



UNIVERSITY
OF TRENTO - Italy

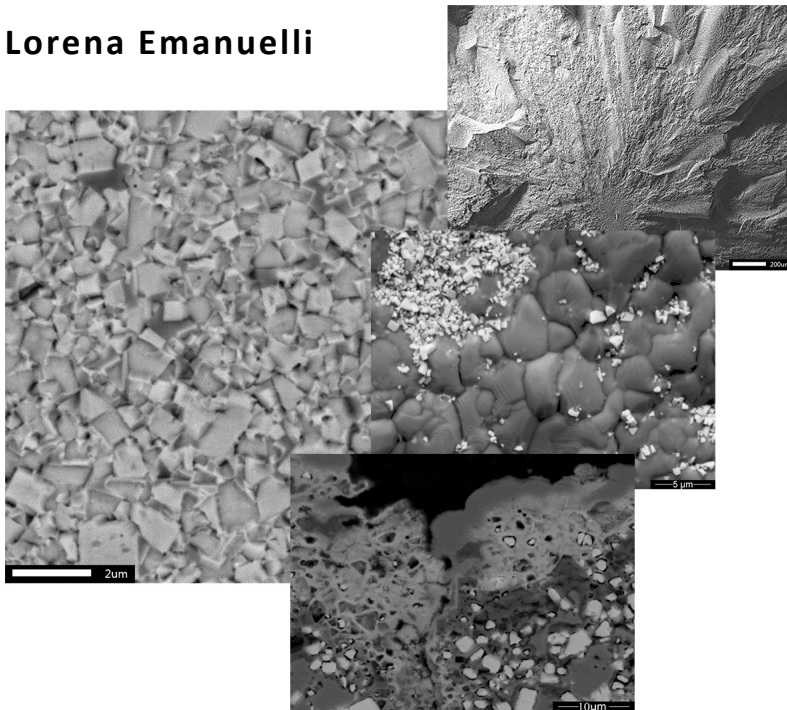
DEPARTMENT OF INDUSTRIAL ENGINEERING

XXX cycle

Doctoral School in Materials, Mechatronics
and Systems Engineering

Study of the properties of cemented carbides from industrial production

Lorena Emanuelli



August 2018

STUDY OF THE PROPERTIES OF CEMENTED CARBIDES FROM INDUSTRIAL PRODUCTION

Lorena Emanuelli

E-mail: lorena.emanuelli@unitn.it

Approved by:

Prof. Alberto Molinari, Advisor
Department of Industrial Engineering
University of Trento, Italy.

Prof. Massimo Pellizzari,
Department of Industrial Engineering
University of Trento, Italy.

Prof. Ilaria Cristofolini
Department of Industrial Engineering
University of Trento, Italy.

Researcher Luis Miguel Llanes
Department of Material Science and
Metallurgy
*Universidad Politecnica de Catalonia,
Barcelona, Spain*

Senior Researcher Christian Gierl
Institute of Chemical Technologies and
Analytics
Technical University of Wien, Austria.

Ph.D. Commission:

University of Trento,
Department of Industrial Engineering

October 2018

**University of Trento
Department of Industrial Engineering**

Doctoral Thesis

**Lorena Emanuelli - 2018
Published in Trento (Italy) – by University of Trento**

To my beloved D. and T.

Abstract

Cemented carbides are composite materials formed by high amount of WC bonded by a soft phase, usually Co. They are used in many applications, such as drawing dies, cutting tools and hot rolls due to their remarkable properties of high hardness and wear resistance. Mechanical properties are strongly related to microstructure, namely the binder amount and the carbide grain size. Increasing the binder content and the carbide grain size, the hardness decreases and the fracture toughness increases.

In this PhD, the correlations between the mechanical properties of WC-Co and the microstructural characteristics, in parts taken from industrial production, were defined. After that, the influence of the residual microporosity on the mechanical properties was evaluated. Considering the production process, another important modification of the final microstructure of WC-Co occurs due to the liquid cobalt migration phenomenon. Based on this, also the liquid cobalt migration that occurs during sintering was investigated. At the end of the thesis, since a few data are available in literature, Thermal Fatigue and oxidation damage in WC-Co were studied.

The main results of this PhD thesis show that the hardness and fracture toughness of WC-Co are defined by the mean binder free path and not by the contiguity since the high standard deviations, the microstructural fineness and also the high carbide grain size scatter. Differently, in case of mechanical strength, also the residual microporosity that depends on the dewaxing stage must be defined. Furthermore, the dewaxing stage acts on the liquid cobalt migration that affects the surface properties and also the final microstructure of the WC-Co part in industrial production. At the end, considering the damages that occur during high temperature applications, the TF and oxidation resistance of WC-Co results affected by the Co content: high cobalt content leads to a better condition of TF damage and a higher oxidation resistance.

Table of contents

Chapter I

Introduction.....	1
-------------------	---

Chapter II

Production of cemented carbide.....	5
2.1. Processing Technologies.....	6
2.1.1. Milling.....	6
2.1.2. Granulation	7
2.1.3. Compaction.....	8
2.1.4. Dewaxing	9
2.1.5. Presintering.....	10
2.1.6. Sintering.....	10
2.2. Liquid phase sintering (LPS)	14

Chapter III

Microstructure and mechanical properties of cemented carbide ...	23
3.1. Microstructural parameters of WC-Co	23
3.1.1. Grain size.....	24
3.1.2. Carbide contiguity	27
3.1.2.1. Effect of Co content and D_{WC} on the contiguity.....	28
3.1.3. Mean binder free path.....	31
3.1.3.1. Effect of Co content and D_{WC} on the λ_{Co}	31
3.2. Mechanical properties of WC-Co.....	33
3.2.1. Hardness.....	34
3.2.1.1. Effect of the Co content, D_{WC} , C and λ_{Co} on the HV.....	35
3.2.2. Fracture Toughness.....	39
3.2.2.1. Effect of the Co content, D_{WC} , C and λ_{Co} on the K_{IC}	42
3.3. Conclusion.....	46

Chapter IV

Mechanical strength of cemented carbide	49
4.1. Introduction	49
4.2. Materials and experimental procedure	56
4.3. Results and discussion.....	58

Chapter VII	
Conclusions	133
List of abbreviation and acronyms	135
References	137
Scientific Production	145
Acknowledgements	147

Chapter I

Introduction

Cemented carbide is a composite material, produced by powder metallurgy (PM), which consists on a high amount of tungsten carbides bonded together by a soft and ductile binder phase, usually Co or Ni. This material is widely used in machining industry due to its remarkable combination of high hardness, wear resistance and toughness. Its development takes place mainly to replace diamond wire drawing dies for W filaments [Upadhyaya, 1998].

By varying the amount of the two phases and the carbide grain size, it is possible to modify the microstructural characteristics of WC-Co, namely contiguity and mean binder free path, and, consequently, to affect the mechanical properties of the material [Brookes, 1992; Santhanam, 1990; Upadhyaya, 1998]. Indeed, increasing the binder content and the D_{WC} , hardness decreases and fracture toughness increases [Brookes, 1992; Santhanam, 1990; Upadhyaya, 1998]. Higher binder amount and D_{WC} tend to decrease the contiguity and to increase the mean binder free path. An increased mean binder free path means a great amount of binder between carbides that is detrimental in terms of hardness, but it increases the fracture toughness since the soft phase offers a high resistance to the possible crack propagation. Differently, higher contiguity means higher amount of carbide-carbide contacts that affects the hardness of the material.

Nevertheless, considering the mechanical strength of WC-Co, the theoretical value is not reached in practice since the presence of defects in the structure or at the surface. The fracture load is not only a function of the intrinsic strength of the WC-Co but is especially a function of the nature and distribution of the defects within the structure since almost all the bending fractures in WC-Co start from internal defects and not at the tensile surface of the test specimen [Li, 2013; Morrell, 1999; Prokopiv, 2008, Sarin, 2014]. An important defect that acts drastically on the strength of a brittle material is the porosity. Nevertheless, today, almost all the commercial WC-Co grades present a negligible amount of residual porosity that it is usually defined according to ASTM B276-05. Despite this, with this standard, it is possible to evaluate only porosity higher than the WC grain size and not the residual microporosity that it is a feature not easy to control in industrial production. Indeed, it was observed that samples from same lot, with same structural parameters, residual porosity, coercive force, hardness and density are often different in strength and plasticity [Li, 2013; Prokopiv, 2008].

Cemented carbide is also used in hot tools subject to cyclic temperature variations and, in turn, to the thermal fatigue damage [Ishihara, 1999; Lagerquist, 1975; Ning, 1997; Tumanov, 1966; Upadhyaya, 1998]. In this condition the material needs a minimum fracture toughness in order to increase the resistance to the nucleation and propagation of cracks. For this reason, the common WC-Co used for the hot applications is characterized by a high binder amount and carbide grain size. Moreover, in these applications, due to the high temperature and the presence of a cooling media, also the oxidation resistance is important [Basu, 1996; Bhaumik, 1992; Casas, 2001; Del Campo, 2009; Gu, 2012; Voitovich, 1996]. The main oxides that are formed during the oxidation of cemented carbide composed by WC and Co are WO_3 , $CoWO_4$ and Co oxides [Basu, 1996; Bhaumik, 1992; Casas, 2001; Del Campo, 2009; Gu, 2012; Voitovich, 1996]. In this case, the oxidation resistance of WC-Co increases by increasing the binder content since the formation of a higher amount of $CoWO_4$, which is denser and more protective than the WO_3 .

It is evident that it is possible to customize the properties in relation to specific applications by changing the chemistry and the microstructural parameters of WC-Co.

Another important aspect that must be taken into account in the tool applications is the surface modification that can occur during the production of the material. In case of cemented carbide, during sintering under specific condition, the liquid Co migration takes place, which leads to the formation of a Co gradient from the surface to the bulk of sintered cemented carbide changing the surface and bulk condition of the part [Brookes, 2010; Eso, 2008; Eso, 2005; Fan, 2008; Fan, 2009A; Fan, 2009B; Fan, 2009C; Fan, 2013; García, 2016; Guo, 2010; Guo, 2011; Janisch, 2010; Konyashin, 2012; Konyashin, 2013; Konyashin, 2014A; Konyashin, 2014B; Liu, 2004; Liu, 2006; Sachet, 2013; Sachet, 2012; Taniguchi, 1989]. A lower Co amount on the surface and a higher Co content in the bulk permits a trade-off between the wear resistance and the fracture toughness [Eso, 2008; Eso, 2005; Fan, 2009; Fan, 2008; Fan, 2013; Guo, 2011; Konyashin, 2012; Konyashin, 2013; Liu, 2004; Liu, 2006]. Differently, the migration of cobalt towards the surface that leads to the Co layer formation, also called “Co capping”, is detrimental in case of wear resistance. [Brookes, 2010; Fan, 2009A; Fan, 2009B; Fan, 2009C; García, 2016; Guo, 2010; Janisch, 2010; Taniguchi, 1989; Sachet, 2013; Sachet, 2012].

The fundamental goal of this PhD thesis is to understand if the mechanical properties of WC-Co could be really defined by the microstructural parameters, namely the mean binder free path and the carbide contiguity, also in case of parts taken from industrial production. For this reason, in the first part of this PhD thesis, the influence of the contiguity and the mean binder free path on the mechanical properties of cemented carbides applied to the production of wire drawing dies was investigated. After that, also the influence of the residual microporosity on the mechanical properties was evaluated. The residual microporosity occurs due to a not correct dewaxing stage. Therefore, in industrial production, not only the Co content and WC grain size but also the production process, such as the dewaxing stage, affects the microstructural parameters of the WC-

Co parts and consequently, the mechanical properties. Considering the production process, another important modification of the final microstructure of WC-Co occurs due to the liquid cobalt migration phenomenon. Based on this, in the second part of this PhD thesis, the liquid cobalt migration that occurs during sintering was investigated. At the end, in the third part of this PhD thesis, since only a few data are available in literature, TF and oxidation damage in WC-Co were studied.

Chapter II

Production of cemented carbide

Hardmetal is a composite material, made by powder metallurgy (PM), which consist of a high fraction of hard particles bonded by a soft and ductile binder. This material is called cemented carbide when the hard phase is WC and the soft phase is usually Co or/and Ni. Example of WC-Co microstructures with different Co content and WC grain size are shown in Figure II – 1.

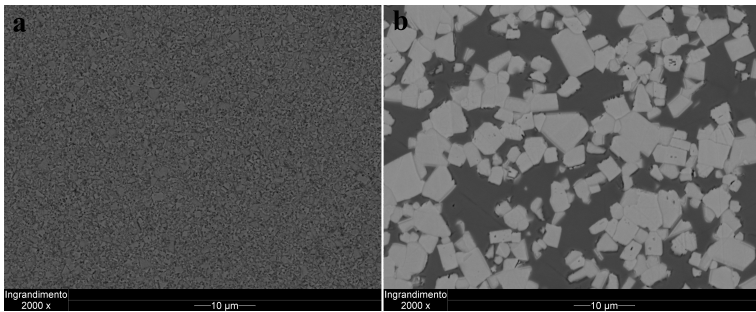


Figure II – 1. WC-Co with 6.5 wt.% Co and $D_{WC}= 0.8 \mu\text{m}$ (a) and 30 wt.% Co and $D_{WC}= 4.7 \mu\text{m}$ (b).

The production of cemented carbide began with the idea of replacing diamond wire drawing dies for W filaments. The company Krupp introduced it to the market on 1927 under the name of Widia (wie Diamant) that means like diamond. This material is widely used in the tool industries due to its remarkable properties of high hardness and wear resistance with a certain amount of toughness.

The production of cemented carbide consists of various operations in which a lot of factors are critical. Figure II – 2 shows a general schematization of the WC-Co production.

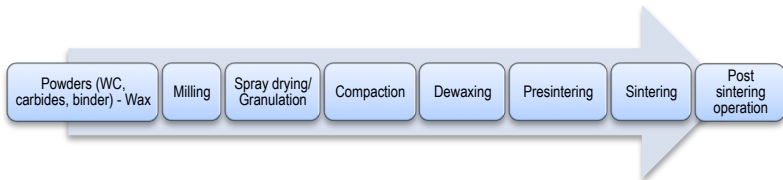


Figure II – 2. General schematization of WC-Co production.

In the present chapter, all the processing technologies used for the WC-Co production have been reported [Upadhyaya, 1998].

2.1 Processing Technologies

The starting materials for the WC-Co production are hard refractory carbides, such as WC, TiC, TaC and their mixed carbides, and a metal binder, usually Co and/or Ni. A small amount of other carbides like NbC, VC and Cr₃C₂ may be used with the purpose of control the grain growth during sintering [Huang, 2008; Poetschke, 2012; Zackrisson, 1998] as shown in Figure II - 3.

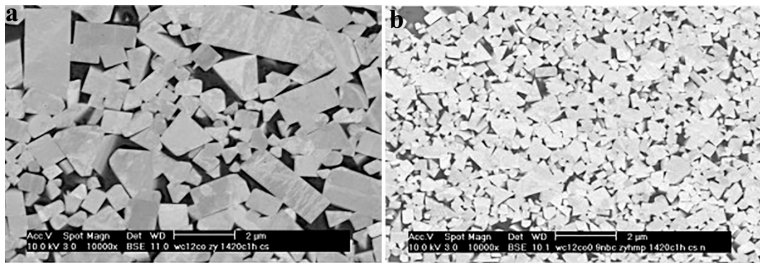


Figure II - 3. WC - 12wt.%Co with 0 (a) and 0.9 (b) wt.% NbC addition [adapted from Huang, 2008].

A wax, usually paraffin wax or polyethylene glycol (PEG), is added to the power mix in order to facilitate the compaction step and to pledge a certain amount of green strength during handling.

2.1.1 Milling

Milling is a mechanical comminution method used in the PM industry in order to reduce the particles size down to the required dimensions by the application of impact and shear forces on the powders. Furthermore, the milling process acts not only on the particles dimensions but also on particle shape (flaking), on the formation of a solid-state alloying (mechanical alloying) or a solid-state blending (incomplete alloying), on the properties and on the uniform distribution in case of mixing of two or more materials [Šalák, 1995; Thümmeler, 1993]. The fracture of the powders during milling creates new active surfaces and increases structural defects of both carbides and binder leading to a more efficient sintering obtaining a homogeneous and pore free sintered WC-Co [German, 1996].

There is a wide variety of milling equipments and the selection depends on the quantity and the composition of the milled powder.

In case of WC-Co production the most used comminution method regards ball milling and the principal aim is to mix the carbides with the metal binder in order to obtain a uniform distribution of the binder. Indeed, the mechanical properties and the porosity absence of the WC-Co are strongly related with the binder distribution into the materials. The common ball milling equipment used in the cemented carbide industry is the cylindrical rotation ball mill [Sun, 2003]. Carbide balls are used in the WC-Co comminution method, in order to contrast the WC hardness and to avoid possible contamination of the powder due to the fragmentation of the balls during milling. In order to reduce the high milling energy, the operation is carried out in a protective liquid (such as acetone, alcohol, etc.) that minimizes the increase in temperature and prevents the powders oxidation that could occur due to the formation of active surfaces during milling.

The most important milling parameters are the ball to powder (BTP) ratio, the milling time and the rotation speed, as reported in Figure II – 4. The BTP ratio is usually equal to 3.0, the milling time could be varied between 48 to 72 h and the critical speed is inversely proportional to the cylindrical drum diameter.

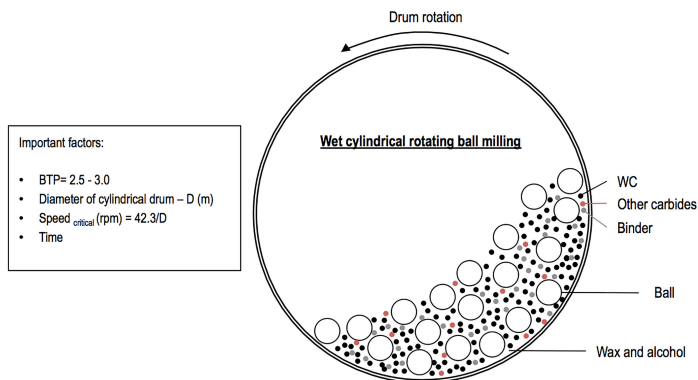


Figure II – 4. Transversal cross section of the cylindrical rotation ball milling.

After milling, a slurry is obtained due to the presence of the protective liquid. For this reason, before the granulation step, the slurry is dried in a closed vessel and the solvent is extracted when its boiling point is reached.

2.1.2 Granulation

The powder obtained after the drying process is not free flowing and has low apparent density because it is very fine. During compaction, the inter-particle friction due to the fine powder, leads to the necessity to apply a higher pressure. For this reason, a granulation step before compaction is introduced in order to create agglomerates with good flow and fill properties.

There are two different granulation methods. The traditional method consists in the prepressing of the dried powder into billets with a low pressure in order to avoid possible welding between the particles. After that, the billets are disintegrated to obtain coarse granules. The coarse granules are sieved in order to eliminate very coarse granules and to select the granules with the proper size for compaction. The alternative granulation method is the spray drying and includes the slurry drying and the granulation. Indeed, in this method, the milled slurry is spray into a preheated inert gas and simultaneously dried. The advantage respect to the traditional method is that the obtained granules are uniform in size, there is less handling and the binder distribution is more uniform since the milled carbide slurry is instantly dried.

2.1.3 Compaction

The aim of compaction is to shape the compacts and improve dimensional control during sintering. The traditional method for the effective green consolidation of WC-Co consists in pressing the powder with a single or double acting press (Figure II – 5) in order to reach a green density of 60% of the theoretical one. Indeed, compacts with less density present, during sintering, higher shrinkage and a worst dimensional control. The double acting press provides a more uniform density and shrinkage distribution compared with the single one.

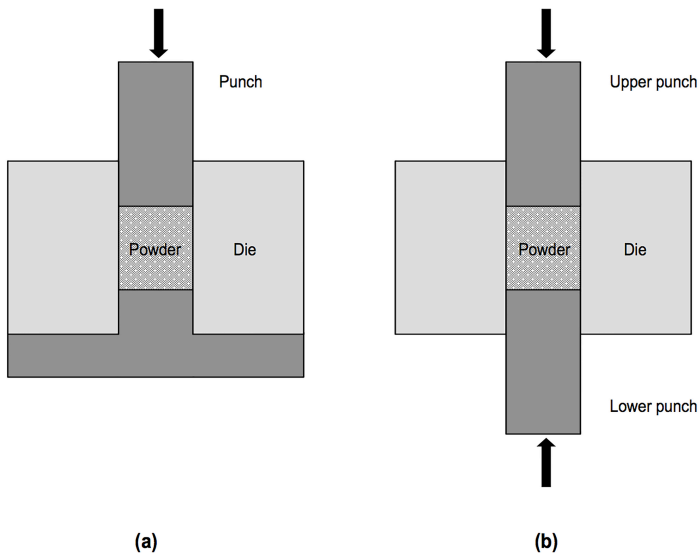


Figure II – 5. Schematization of (a) single and (b) double acting presses.

All the presses are designed in order to press the compacts to a given green density with the use of a constant weight of powder and a constant compacted volume.

In the WC-Co industry, the hydraulic press is used in the production of big size parts and the mechanical one is preferred for the production of tool tips. Today also servo electric presses are in use. The compaction pressure is from 50 to 150 N/mm².

The isostatic compaction is an economical alternative to the traditional one in the production of large parts. In this case, due to the application of a uniform pressure in all directions, an uniform distribution of the density is achieved. However, the resulted compact needs to be presintered in order to preserve the shape before sintering.

Another green consolidation method is extrusion. This method is used when the part presents a very high length to diameters ratio such as drills, reamers and boring tools. The extruded material needs to exhibit a certain plastic flow. For this reason, a high amount of plasticizer like polyvinyl alcohol, PEG, paraffin etc. is added to the powder in order to ideally separate all the particles by a film of plasticizer.

After compaction, the wax or the plasticizer is removed by the dewaxing stage before sintering.

2.1.4 Dewaxing

The wax added in the milling stage in order to facilitate compaction and the handling has to be removed. The common technique used in the hardmetal industry consists in the wax volatilization by heating the compacted WC-Co in a protective atmosphere or in vacuum depending on the type of wax. In this stage it is important that the wax is completely removed in a certain temperature interval in order to avoid possible physical or chemical decomposition of the wax that affects the compact. The compacted WC-Co is heated up in the wax boiling range in order to activate its evaporation.

Considering the paraffin, the correct interval in order to remove all the wax is around 150°C until 250-300°C [Spriggs, 1970]. If the temperature exceeds 400°C, the paraffin wax cracks to form lower paraffins, olefins and free carbon that contaminate the WC-Co. This is the so called paraffin cracking [Chen, 2008]. Differently, in case of PEG it is important to use the hydrogen atmosphere in order to facilitate the evaporation and to prevent possible carbide contamination due to the oxygen derived from the gaseous species that form during PEG decomposition as CO, CO₂, CH₄ and H₂O [Uhrenius, 1975; Leitner, 1992].

In all cases, first of all the wax present on the exposed surfaces evaporates and, when it is completely eliminated, the one in the inner part of the component is able to diffuse to the surface and to evaporate. In the correct temperature and time condition, this process continues until the complete wax evaporation. The use of a gas flow facilitates the evaporation because it quickly removes the gaseous products from the reaction zone.

2.1.5 Presintering

Usually, the compacted WC-Co is produced in simple shape that, in some case, needs to be machined by turning, grinding and drilling. In this situation, a presintering stage at 750-1000°C before machining is performed in order to strengthen the compacted WC-Co and to avoid its breaking. The strengthening that occurs during the presintering stage is due to the solid state sintering of cobalt particles. For most machining operation, a presintering stage at 800°C provides sufficient strength. Increasing the Co amount, the presintering temperature could be decreased to obtain similar strength.

Another important parameter in this stage is the atmosphere that, if not inert, may react with the compacts leading to a surface composition variation. Hydrogen is usefull in order to reduce the possible oxides on the powder after milling but it can also interact with the C present into the material, leading to the possible formation of a third brittle phase (η phase).

2.1.6 Sintering

Sintering is a heat treatment used in PM in order to bond together the particles and to obtain a solid mass. Usually, the particles are smaller than 1 mm in size and can have different shape such as spherical, cubical etc. Small particle sizes mean high surface to volume ratio that leads to a high surface energy. The sintering process tends to reduce the surface energy by reducing the surface area with the formation of particle bonds. The formation of these bonds occurs through with different mechanisms that occur at the atomic level. The different sintering techniques present in the industry are:

- solid-state sintering (SSS) that creates bonding through solid-state diffusion;
- liquid-phase sintering (LPS) that uses the formation of a liquid phase in order to join the particles;
- pressure assisted sintering where a pressure is applied to increase simultaneously particles deformation and bonding;
- new techniques that involve reactions between mixed powders.

In all cases, the particle bonds lead to change in the pore structure and in the microstructure, which affect the material properties. Indeed, properties like strength, ductility, conductivity, magnetic permeability and corrosion resistance are subjected to a drastic improvement during sintering.

A negative aspect in sintering is the oversintering where the properties reach a peak and then decline due to the microstructural coarsening that occurs with the continued heating for a longer time or at a higher temperature [German, 1996].

The sintering technique used in case of WC-Co production is the liquid phase sintering. The sintering temperature is correlated with the eutectic temperature that is formed in the WC-Co system. In this process, even at rather low temperatures, binder spreads and diffuses into WC-WC interfaces. Increasing the temperature, the binder starts to dissolve a certain amount of carbide from the adjacent particles surfaces. This condition leads to the WC surface smoothing and to an easier gliding of the carbides, providing the mechanism of rearrangement in solid-state. This is the reason why shrinkage is observed in the temperature interval below the melting point of the carbide - cobalt eutectic.

During the WC-Co sintering there are some variables that must be considered. The sintering atmosphere is an important parameter because of the possible chemical interactions that occur between the compacts and the surrounding atmosphere. Usually, these chemical interactions involve carbon. The carbon control in WC-Co is very important because a deviation from the stoichiometric value leads to the formation of a third phase as shown in the W-Co-C phase diagram [Fernandes, 2011; Upadhyaya, 1998] (Figure II – 6).

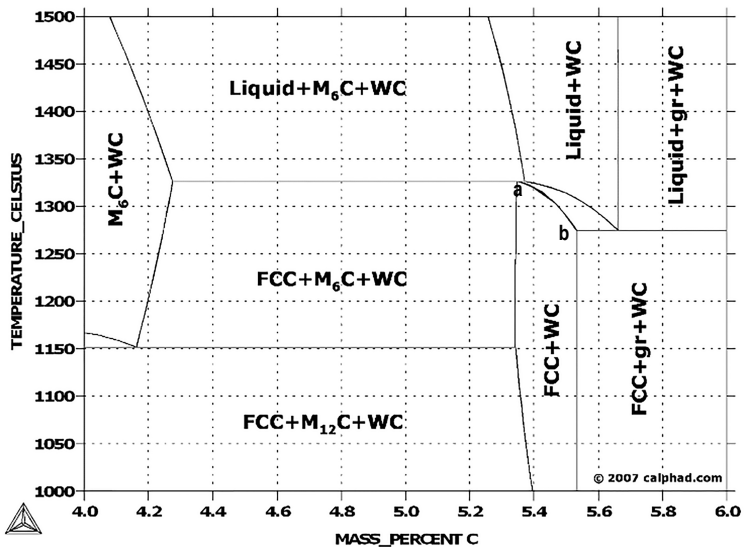


Figure II – 6. Vertical section of WC- 10Co, calculated with Thermo-Calc and SSOL4 thermodynamic database [adapted from the website <http://www.calphad.com>].

The points “a” and “b” in the Figure II – 6 refer respectively to the minimum and maximum carbon contents of a two-phase WC-Co alloy. A carbon deficit leads to the formation of a third brittle phase named η phase. It is a ternary compound of W, Co and C and can exist in two forms, M_6C and $M_{12}C$ [Fernandes, 2007; Formirano, 2016; Peters, 1978]. Micrographs of η phase are reported in Figure II – 7.

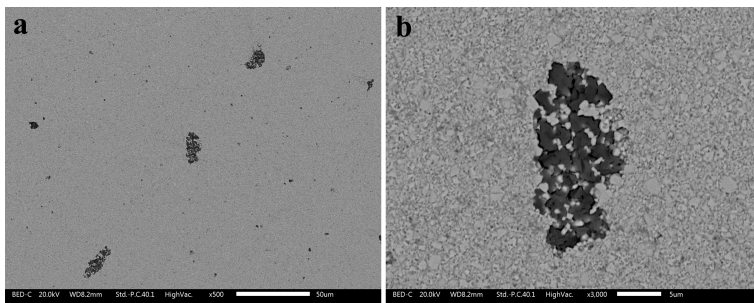


Figure II – 7. SEM micrographs of WC-Co with η phase (a) and detail of η phase (b).

Differently, a carbon excess precipitates as free carbon [Chingbin, 2012; Joost, 2008], as shown in Figure II - 8.

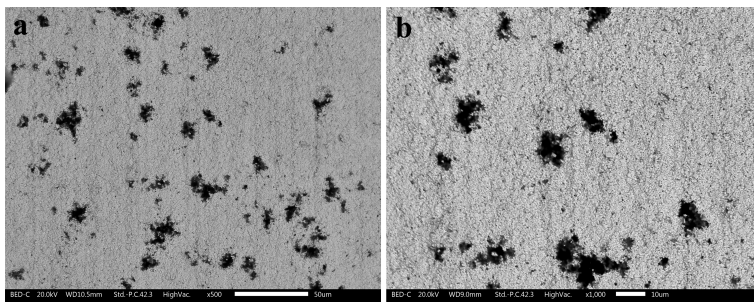


Figure II – 8. SEM micrographs of WC-Co surface with free carbon at 500X (a) and 1000X (b).

Both of these phases deteriorate the mechanical properties of the WC-Co. For this reason, it is important to pay attention to the atmosphere control in order to ensure that the carbon content remain into the two-phase region. An example is the hydrogen atmosphere used to reduce possible oxides present on the compacted WC-Co. The problem is that hydrogen reacts not only with oxygen but also with carbon producing CH_4

and, in turn, leading to decarburization. To avoid this condition, either an equal amount of CH_4 is added to hydrogen or an extra carbon addition is provided. Another solution is sintering in vacuum. In this case, a pressure under a few Torr is required to reduce cobalt losses. Other important factors that must be considered are the sintering temperature and time. The sintering temperature is preliminarily defined by the cemented carbide composition and the sintering time is related with the sintering temperature. Increasing the sintering temperature is possible to decrease the sintering time. Higher sintering temperature or longer sintering time leads to the microstructural coarsening that affects the WC-Co properties [Mannesson, 2011] as shown in Figure II - 9.

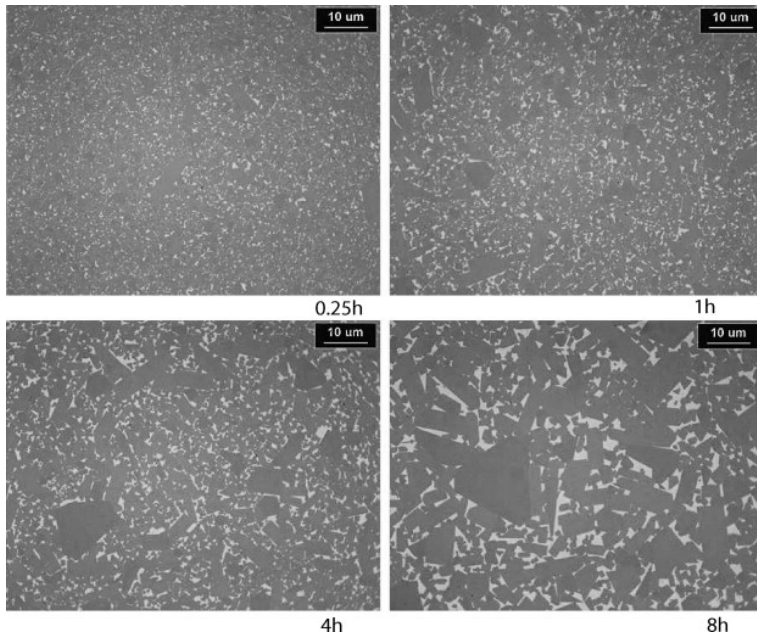


Figure II – 9. Effect of the sintering time on the WC grain growth in cemented carbides [adapted from Mannesson, 2011].

Hence, a compromise in terms of temperature and time has to be reached in order to minimize coarsening, to optimize the densification and to avoid distortion of the parts. Also the heating and the cooling rates play an important role in the final properties of WC-Co. High heating rate reduces the time for the dewaxing stage and the wax vapor creates cracks or void into the compact, since the gaseous species are unable to escape sufficiently fast from the parts. Moreover, high heating rate after the formation of the eutectic liquid is detrimental due to the formation of a high temperature gradient that causes local volume variation and consequently distortion of the compact. Differently, the

cooling rate has effect on the solidification porosity and on the impurity segregation at the WC-Co interface that leads to an embrittlement of the compact.

In the next subchapter a detailed explanation about liquid phase sintering is reported.

2.2 Liquid phase sintering (LPS)

In LPS the three main phenomena that must be taken into account are the solid solubility in the liquid, wetting of the solid grains by the liquid and the solid-phase diffusion in the liquid phase [German, 1996; Mchugh, 1997]. It is essential that the liquid wets the solid particles and has certain solubility for the solid. Due to the presence of a wetting liquid, the capillary force acts on the solid particles in order to eliminate porosity and reduce the interfacial area. For this reason, there is a high diffusion rate respect to the SSS. The microstructure evolution at high temperature is dominated by the surface energy. Indeed, a negative is the microstructural coarsening that may occur in the case of higher sintering temperature or longer sintering time.

In Table II – 1 the some possible solubility combinations in LPS are summarized.

	Solid solubility in liquid	Liquid solubility in solid	Results	Example of systems
1	Low	Low	Limited densification, rearrangement	W-Cu
2	Low	High	Swelling, transient liquid	Fe-Cu
3	High	Low	Extensive densification	WC-Co
4	High	High	Swelling and densification	Cu-Sn

Table II – 1. Schematization of the interactions and sintering behavior depending on the solubility interaction during LPS.

When the surface energies prevail, as in case of WC-Co system, the densification occurs as shown in Figure II – 10.

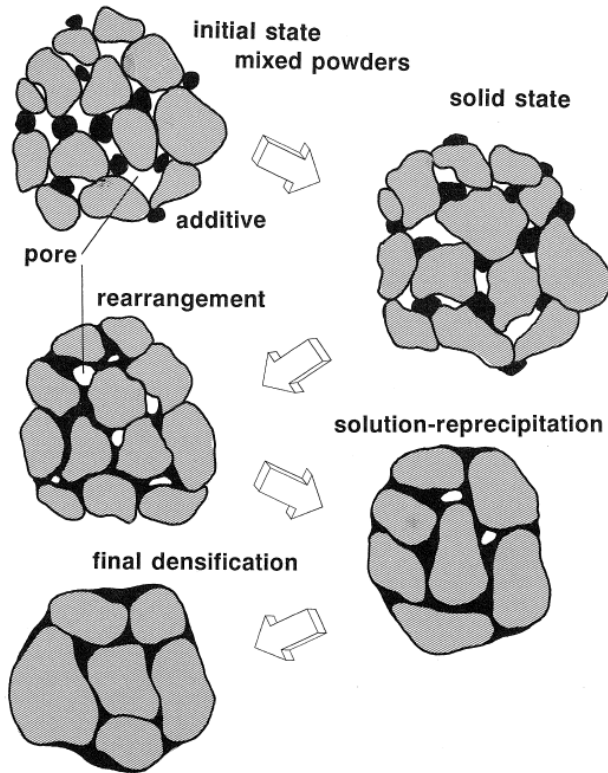


Figure II – 10. Schematization of the LPS stage in the WC-Co sintering [adapted from German, 1996].

During the heating of the mixed powders, firstly solid-state sintering occurs. In this stage, in case of WC-Co, the binder phase starts to diffuse by leading to considerable densification [Macedo, 2003]. This is driven by the chemical concentration gradient into the system. After that, the densification becomes dependent on the liquid phase amount during the rearrangement, solution-recipitation and final densification stages. Indeed, the final stage of the LPS is controlled by the densification due to the solidification of the liquid Co that is slow because of the rigid WC skeleton. It is clear that the total densification is due to the overlapping phenomena of rearrangement, solution and recipitation and solid phase sintering that occur after the liquid phase formation [Allibert, 2001; German, 1996; Porat, 1996], as shown in Figure II – 11. It is evident that, even if the logarithmic scale is only approximate, densification by rearrangement is fast and the final stage, where it is controlled by the solid structure, is slow.

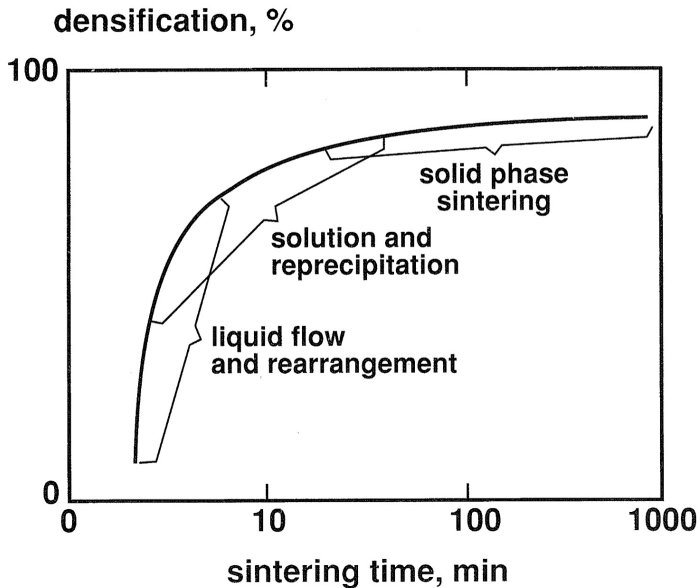


Figure II - 11. LPS densification versus the sintering time [adapted from German, 1996].

It is evident that almost all the densification occurs in the rearrangement and the solution-reprecipitation stages. Prolonged holding of material at sintering temperature leads to negative microstructural modification such as the excessive solid particle growth.

In order to understand better the LPS of WC-Co the three main stages where the WC-Co densification occurs are summarized below.

1. Liquid flow and rearrangement

In this stage, the first liquid is formed and spreads fast over the particles in order to minimize the total surface energy. As soon as the liquid penetrates the WC-WC boundaries, a high capillary force exerted on the WC leads to the particle rearrangement and a rapid densification occurs. The capillary force brings the WC particles closer and, due to the irregular shape of the WC, the misalignment of the center of gravity gives a torque. This torque is responsible for a rapid rearrangement and brings flat surfaces into contact. The minimization of the total surface energy is also important for the pore elimination that takes place simultaneously to the densification. The maximum amount of densification during rearrangement depends on many important factors as the liquid amount, particle size, solubility of the solid in liquid, contact angle etc.

II. Solution and reprecipitation

The solution and reprecipitation of WC, which occur concurrently and after the rearrangement, become dominant in this stage. In case of a low Co amount, where the liquid volume is not sufficient to fill all the voids after rearrangement, the solution/reprecipitation mechanism acts significantly on the densification of WC-Co. During this stage the densification is associated with grain shape accommodation, dissolution of small particles with reprecipitation on large particles and coalescence of contacting grains that involves grain boundary migration. The increased grain size due to the solution and reprecipitation leads to a reduction of the pore size. At the end of this stage, pores are eliminated or stabilized by a trapped atmosphere.

III. Solid phase sintering

In many cases, the full densification is reached in the first two stages and further holding at sintering temperature does not contribute to the densification but only to microstructural changes. These variations have an important effect on the WC-Co properties such as wear resistance, toughness, strength, magnetic properties etc. The microstructural coarsening takes place in parallel with the densification and prevails in this last stage. Also in this case, the driving force is the surface energy minimization. Indeed, due to the grain growth, the small grain dissolve in favor of the large grains. For this reason, the mean grain size and the mean distance between carbides increase by increasing the sintering time.

As has been mentioned previously, the phase diagram, the surface energy, the wettability, the solubility of the liquid phase in the solid phase and of the solid phase in the liquid phase and the capillarity force are the principal thermodynamic and kinetic factors in the LPS.

As shown in paragraph 2.3 the phase diagram is important in order to consider the different phases that it possible to obtain at a certain temperature depending on the starting composition. Therefore, it is useful since it gives information regarding the temperature that must be reached in order to obtain the liquid phase. In this way, knowing the composition, it is possible to define the correct sintering temperature. A typical sintering temperature is slightly above the eutectic temperature considering a composition in the liquid – solid region.

The other important parameter in the LPS is the surface energy that is the driving force of the process. In condition with a high fraction of solid, the porosity and its associated surface energies are eliminated by grain shape accommodation that depends on the relative energy of the solid-liquid interface. This minimization of the surface energy starts with the particle rearrangement due to the liquid that wets the solid phase and continues with the solution-reprecipitation leading to pore elimination due to grain adjustment. At the end, the microstructural coarsening occurs and the mean grain size

increases. The equation [2.1] is used for the driving force in the LPS and considers the pressure difference between two curved liquid surfaces that depends on the radii of curvature (R_i and R_j) and the liquid vapor surface energy γ_{LV} .

$$\Delta P = \gamma_{LV} \cdot \left(\frac{1}{R_i} + \frac{1}{R_j} \right) \quad [2.1]$$

By convention, the sign is positive if the radius of curvature is inside the liquid. From this equation it is clear that the minimum of pressure across a surface is obtained for a flat surface (no net curvature) or when the two radii are equal and opposite, as in a saddle surface.

The solid wettability by liquid is a natural concern in the LPS and depends on different surface energies in the system liquid – solid – vapor as shown in Figure II – 12 [German, 1996; Mittal, 2008].

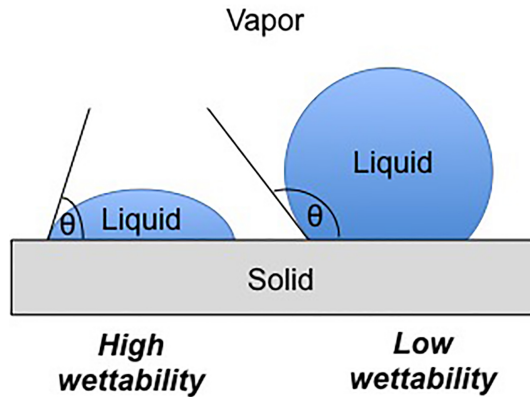


Figure II – 12. Geometric representation of the solid-liquid-vapor equilibrium condition for high and low wettability.

The degree of wetting is characterized by the contact angle θ and its value depends on the balance of the three surface tensions as shown in equation [2.2].

$$\gamma_{SV} = \gamma_{SL} + \gamma_{LV} \cdot \cos \theta \quad [2.2]$$

γ_{SV} , γ_{SL} and γ_{LV} refer to the solid-vapor, solid-liquid and liquid-vapor surface tensions. Surface impurities and temperatures drastically influence the wettability. Increasing the temperature, the solubility increases and the contact angle decreases.

Considering the solubility, in a classic LPS, the solid is soluble in the liquid but the solubility of liquid in solid is very low. Indeed, a high liquid solubility in the solid leads to a transient liquid phase and compact swelling during heating. Differently, high solid solubility in the liquid and no liquid solubility in the solid favor the densification that is very important in the sintering process. In Figure II – 13 the schematization of the different conditions described above is reported.

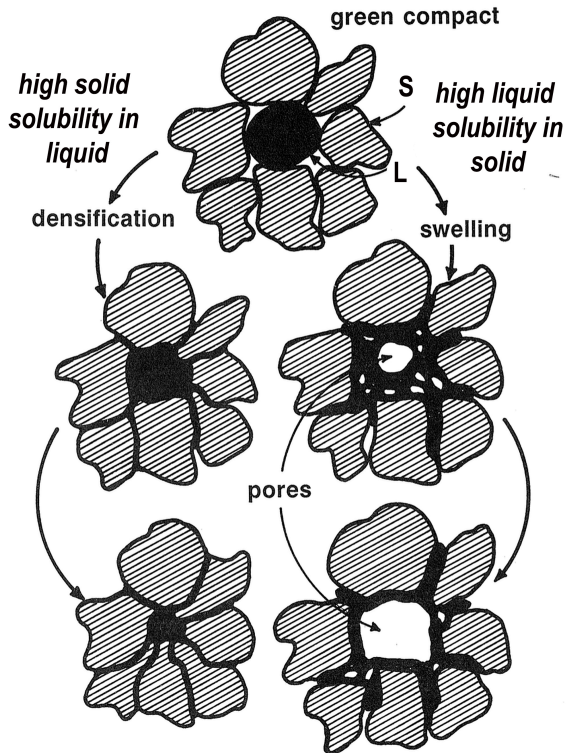


Figure II – 13. Schematization of swelling and densification [adapted from German, 1996].

A thin pipe, as the space between WC grains, and a wetting liquid, such as the Co liquid, leads to the capillarity. This phenomenon regards the capability of a liquid to flow against gravity in a narrow space, therefore a smaller capillary size scale favors it. It depends on two forces: cohesion between similar molecules or atoms of a liquid and attraction between the molecules or atoms of liquid with the particles of forming the tube that are in contact with the liquid. Indeed, considering these two forces, the height of a liquid inside a tube is defined by the equation [2.3].

$$h = \frac{2\gamma \cdot \cos \vartheta}{\rho \cdot g \cdot r} \quad [2.3]$$

where γ is the liquid – air surface tension, ϑ is the contact angle, ρ is the liquid density, g is the local acceleration due to the gravity and r is the radius of tube.

From the equation [2.3] it is evident that the capillary height increases by decreasing the tube radius. This means that, in LPS, the wetting liquid flows preferentially into the smallest pore leaving behind the large one. Considering the LPS, the capillarity becomes important in terms of densification: when the liquid forms, the capillarity creates a strong surface densification force on the solid leading to the rearrangement, densification and contact flattening. It is possible to define the capillarity force in the LPS considering the two spheres model shown in Figure II – 14.

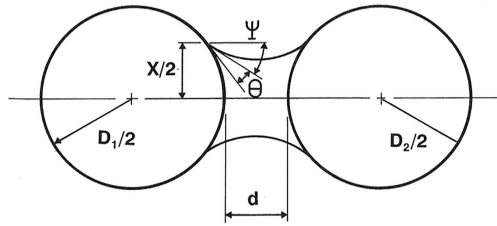


Figure II – 14. Two spheres model with a liquid bridge [adapted from German, 1996].

The force between the two spherical particles is given by the pressure difference between the liquid meniscus and the vapor, and the surface energy between liquid and vapor (γ_{LV}). The pressure difference (ΔP) is related with the liquid curvature that depends on the liquid content, contact angle (ϑ), particles spacing and size. For this reason is possible to define the capillarity force as reported in the equation [2.4].

$$F = \frac{\pi}{4} \cdot X^2 \cdot \Delta P + \pi \cdot X \cdot \gamma_{LV} \cdot \cos \psi \quad [2.4]$$

Where X is the meniscus diameter and ψ the angle reported in Figure II – 14.

The capillarity force is attractive and achieves zero separation between the particles leading to the densification during LPS with a wetting liquid. Differently, a poor wetting liquid leads to the formation of a repulsion force that separates the particles as shown in Figure II – 15.

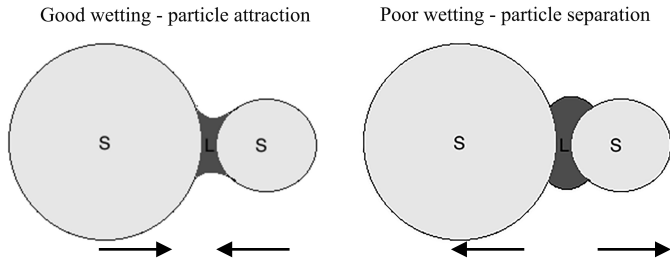


Figure II – 15. Effect of the solid wettability by liquid on the capillarity force.

Chapter III

Microstructure and mechanical properties of cemented carbide

Part of this chapter has been published in:

L. Emanuelli

“**Caratterizzazione microstrutturale del WC-Co**”,
LA METALLURGIA ITALIANA, n. 11/12 (2017), p. 52-55.

L. Emanuelli, A. Molinari, G. Arrighetti, G. Garoli

“**Dependence of the mechanical properties on the microstructural parameters of WC-Co**”,
Submitted to Powder Metallurgy Progress.

Mechanical properties of WC-Co are strongly related to chemical composition and microstructure, namely to the binder content and carbide grain size. Increasing the binder content and the WC grain size, hardness decreases and fracture toughness increases [Brookes, 1992; Santhanam, 1990; Upadhyaya, 1998]. For this reason it is possible to customize the properties in relation to specific applications by changing the chemistry and the microstructural parameters. Actually, these correlations are related to the influence of the Co content and D_{WC} on the contiguity and on the mean binder free path, which are the microstructural parameters that affect the mechanical properties. Indeed, higher mean binder free path and lower contiguity mean a great amount of Co between carbides that is detrimental in terms of hardness but increases the fracture toughness since Co offers higher resistance to crack propagation. In this chapter the method used to evaluate the just mentioned microstructural parameters is summarized. Moreover, in order to confirm what is reported in literature, the mechanical properties of typical industrial cemented carbides with a medium/low Co content are investigated in correlation with Co content and D_{WC} and also, more precisely, with contiguity and mean binder free path.

3.1 Microstructural parameters of WC-Co

The microstructural parameters that affect the mechanical properties of WC-Co are the WC grain size (D_{WC}), the carbide contiguity (C) and the mean binder free path (λ_{Co}). These parameters and the method used for their measurement are summarized in the next paragraphs. Seventeen different WC-Co samples were investigated and at least

four micrographs for each samples were used in order to define the microstructural parameters.

3.1.1 Grain size

D_{WC} is the grain size of WC after the sintering process. Using this parameter and the starting dimension of the WC powder, it is possible to understand if grain growth occurs during sintering. It is an important parameter to understand the goodness of the sintering process and the effective role of the grain growth inhibitors (Cr_3C_2 , VC and NbC) that are possibly added to the powders in order to prevent the grain coarsening. The most common way used for the measurement of D_{WC} is through quantitative metallographic techniques. One of these techniques is the linear intercept method (Figure III – 1) and is important because it is able to quantify the mean D_{WC} and to define the size distribution [Bennett, 2000]. This method requires a polished and etched cross section of the WC-Co sample and the acquisition of calibrated micrographs. On these images straight lines are drawn that must intercept at least 20 grains for each line to reach a total of at least 200 grains. The length of each grain is measured using a calibrated rule and the mean linear intercept grain size is defined with the equation [3.1].

$$l_{av} = \frac{\sum l_i}{n} \quad [3.1]$$

Where l_{av} is the mean linear intercept grain size, l_i is the measured length of each individual intercept and n is the number of WC grains intercepted.

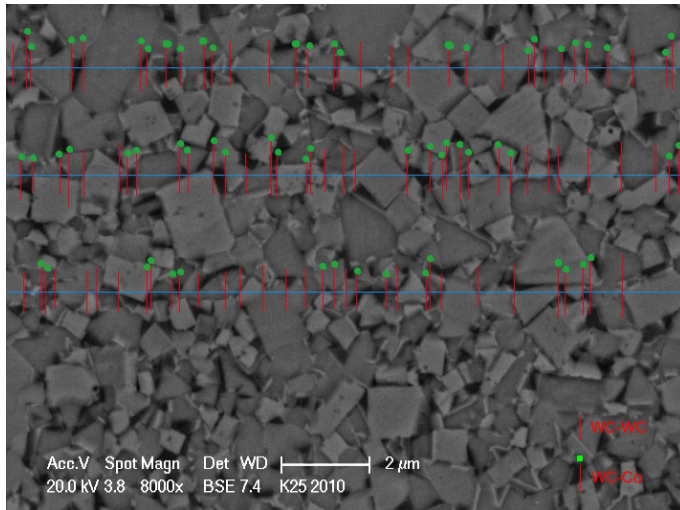


Figure III – 1. Example of the linear intercept method used in order to evaluate the D_{WC} .

Considering the uncertainty of the measurement, in this work the D_{WC} values are rounded to two digits. The equation [3.1] refers to measurements made in one-dimension and no assumptions regarding the shape of the grains were taken into account. Another technique is the Jefferies method that, based on point or area counting grains, calculates the WC average area and the equivalent diameter for the two-dimensional size of WC. Respect to the linear intercept method, this does not supply a grain size distribution [Jefferies, 1916]. In order to define the three-dimensional mean grain size, a new method for its calculation was proposed [Engqvist, 2002]. In this method, the three-dimensional grain size was evaluated by dissolving the binder and estimating the largest diameter of each WC by SEM. It was observed that the results of the three-dimensional method and the linear intercept method are comparable if the values of the linear intercept method are transformed into three-dimension with the equation [3.2].

$$D_{WC} = \frac{\sum l_i^4}{\sum l_i^3} \quad [3.2]$$

From these methods it is possible to define the correct procedure for measuring the average D_{WC} : in the following the procedure of the linear intercept method will be adopted with the correction for the three-dimensionality of the WC particles. Some D_{WC} values obtained by this method on hardmetals from the industrial production of a company are summarized in Table III - 1.

Samples	WC (%)	Co (%)	Other carbide (%)	WC powder size (μm)	I_{av} (μm)	D_{wc} (μm)
A	93.7	6.0	0.3 Cr ₃ C ₂	0.8	0.49 ± 0.25	0.95
B	93.8	6.0	0.2 Cr ₃ C ₂	0.8	0.44 ± 0.20	0.74
C	93.5	6.0	0.5 Cr ₃ C ₂	0.8	0.40 ± 0.19	0.69
D	93.2	6.5	0.3 Cr ₃ C ₂	0.8	0.44 ± 0.22	0.82
E	93.2	6.5	0.3 Cr ₃ C ₂	0.8	0.44 ± 0.23	0.85
F	93.2	6.5	0.3 Cr ₃ C ₂	0.8	0.47 ± 0.22	0.83
G	93.2	6.5	0.3 Cr ₃ C ₂	0.8	0.45 ± 0.22	0.77
H	93.2	6.5	0.3 Cr ₃ C ₂	0.8	0.43 ± 0.19	0.70
I	93.3	6.5	0.3 Cr ₃ C ₂	0.8	0.41 ± 0.20	0.71
L	92.7	7.0	0.3 (W,Nb)C	1.1	0.53 ± 0.30	1.07
M	92.7	7.0	0.3 VC	1.2	0.42 ± 0.21	0.71
N	90.7	9.0	0.3 Cr ₃ C ₂	0.8	0.44 ± 0.23	0.83
O	91.0	9.0	-	1.0	0.61 ± 0.35	1.27
P	90.7	9.0	0.3 Cr ₃ C ₂	0.8	0.41 ± 0.22	0.86
Q	91.0	9.0	-	1.0	0.50 ± 0.26	0.97
R	88.0	12.0	-	1.0	0.58 ± 0.33	1.60
S	88.0	12.0	-	1.0	0.54 ± 0.34	1.45

Table III – 1. I_{av} and D_{WC} values for different industrial cemented carbides.

To better investigate the final D_{WC} , the data reported in Table III – 1 are plotted in Figure III -2.

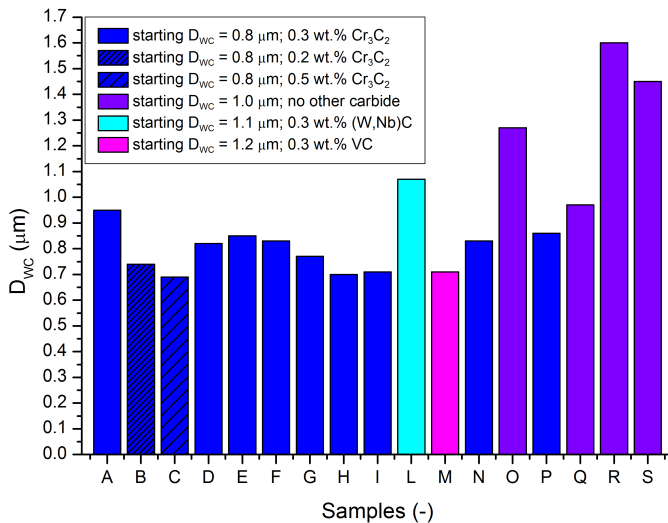


Figure III – 2. D_{wc} for the different industrial cemented carbides.

In the compositions with 6.0 wt. % of Co (A, B and C), an increase of 0.3 wt.% of Cr_3C_2 has not a visible effect on the WC grain size measured with the linear intercept method and the three-dimensional correction.

Analyzing the materials with 7.0 wt. % of Co and different grain growth inhibitor (L and M), it is clear that the addition of VC leads to a very good grain size refinement respect to the (W,Nb)C that acts only as a grain growth inhibitor.

Even if with the same composition and starting grain size, the D_{WC} of materials with 6.5 wt.% Co (D, E, F, G, H and I) and 12 wt.% Co (R and S) varies of about $0.15 \mu\text{m}$. In case of materials with 9.0 wt.% of Co, without any inhibitor and the same starting grain size (O and Q), the final D_{WC} differs of a value higher than $0.15 \mu\text{m}$. These differences are justified considering the inhomogeneity of the carbide grain size in the cemented carbides. Indeed, analyzing the linear intercept values obtained in material O, 4 grains with a dimension (l_i) higher than $1.5 \mu\text{m}$ were found. Differently, in material Q only a grain is higher than $1.5 \mu\text{m}$ and there are more length between 0.2 and $0.4 \mu\text{m}$ as shown in the Figure III – 3. For this reason, only a difference in the grain size higher than $0.20 \mu\text{m}$ is to be considered relevant in the comparison between two or more cemented carbides.

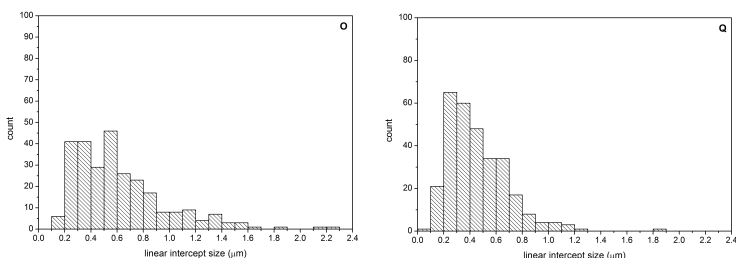


Figure III – 3. Grain size distributions of materials O and Q.

3.1.2 Carbide contiguity

The carbide contiguity is a measure of the contacts between carbide grains. In literature there are some contradictions in terms of the degree of carbide contiguity: some of them consider the existence of a continuous binder phase that embeds dispersed carbides, others assume the presence of a carbide skeleton into the material. For authors that consider the carbides dispersed and embedded in a continuous binder phase, only the binder phase has an important role in the plastic deformation of WC-Co. Differently, for the works that consider the WC-Co characterized by the presence of a carbide skeleton, the plastic deformation acts also on the carbides since the carbide skeleton has to deform compatibly with the binder [Upadhyaya, 1998]. A quantitative measurement of this skeleton is the contiguity that is defined as the surface area of

carbide-carbide contacts as a fraction of the total area [German, 1996; Jia, 1998, Upadhyaya, 1998]. It is measured on a two-dimensional cross-section using the number of intercepts per unit length of the test line. It is defined by the equation [3.3].

$$C = \frac{2 \cdot N_{L_{WC-WC}}}{2 \cdot N_{L_{WC-WC}} + N_{L_{WC-Co}}} \quad [3.3]$$

Where $N_{L_{WC-WC}}$ and $N_{L_{WC-Co}}$ are the number of intercepts per unit length of test line for the WC-WC grain boundary and WC-Co interface, respectively.

The contiguity is correlated with the cobalt content, the sintering time and, in a less effective way, with the sintering temperature. Increasing the binder content, the contiguity decreases since the probability to have WC-WC boundary decreases. The contiguity also decreases by increasing the sintering time and temperature.

3.1.2.1 Effect of the Co content and the D_{wc} on the contiguity

In order to understand the effect of the different composition and the grain size on the contiguity, different industrial cemented carbides were studied and the results are reported in Table III - 2.

Samples	WC (%)	Co (%)	Other carbide (%)	D_{wc} (μm)	C (-)	dev.st C (-)
A	93.7	6.0	0.3 Cr ₃ C ₂	0.95	0.56	0.08
B	93.8	6.0	0.2 Cr ₃ C ₂	0.74	0.56	0.04
C	93.5	6.0	0.5 Cr ₃ C ₂	0.69	0.53	0.05
D	93.2	6.5	0.3 Cr ₃ C ₂	0.82	0.62	0.12
E	93.2	6.5	0.3 Cr ₃ C ₂	0.85	0.61	0.09
F	93.2	6.5	0.3 Cr ₃ C ₂	0.83	0.53	0.09
G	93.2	6.5	0.3 Cr ₃ C ₂	0.77	0.56	0.06
H	93.2	6.5	0.3 Cr ₃ C ₂	0.70	0.52	0.06
I	93.3	6.5	0.3 Cr ₃ C ₂	0.71	0.55	0.09
L	92.7	7.0	0.3 (W,Nb)C	1.07	0.50	0.09
M	92.7	7.0	0.3 VC	0.71	0.56	0.05
N	90.7	9.0	0.3 Cr ₃ C ₂	0.83	0.54	0.13
O	91.0	9.0	-	1.27	0.51	0.11
P	90.7	9.0	0.3 Cr ₃ C ₂	0.86	0.55	0.05
Q	91.0	9.0	-	0.97	0.54	0.11
R	88.0	12.0	-	1.60	0.44	0.11
S	88.0	12.0	-	1.45	0.48	0.06

Table III – 2. Contiguity values for different industrial cemented carbides.

Analyzing the data reported in Table III – 2 it is evident the high standard deviations of the contiguity for all studied materials. This is attributed to the difficulty in

the measurement of the WC-WC grain boundaries and WC-Co interface in a SEM micrograph (Figure III – 4).

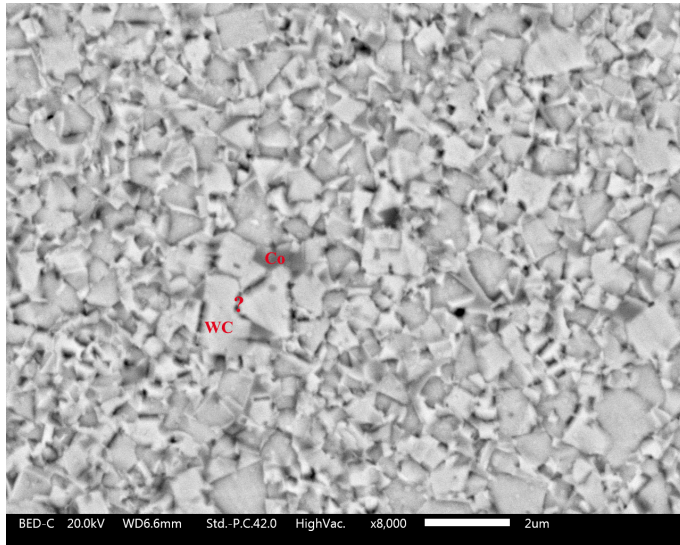


Figure III – 4. Example of the difficulties that occur in the measurement of the WC-WC grain boundaries and WC-Co interface.

It is complicated to understand if there is a very thin layer between two carbides or if the carbides are in contact from each other. This is due to the resolution limitation of the W filament SEM that leads to no precise information about the distribution of binder between the carbides [Upadhyaya, 1998]. Therefore, the contiguity values depend also on the operator that makes the measurement. So high standard deviations bring about to a difficult understanding of the possible correlation between the contiguity and the composition, grain size and mechanical properties as shown below.

The effect of Co amount on contiguity is reported in Figure III –5.

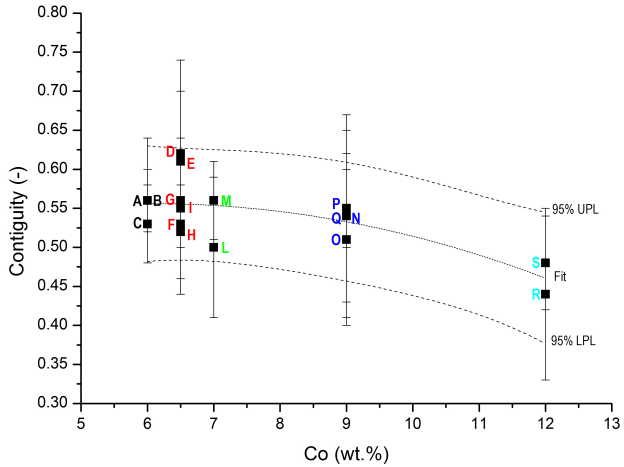


Figure III - 5. Contiguity vs Co content.

The effect of the Co amount on the contiguity is not so evident due to the high standard deviations since the microscope resolution limitation. Nevertheless, considering the prediction lines with a confidence of 95%, it is possible to conclude that higher cobalt amount tends to slightly decrease the contiguity.

The correlation between the contiguity and D_{wc} is reported in Figure III - 6.

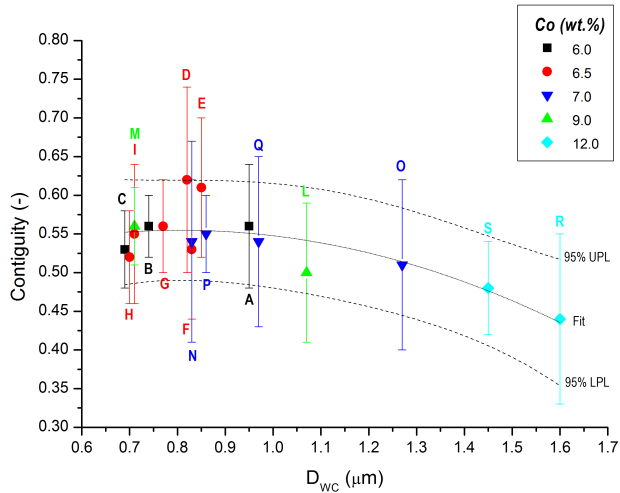


Figure III - 6. Contiguity vs D_{wc} .

As for the correlation between contiguity and binder content, considering the prediction lines, higher D_{WC} tends to slightly decrease the contiguity since, at equal volume, higher D_{WC} means less carbide – carbide contacts that decrease contiguity.

3.1.3 Mean binder free path

The mean binder free path is the thickness of the binder layer between the carbides and depends on both the binder amount and the carbide grain sizes [Jia, 1998, Upadhyaya, 1998]. It is defined by the equation [3.4].

$$\lambda_{Co} = \frac{1}{1-C} \cdot d_{WC} \cdot \frac{V_{Co}}{V_{WC}} \quad [3.4]$$

Where V_{Co} and V_{WC} are the volume fraction of Co and WC, respectively. The d_{WC} refers to the mean carbide grain size [Gurland, 1984] and is defined by the equation [3.5].

$$d_{WC} = \frac{2 \cdot V_{WC}}{2 \cdot N_{L_{WC-WC}} + N_{L_{WC-Co}}} \quad [3.5]$$

Inserting the equation [3.3] and [3.5] into the equation [3.4] it is possible to define the mean binder free path depending on the volume fraction of the binder content and the number of intercepts per unit length of the test mine for WC-Co interface, as shown in equation [3.6].

$$\lambda_{Co} = \frac{2 \cdot V_{Co}}{N_{L_{WC-Co}}} \quad [3.6]$$

Sometimes, an indirect way to evaluate the λ_{Co} is the coercive force measurement. Indeed, it exists a linear correlation between the reciprocal λ_{Co} and the coercive force [Exner, 1966].

As reported previously, due to microscope resolution limitation, precise information about the distribution of binder between the carbides is still inadequate. The mean binder free path results strongly related with the composition of WC-Co and the final WC grain size as shown below.

3.1.3.1 Effect of the Co content and the D_{WC} on the λ_{Co}

The values of the λ_{Co} for the differently industrial cemented carbides are shown in Table III - 3.

Samples	WC (%)	Co (%)	Other carbide (%)	D _{wc} (μm)	λ _{Co} (μm)	dev.st λ _{Co} (μm)
A	93.7	6.0	0.3 Cr ₃ C ₂	0.95	0.15	0.02
B	93.8	6.0	0.2 Cr ₃ C ₂	0.74	0.13	0.01
C	93.5	6.0	0.5 Cr ₃ C ₂	0.69	0.11	0.01
D	93.2	6.5	0.3 Cr ₃ C ₂	0.82	0.16	0.04
E	93.2	6.5	0.3 Cr ₃ C ₂	0.85	0.15	0.03
F	93.2	6.5	0.3 Cr ₃ C ₂	0.83	0.14	0.03
G	93.2	6.5	0.3 Cr ₃ C ₂	0.77	0.14	0.01
H	93.2	6.5	0.3 Cr ₃ C ₂	0.70	0.13	0.02
I	93.3	6.5	0.3 Cr ₃ C ₂	0.71	0.13	0.02
L	92.7	7.0	0.3 (W,Nb)C	1.07	0.16	0.03
M	92.7	7.0	0.3 VC	0.71	0.14	0.01
N	90.7	9.0	0.3 Cr ₃ C ₂	0.83	0.18	0.06
O	91.0	9.0	-	1.27	0.24	0.05
P	90.7	9.0	0.3 Cr ₃ C ₂	0.86	0.17	0.02
Q	91.0	9.0	-	0.97	0.21	0.05
R	88.0	12.0	-	1.60	0.26	0.06
S	88.0	12.0	-	1.45	0.29	0.04

Table III – 3. contiguity values for different industrial cemented carbides.

Plotting the λ_{Co} as a function of the Co amount it is possible to highlight that the mean binder free path is strongly related to the cobalt amount (Figure III – 7).

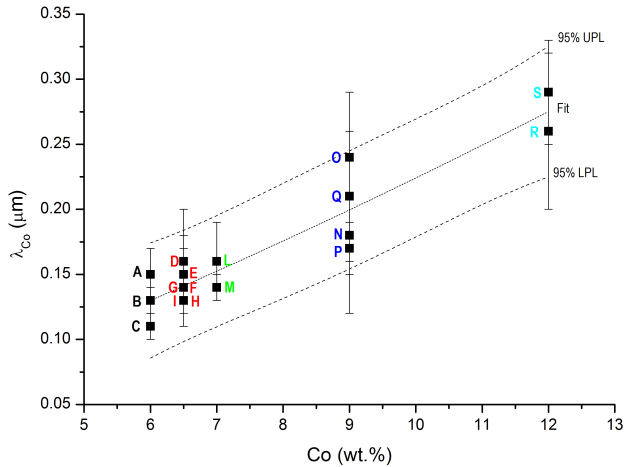


Figure III – 7. Mean binder free path vs Co content.

As previously reported, the mean binder free path is characterized by a quite high standard deviation since the microscope resolution limitation.

It is clear that, considering the prediction lines with a 95% confidence, higher cobalt amount means higher λ_{Co} . Because of different values of λ_{Co} for the same cobalt contents, it is possible to conclude that it depends also on other microstructural parameters as the D_{WC} as shown in Figure III – 8.

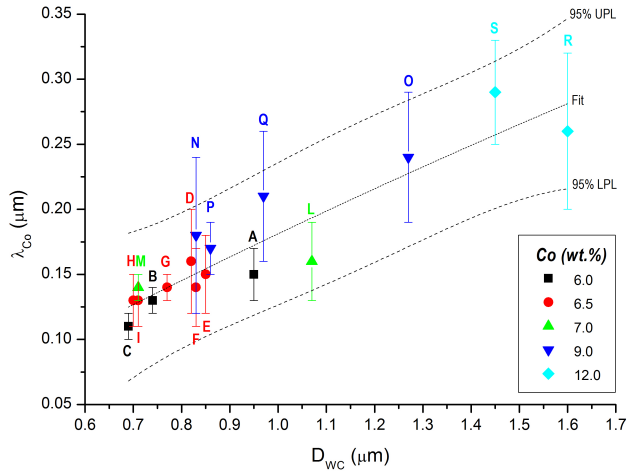


Figure III – 8. Mean binder free path vs D_{WC} .

Comparing the Figure III – 7 and III – 8, it is evident that the λ_{Co} is strongly related not only with the cobalt amount but also with the D_{WC} : higher cobalt amount and higher D_{WC} mean higher λ_{Co} .

In the following subchapter the mechanical properties of typical industrial cemented carbides and the correlation with the chemical composition and D_{WC} and, more precisely, with the contiguity and mean binder free path are reported.

3.2 Mechanical properties of WC-Co

The cemented carbides are used for their hardness and wear resistance with a certain amount of toughness. The methods used for the determination of WC-Co mechanical properties are defined by industry or national standards. The most important properties of WC-Co are the hardness and the fracture toughness and they are strongly related to the contiguity and the mean binder free path, which are affected by the chemical composition and the microstructure. In order to confirm what is reported in literature, these properties and the correlation with the Co content and D_{WC} and also, with the contiguity and mean binder free path are reported below.

3.2.1 Hardness

The hardness is one of the most important properties of WC-Co since it is used as a measure of the wear resistance of the material. Hardness is the resistance that the material opposes to the indentation of a penetrator with a higher hardness, such as diamond. The standards used for the WC-Co hardness are the ASTM B-294 and the ISO 3878, where Rockwell A and Vickers are defined as the most common tests for the WC-Co hardness [Brookes, 1992; Dobrzański, 2010; Jia, 1998; Schubert, 1998]. In this work, as recommended by ISO 3878, Vickers hardness with a load of 30Kg was used.

The HV was calculated from the indentation diagonals according to the equation [3.7].

$$HV = 1.854 \cdot \frac{F}{d^2} \quad [3.7]$$

Where d, in mm, is the mean diagonal of indentation defined by equation [3.8] and F is the load in Kg. The HV is defined as Kg/mm².

$$d = \frac{d_1 + d_2}{2} \quad [3.8]$$

Where d₁ and d₂, in mm, are the two indentation diagonals.

The hardness of the different industrial cemented carbides studied in this chapter is shown in Table III - 4.

Samples	WC (%)	Co (%)	Other carbide (%)	D _{wc} (μm)	HV30 (Kg/mm ²)	dev.st HV30 (Kg/mm ²)
A	93.7	6.0	0.3 Cr ₃ C ₂	0.95	1836	16
B	93.8	6.0	0.2 Cr ₃ C ₂	0.74	1887	23
C	93.5	6.0	0.5 Cr ₃ C ₂	0.69	1916	12
D	93.2	6.5	0.3 Cr ₃ C ₂	0.82	1912	5
E	93.2	6.5	0.3 Cr ₃ C ₂	0.85	1882	17
F	93.2	6.5	0.3 Cr ₃ C ₂	0.83	1844	12
G	93.2	6.5	0.3 Cr ₃ C ₂	0.77	1835	23
H	93.2	6.5	0.3 Cr ₃ C ₂	0.70	1864	15
I	93.3	6.5	0.3 Cr ₃ C ₂	0.71	1861	7
L	92.7	7.0	0.3 (W,Nb)C	1.07	1691	16
M	92.7	7.0	0.3 VC	0.71	1790	17
N	90.7	9.0	0.3 Cr ₃ C ₂	0.83	1653	35
O	91.0	9.0	-	1.27	1534	14
P	90.7	9.0	0.3 Cr ₃ C ₂	0.86	1686	11
Q	91.0	9.0	-	0.97	1607	10
R	88.0	12.0	-	1.60	1404	8
S	88.0	12.0	-	1.45	1404	13

Table III – 4. HV30 values for different industrial cemented carbides.

All the hardness values refer to the mean values of at least three individual indentations. The diagonals of the indentation were measured using the Zeiss Axiophot optical microscope at a magnification of 200X.

As reported in literature [Jia, 1998; Schubert, 1998; Upadhyaya, 1998] the hardness is related with the composition and microstructure parameters. The correlations between the hardness and the Co content, D_{WC} , contiguity and mean binder free are reported below.

3.2.1.1 Effect of the Co content, D_{WC} , C and λ_{Co} on the HV

Figure III – 9 shows the correlation between the hardness and the Co amount in different industrial WC-Co.

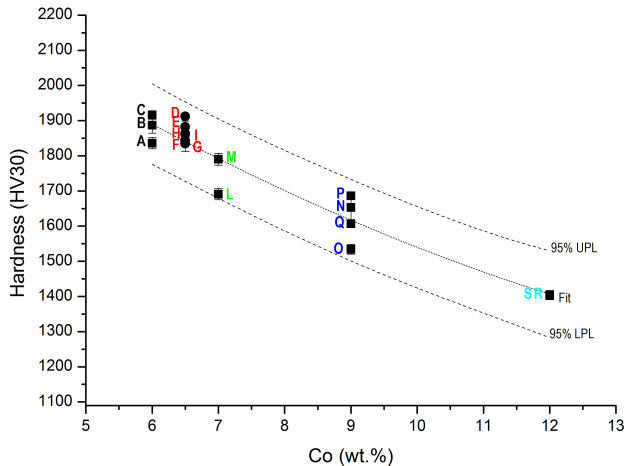


Figure III – 9. Hardness vs Co content.

From this graph it is clear that an increased Co amount leads to a decreased hardness. Nevertheless, the different values regarding the same amount of binder refer to other microstructural difference as the D_{WC} , as shown in Figure III – 10.

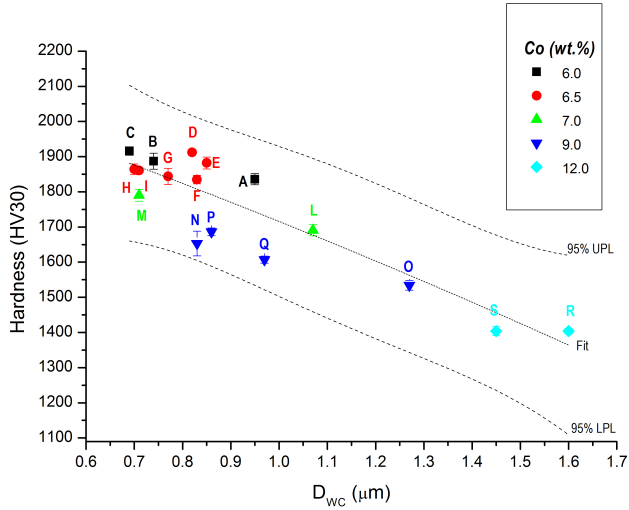


Figure III – 10. Hardness vs D_{WC} .

The figure displays a general trend whereby the increase in D_{WC} decreases hardness. Such a trend may be also recognized in specimens with 6.0, 7.0 and 9.0 wt.% Co, where the difference in D_{WC} is of the order of 0.4-0.5 μm . When the difference is smaller, as in specimens with 6.5 and 12.0 wt.% Co, the effect is not observed, as reported in paragraph 3.1.1, since the impossibility to define the D_{WC} standard deviation with the equation [3.2]. Indeed, information regarding the grain size distribution homogeneity is given by the mean linear intercept grain size (l_{av}) obtained with the 2D equation [3.1] that presents a high standard deviation, as shown in Table III - 1. For this reason it is better to consider the l_{av} with its standard deviation in order to highlight the real influence of the grain size on the hardness, as shown in Figure III - 11.

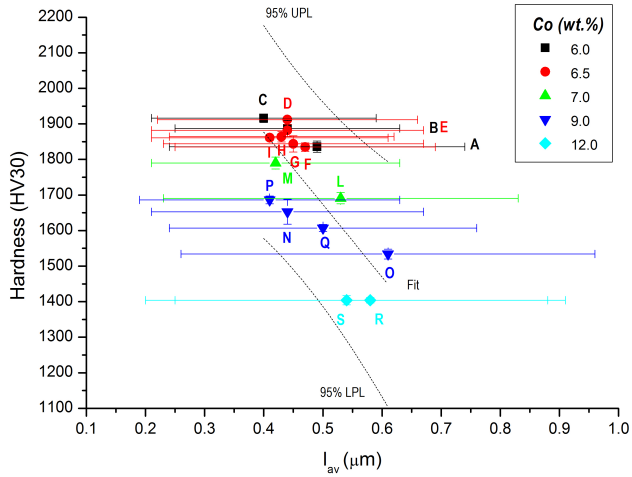


Figure III – 11. Hardness vs I_{av} .

It is evident that the high standard deviation of the I_{av} gives a difficult interpretation of the data. Considering grades with 6.5 and 12.0 wt.% of Co, the specimens present the same I_{av} leading to no differences in terms of hardness. Differently, considering the material A respect to material B and C in grade with 6 wt.%, it is clear that the lower hardness is due to a slightly higher I_{av} . Same consideration holds for grade with 9.0 wt.% of Co.

It is possible to conclude that the hardness depends on the Co content and the D_{wc} : increasing the Co amount and the D_{wc} , the hardness decreases. This dependency is justified considering that the Co content and the D_{wc} act on the contiguity and the mean binder free path, which affect the hardness of the material. Therefore, it is more accurate to correlate the hardness with the contiguity and the mean binder free path as shown below.

In Figure III – 12 is reported the correlation between hardness and contiguity.

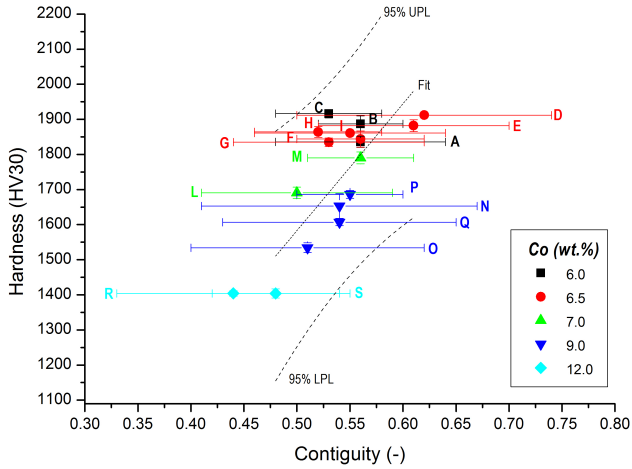


Figure III – 12. Hardness vs Contiguity.

The high standard deviations of the contiguity values in the analyzed materials make data interpretation difficult. As reported in paragraph 3.1.2.1, the difficulty in the measurement of contiguity leads to a high scatter. Considering the fit line it seems that increasing the contiguity, the hardness increases. However, the prediction lines with 95% of confidence underline that the hardness values that could be obtained for a constant contiguity are very different. For example, considering 0.5 of contiguity, it is possible to obtain hardness that varies from 1257 and 1917 HV. Therefore, it is not possible to define a particular trend comparing the hardness and the contiguity in case of typical commercial cemented carbides.

The influence of the mean binder free path on the hardness is visible in Figure III – 13.

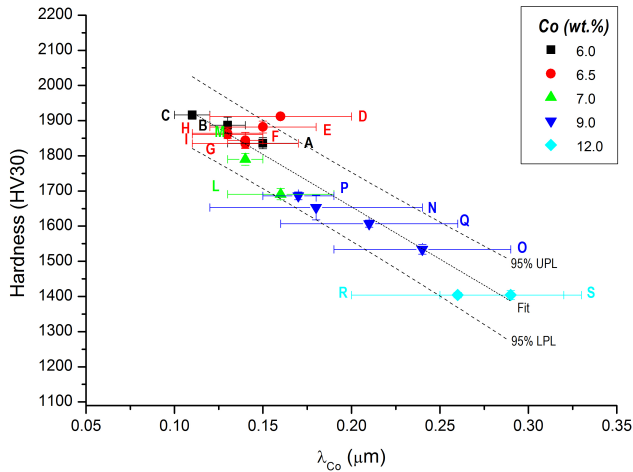


Figure III – 13. Hardness vs λ_{Co} .

As reported in paragraph 3.1.3.1, the mean binder free path increases by increasing both the Co amount and the D_{WC} . For this reason, it is evident that the mean binder free path, which depends on the Co content and D_{WC} , acts on the hardness of WC-Co. Considering the prediction line with a 95% of confidence, higher mean binder free path leads to a lower hardness. This is justified considering that higher mean binder free path means greater Co thickness between carbides that reduce the hardness of the material.

3.2.2 Fracture Toughness

The fracture toughness is the material resistance to crack propagation and is ideally independent of specimen dimension, geometry and finish. It is usually correlated with K_{IC} that refers only to plain strain fracture toughness. It is not possible to measure K_{IC} with the recommended standards, since the difficulty in precrack this hard material by fatigue due to the fact that the precrack stress is very similar to the critical stress intensity factor K_{IC} [Upadhyaya, 1998]. A lot of works tried to define a new method for the determination of fracture toughness without any attractive effect on the industry since the relative large and complex design of the test samples.

The most common method used for the measurement of the fracture toughness has become the Palmqvist method [Brookes, 1992; Dobrzański, 2010; Jia, 1998; Schubert, 1998; Shetty, 1985; Spiegler, 1990; Upadhyaya, 1998]. This method is used for the brittle material and consists on the measurement of the crack lengths that are formed at the four corners of a Vickers hardness indentation (Figure III – 14).

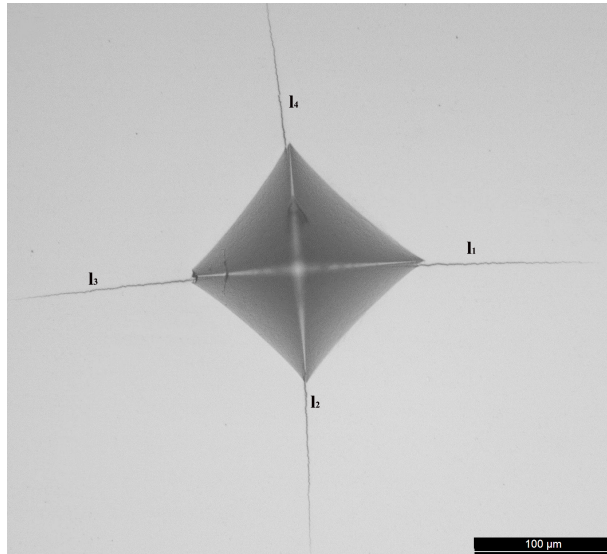


Figure III – 14. Micrograph of the Vickers hardness indentation in WC-Co.

Therefore, the fracture toughness is defined by the equation [3.9] [Schubert, 1998].

$$K_{IC} = A \cdot \sqrt{H} \cdot \sqrt{\frac{P}{\sum l_i}} \quad [3.9]$$

Where A is equal to $0.0028 \text{ m}^{1/2} / \text{mm}^{1/2}$, H is the Vickers hardness in N/mm^2 , P is the load in N, and l_i are the crack lengths in mm. The K_{IC} is defined as $\text{MPa} \cdot \text{m}^{1/2}$. As for the hardness, the fracture toughness values refer to the mean values of at least three individual indentations. The crack lengths were measured using the Zeiss Axiophot optical microscope at a magnification of 500X. From this equation it is evident that the fracture toughness is strongly related with the hardness. The resulted fracture toughness and hardness values for the differently industrial cemented carbides studied in this work are shown in Table III - 5.

Samples	WC (%)	Co (%)	Other carbide (%)	D _{WC} (μm)	HV30 (Kg/mm ²)	dev.st HV30 (Kg/mm ²)	K _{IC} (MPa m ^{1/2})	dev.st K _{IC} (MPa m ^{1/2})
A	93.7	6.0	0.3 Cr ₃ C ₂	0.95	1836	16	9.95	0.10
B	93.8	6.0	0.2 Cr ₃ C ₂	0.74	1887	23	9.60	0.12
C	93.5	6.0	0.5 Cr ₃ C ₂	0.69	1916	12	9.70	0.12
D	93.2	6.5	0.3 Cr ₃ C ₂	0.82	1912	5	9.85	0.03
E	93.2	6.5	0.3 Cr ₃ C ₂	0.85	1882	17	9.73	0.12
F	93.2	6.5	0.3 Cr ₃ C ₂	0.83	1844	12	9.69	0.12
G	93.2	6.5	0.3 Cr ₃ C ₂	0.77	1835	23	9.82	0.14
H	93.2	6.5	0.3 Cr ₃ C ₂	0.70	1864	15	10.08	0.08
I	93.3	6.5	0.3 Cr ₃ C ₂	0.71	1861	7	9.77	0.14
L	92.7	7.0	0.3 (W,Nb)C	1.07	1691	16	10.31	0.08
M	92.7	7.0	0.3 VC	0.71	1790	17	9.95	0.11
N	90.7	9.0	0.3 Cr ₃ C ₂	0.83	1653	35	11.38	0.55
O	91.0	9.0	-	1.27	1534	14	13.21	0.39
P	90.7	9.0	0.3 Cr ₃ C ₂	0.86	1686	11	11.23	0.14
Q	91.0	9.0	-	0.97	1607	10	11.27	0.26
R	88.0	12.0	-	1.60	1404	8	15.16	1.55
S	88.0	12.0	-	1.45	1404	13	13.41	0.70

Table III – 5. K_{IC} values for different industrial cemented carbides.

In Figure III-15 is reported the fracture toughness respect to the hardness in order to highlight their correlation.

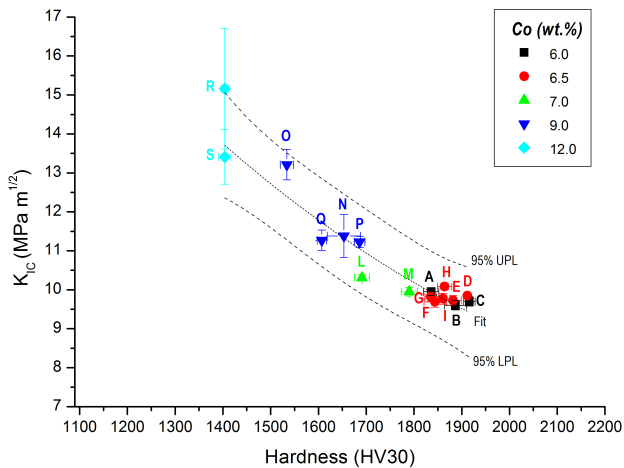


Figure III – 15. Fracture toughness vs hardness.

As reported in literature [Brookes, 1992; Dobrzański, 2010; Jia, 1998; Schubert, 1998; Shetty, 1985; Spiegler, 1990; Upadhyaya, 1998], the hardness and the fracture toughness of WC-Co are inversely proportional: higher hardness means lower fracture toughness.

As for the hardness, the fracture toughness is strongly related with the composition and the microstructure parameters [Brookes, 1992; Jia, 1998; Schubert, 1998; Upadhyaya, 1998] as shown below.

3.2.2.1 Effect of the Co content, D_{WC} , C and λ_{Co} on the K_{IC}

In Figure III – 16 is reported the correlation between the fracture toughness and the Co amount in the different industrial WC-Co.

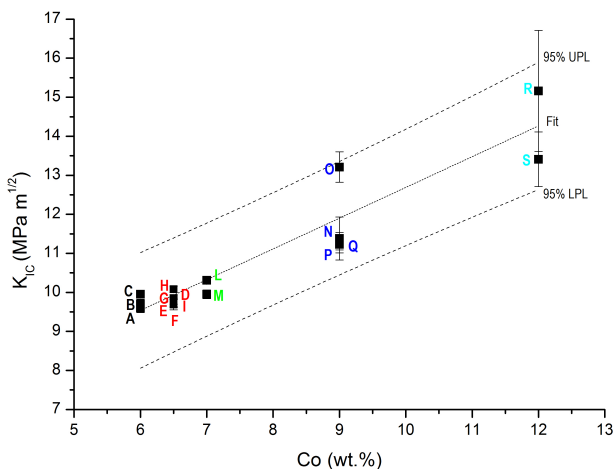


Figure III – 16. Fracture toughness vs Co content.

This graph highlights the correlation between the fracture toughness and the binder amount: an increased Co amount leads to a decreased hardness. The different values regarding the same amount of binder refer to other microstructural difference as the D_{WC} . For this reason, the correlation between fracture toughness and D_{WC} is shown in Figure III - 17.

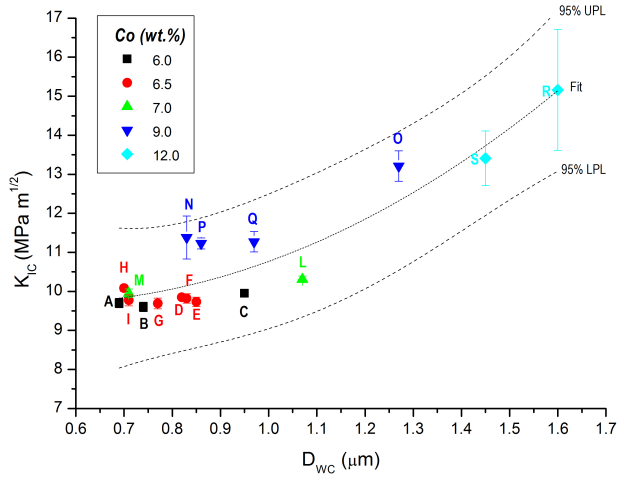


Figure III – 17. Fracture toughness vs D_{WC} .

The fracture toughness depends not only on the binder amount but also on the D_{WC} . This correlation is not evident considering D_{WC} in the interval between 0.7 and 1.1 mm but becomes clear considering higher D_{WC} . Indeed, the figure displays a general trend whereby the increase in D_{WC} increases fracture toughness. As for the hardness, such a trend may be also recognized in specimens with 6.0, 7.0 and 9.0 wt.% Co, where the difference in D_{WC} is of the order of 0.4-0.5 μm . When the difference is smaller, as in specimens with 6.5 and 12.0 wt.% Co, the effect is not observed, since the impossibility to define the D_{WC} standard deviation. For this reason it is better to consider the l_{av} with its standard deviation in order to highlight the real influence of the grain size on the fracture toughness, as shown in Figure III - 18.

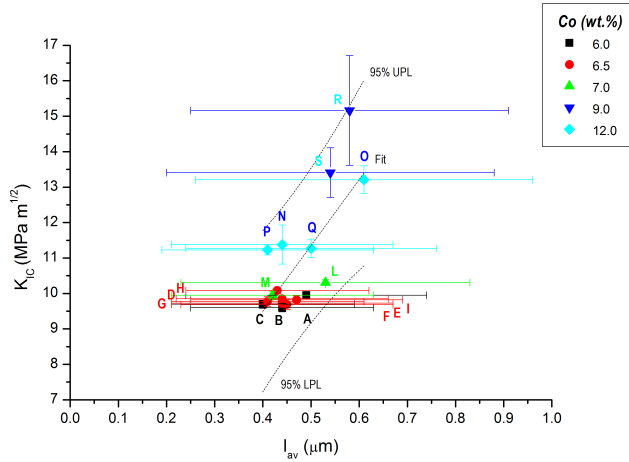


Figure III – 18. Fracture toughness vs l_{av} .

As already reported for the hardness, it is evident that the high standard deviation of the l_{av} gives a difficult interpretation of the data. Considering grades with 6.5 and 12.0 wt.% of Co, the specimens present the same l_{av} leading to no differences in terms of mechanical properties. Differently, considering the material A respect to material B and C in grade with 6 wt.%, it is clear that the higher fracture toughness is due to a slightly higher l_{av} . Same consideration holds for grade with 9.0 wt.% of Co.

In conclusion, the fracture toughness increases by increasing the Co content and the D_{WC} . A just mention before, this dependency is justified considering that the Co content and the D_{WC} act on the contiguity and the mean binder free path, which affect the fracture toughness of the material. Therefore, it is more accurate correlate the fracture toughness with the contiguity and the mean binder free path as shown below.

In Figure III – 19 the correlation between fracture toughness and contiguity is reported.

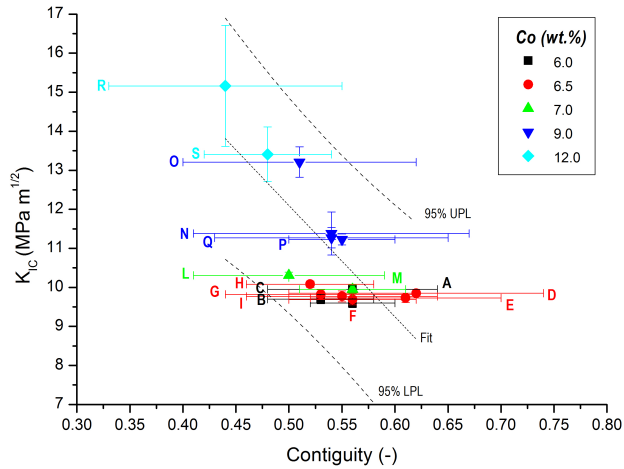


Figure III – 19. Fracture toughness vs contiguity.

As for the hardness, the high standard deviations of the contiguity values in the analyzed materials make data interpretation difficult. Considering the fit line seems that increasing the contiguity, the fracture toughness decreases. However, the prediction lines with 95% of confidence underline that the fracture toughness values that could be obtained for a constant contiguity are very different. For example, considering 0.5 of contiguity, it is possible to obtain fracture toughness that varies from 9.33 and 14.86 $\text{MPa m}^{1/2}$. Therefore, it is not possible to define a particular trend comparing the K_{Ic} and the contiguity in case of industrial cemented carbides.

The influence of the mean binder free path on the fracture toughness is visible in Figure III – 20.

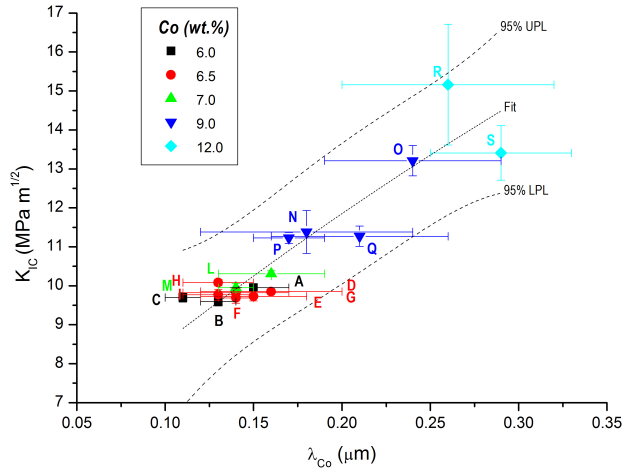


Figure III – 20. Fracture toughness vs mean binder free path.

Considering the prediction lines with a 95% of confidence, the fracture toughness increases by increasing the mean binder free path. Indeed, higher mean binder free path means a great amount of Co between carbides that is detrimental in terms of hardness but increases the fracture toughness since Co offers higher resistance to the possible crack propagation.

3.3 Conclusion

The production of WC-Co starts with a certain composition and WC grain size. The sintering process is defined in order to obtain a defined composition of the bulk after the process. It is well known that, due to the dissolution and reprecipitation phenomenon and the high sintering temperature, the WC grain size can increase leading to grain coarsening and this has an important effect on the mechanical properties of the final material. For this reason, the microstructure characterization of WC-Co consists not only on the measurement of the microstructural parameters such as the contiguity and the mean binder free path, but also on the measurement of the D_{WC} after the sintering process.

The contiguity and the mean binder free path are parameters that depend on the Co content and the final D_{WC} of the investigated industrial WC-Co. These correlations are summarized as follow.

- Due to the high standard deviations of contiguity values since the microscope resolution limitation, no clear correlations with Co content and D_{WC} were defined. Nevertheless, considering the prediction lines with a confidence of 95%, it is possible to conclude that higher cobalt amount and D_{WC} tend to slightly decrease the contiguity;
- Even if with quite a high standard deviation due to the microscope resolution limitation, the analyses highlight that an increased Co content and D_{WC} leads to an increased mean binder free path.

The mechanical properties of commercial cemented carbides are strongly related to the Co content, D_{WC} and, more precisely, to the contiguity and the mean binder free path, as reported in literature. These correlations are summarized as follow.

- An increase in Co content and D_{WC} leads to a higher mean binder free path, which affects the mechanical properties by decreasing the hardness and increasing the fracture toughness;
- No correlation is visible between the mechanical properties and the contiguity since the resolution limitation of the W filament SEM.

Chapter IV

Mechanical strength of cemented carbide

Part of this chapter has been presented and published in:

L. Emanuelli, A. Molinari, G. Arrighetti, G. Garoli

“Analysis of transversal rupture strength of different WC-Co Cemented carbides”,

Accepted in Proceedings EuroPM2018, Bilbao, Spain, 14 - 18 October 2018.

Even if cemented carbide results very strong due to its composition, its real strength is not reached in practice since the presence of defects in the structure or at the surface that increase the local stress concentration during the application of a stress. Indeed, the fracture load is not only a function of the intrinsic strength of the WC-Co, which depends on the chemical composition and microstructural properties of the material, but is especially a function of the nature and distribution of the defects within the structure leading to consider the cemented carbides as a high strength brittle materials. Due to the large scatter of the experimental results, the WC-Co strength is usually analyzed by means of Weibull theory.

In this Chapter, mechanical strength of different WC-Co grades that is usually defined by the transversal rupture strength (TRS) was measured by means of the three-point bend test defined by ISO 3327 and ASTM B406-96. Weibull theory was used in order to investigate the TRS values since the large scatter. Grade with the intermediate Co concentration presents a bi-modal Weibull distribution with lower or equal characteristic strengths (σ_0) compared to grade with the lower Co amount. This different behaviour could be justified analyzing the residual microporosity and the fracture surfaces of the different grades. In order to compare TRS with mechanical properties, namely hardness and fracture toughness, microstructure and composition, mean TRS values with standard deviations were evaluated. After that, the influence of chemical composition and microstructural parameters on mechanical properties was evaluated.

4.1 Introduction

The mechanical strength of WC-Co, usually TRS, is the maximum stress reached before failure during a bending test [Brookes, 1992; Santhanam, 1990; Sarin, 2014; Upadhyaya, 1998]. It is a combination of shear strength, compressive strength and tensile strength and it is usually used as a measure of toughness of the sintered WC-Co. Even if cemented carbide results very strong due to its composition, its real strength is

not reached in practice since the presence of defects in the bulk or at the surface, namely porosities or voids, microporosity, inclusions, free carbon, μ phase, abnormally large WC grains, segregation areas and binder lakes, which increase the local stress concentration during the application of a stress [Li, 2013; Morrell, 1999; Prokopiv, 2008]. With the fractographic analysis it is possible to highlight that almost all the fractures in WC-Co start from internal defects in the material and not at the tensile surface of the test specimen [Morrell, 1999; Sarin, 2014]. For this reason, the fracture load is not only a function of the intrinsic strength of the WC-Co that depends on chemical composition and microstructural properties of the material, but is especially a function of the nature and distribution of the defects within the specimen. It is clear that it is not possible to confuse this mechanical strength with the fracture toughness measured by the Palmqvist method shown in Chapter III, which investigate a very small volume of the material and therefore is not subjected to the defects present into it.

Considering the fracture mechanism in a material, in general there are three stages of fracture: crack initiation on defects, subcritical crack growth since the increase of the load and final the catastrophic crack propagation or, in other words, crack propagation [Chermant, 1976; Exner, 2001; Hong, 1983; Johannesson, 1988; Osterstock, 1983; Sigl, 1987]. The subcritical crack growth in WC-Co occurs only at high temperature under fatigue or creep tests [Johannesson, 1988]. Differently, considering the fracture of a typical WC-Co at room temperature, it is characterized by brittle fracture behaviour with only two fracture stages: the crack initiation on a defect and the subsequently catastrophic crack propagation without any subcritical crack growth [Exner, 2001; Johannesson, 1988; Osterstock, 1983; Sigl, 1987].

The possible fracture origin types in case of brittle materials are summarized in Figure IV – 1 and IV - 2.

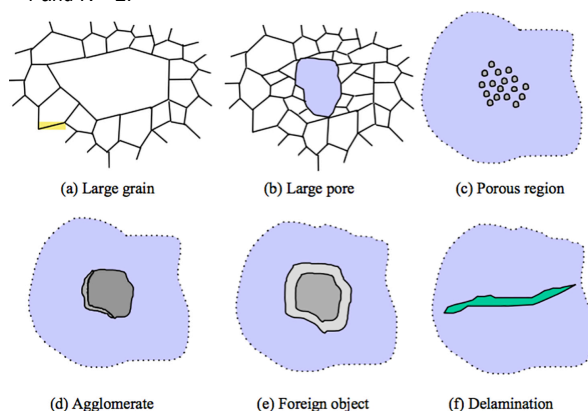


Figure IV – 1. Schematic representation of different fracture origin types _1 [adapted from Morrell, 1999].

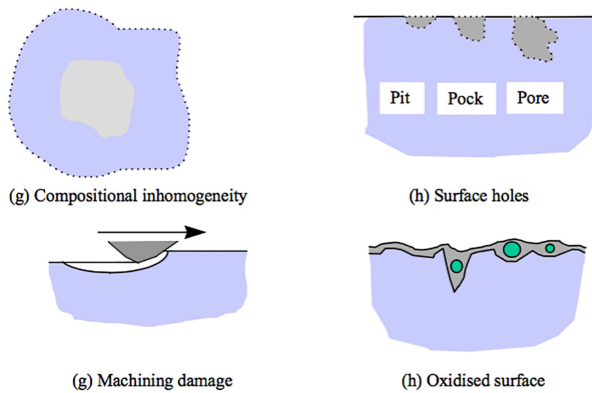


Figure IV – 2. Schematic representation of different fracture origin types _2 [adapted from Morrell, 1999].

Considering the WC-Co, agglomerates refer to particles that during sintering densify differently respect to the surrounded material and tend to shrink away from the normal matrix. Differently, compositional inhomogeneities are regions rich in metallic binder or carbon. The overall appearance of fracture origins in a flexural strength test for WC-Co samples are similar to those found in high strength ceramics and could be schematized as in Figure IV – 3.

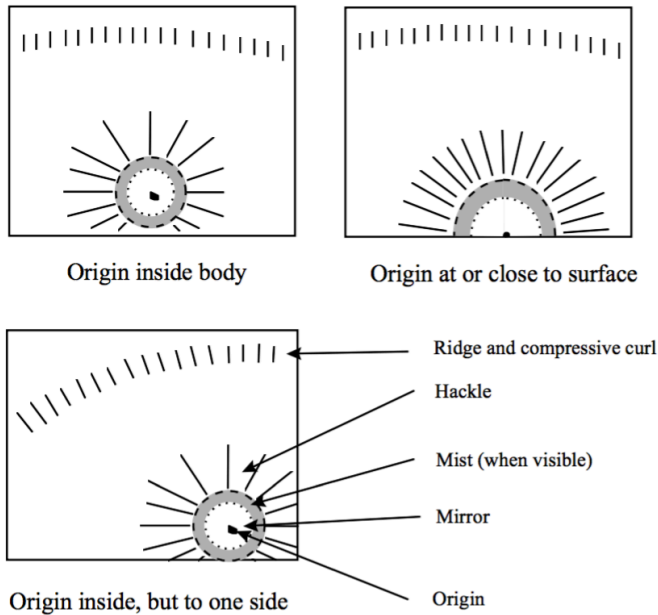


Figure IV – 3. Schematic of the macro appearance of the fracture origins in flexural test bars for brittle materials [adapted from Morrell, 1999].

As shown in Figure IV – 3 on a fracture surface of a brittle material after a flexure test it is possible to observe:

- the fracture origin;
- around it the mirror region that is smooth and refers to the initial part of the fracture surface;
- the mist region that is rougher due to a critical speed of the crack and surrounding these regions, the hackle region where cracks propagate in different directions.

Obviously, this appearance is affected by the defect position that could be inside the specimen, close to the surface or inside the specimen but to one side.

The behaviour of TRS with the chemical composition was widely investigated in literature. First investigations underline that the TRS reaches a maximum between 15 – 20 wt.% Co, and with further additions of binder, decreases [Engle, 1942; Sandford, 1947].

Differently, Gurland et al. [Gurland, 1955] consider the influence of the mean binder free path on the TRS at a constant Co content. They found that the TRS initially increases, reaches a maximum and subsequently decreases with further increase of the mean binder free path. The maximum is observed for materials with Co content between 12 and 25 wt.%. The authors justified this behaviour considering that TRS increases as the film of binder metal becomes thinner but subsequently the strength is reduced by the increased amount of the brittle phase and incomplete dispersion of the WC grains. In other words, for small mean binder free path, fracture mechanisms are governed by the brittle fracture of WC; differently, the mechanical strength was determined by the plastic deformation of binder in case of high mean binder free path. Both the maximum value of TRS and the corresponding mean binder free path increase by increasing the Co content. Differently, materials with Co amount lower than 12 wt.%, present an increase in TRS with mean binder free path without reaching any maximum value.

Considering the influence of WC grain size on TRS at a certain Co content, the general trend presents first an increase of TRS up to a maximum value and a decrease with further increase of the grain size [Exner, 1970].

A more recent work found that the rupture force in a three-point bend test remains quite constant between 5 to 10 wt.% of Co and increases reaching a maximum at 15 wt.% of Co. Differently, the rupture force decreases by increasing grain size up to 20 μm and, furthermore, remains constant [Okamoto, 2005].

Nevertheless, in all these works it was not considered the effect of process parameters on the TRS evolution with chemical composition and microstructure. Indeed, the presence of a TRS maximum by increasing Co content, mean binder free path and WC grain size was not always observed considering different production processes [Ivnsen, 1963]. Indeed, the production processes such as milling of the powder and sintering stage act on the final microstructure of WC-Co part and on its defectiveness.

As reported previously, the presence of defect, such as porosity, and in details its size and location in the structure, affects drastically the strength of WC-Co [Cha, 2008]. Therefore, a direct relation between TRS and intrinsic mechanical properties, namely the hardness and fracture toughness, is visible only when the microporosity is negligible [Fang, 2005]. A typical correlation between TRS and hardness in case of hardmetals with different composition is reported in Figure IV – 4 [Almond, 1983].

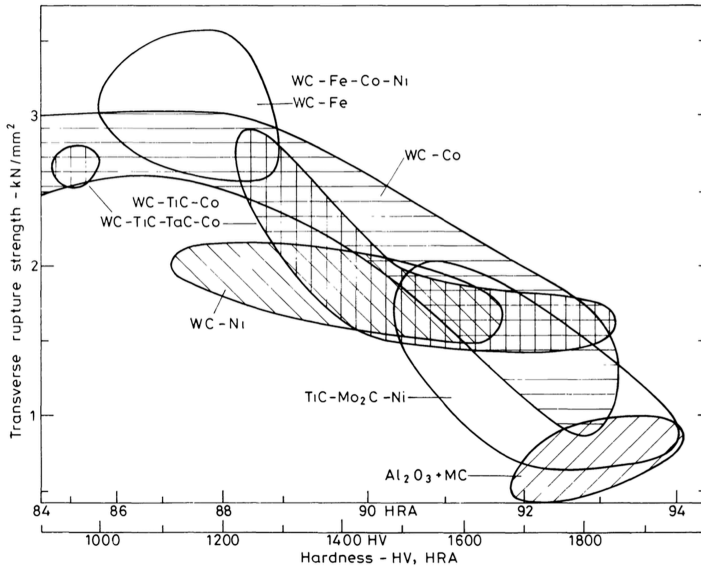


Figure IV – 4. Typical TRS and hardness range for WC-Co with different compositions [adapted from Almond, 1983].

As it has just been mentioned, the porosity is a defect that acts drastically on the mechanical strength of a brittle material. Nevertheless, today, due to the advance in the production of WC-Co, most of the commercial WC-Co grades present an almost pore-free structure (densification higher than 99%). It means that these materials present a negligible amount of residual porosity that it is usually defined with three different scales (A, B and C) depending on the pore size and distribution according to ASTM B276-05. Despite this, with these standards, it is possible to evaluate only porosity bigger than the WC grain size but not the possible residual microporosity that it is also a critical aspect of the mechanical strength of WC-Co grades. Indeed, it was observed that samples from the same lot, with the same structural parameters, residual porosity, coercive force, hardness and density are often different in strength and plasticity [Li, 2013; Prokopiv, 2008]. These differences in terms of strength and plasticity could be justified considering the residual microporosity. The evaluation of the microporosity consists on SEM analysis with the opportune correction of brightness and contrast in order to distinguish the binder phase (grey) from the microporosity (black) at high magnification depending on the material composition and microstructure [Prokopiv, 2008].

All the defects present in the microstructure of WC-Co, which lead to the catastrophic failure, are the cause for the wide scatter of the measured TRS. The width

of the TRS scatter is measured by Weibull distribution and modulus [Weibull, 1951]. In some case, due to the various types and sizes of the defect, it possible to observe a multi-modal Weibull distribution [Weibull, 1951; Tarragó, 2017]. From Weibull theory in case of brittle material, the probability of failure is defined as the probability that fracture takes place at a stress equal to or lower than a given value and is defined by the equation [4.1] [Danzer, 1992; Jayatilaka, 1977; Torres, 2014; Weibull, 1951].

$$P_f(\sigma, V) = 1 - e^{-\frac{V}{V_0} \left(\frac{\sigma}{\sigma_0}\right)^m} \quad [4.1]$$

where m is the Weibull modulus that describes the scatter of the strength, σ_0 is the characteristic strength that is the stress at which, for a specimen with $V=V_0$, the failure probability is equal to 63.21% (equation [4.2]).

$$P_f(\sigma, V) = 1 - e^{-(1)^m} = 63.21\% \quad [4.2]$$

From this equation it is clear that the failure probability increases by increasing the stress (σ) and the size of the sample (V). Considering the size effect, higher dimension of samples means higher probability to have a lot of flaws and also with a big size. Indeed, smaller part has a lower probability of failure than a large one, under the same stress condition. In order to scale brittle material strength from one component size to another, the so-called effective volumes and surfaces were defined and were given by equations [4.3] and [4.4], respectively [Bhushan, 2016; Klünsner, 2011; Torres, 2014].

$$S_{eff} = \int_{\sigma>0} \left(\frac{\sigma(\vec{r})}{\sigma_r}\right)^m dS \quad [4.3]$$

$$V_{eff} = \int_{\sigma>0} \left(\frac{\sigma(\vec{r})}{\sigma_r}\right)^m dV \quad [4.4]$$

where σ_r is the arbitrary reference stress (usually the maximum in the stress field). The integration is done only in the surface or volume where there is a tensile stress field ($\sigma > 0$). Considering the simple case of a three-point bend test and the specimen geometry, the calculation of the two integral can be made analytically [Quinn, 2003]. These parameters become important in order to compare correctly the TRS values obtained with different method and sample geometry and dimension as shown in equations [4.5] and [4.6] [Bhushan, 2016; Quinn, 2003; Sōmiya, 1984].

$$\frac{\sigma_1}{\sigma_2} = \left(\frac{V_{eff2}}{V_{eff1}}\right)^{1/m} \quad [4.5]$$

$$\frac{\sigma_1}{\sigma_2} = \left(\frac{S_{eff2}}{S_{eff1}} \right)^{1/m} \quad [4.6]$$

where σ_1 and σ_2 are the mean strength of specimens type 1 and 2, V_{eff1} and V_{eff2} are the effective volumes of specimens type 1 and 2 and S_{eff1} and S_{eff2} are the effective surfaces of specimens type 1 and 2.

The volume-based Weibull analysis, equation [4.5], is used when the failure initiating defect exist within material. Differently, the equation [4.6] is used when failure mainly occurs due to surface flaws [Bhushan, 2016]. When the surface defects become the main failure reason, it is clear that also the surface preparation must be taken into account.

The experimental investigation of the WC-Co mechanical strength requires a large number of samples and a specific sample preparation in order to define a correct failure probability.

Furthermore, measurement uncertainty (MU) exists. Indeed, Bermejo et al. [Bermejo, 2012] demonstrate that for strength testing of brittle materials a high precision (MU < 5%) is necessary in case of high Weibull modulus ($m \geq 20$). In this condition, considering bend testing, samples longer than 30 mm are necessary. Differently, in case of low Weibull modulus ($m \leq 10$) even no precise measurement system, which leads to a MU around 10%, can be accepted for the correct determination of the strength distribution.

In this Chapter, the TRS of different WC-Co grades was measured by means of three-point bend test defined by ISO 3327 and ASTM B406-96. Due to the large scatter, the obtained results were analyzed within the Weibull theory. In order to justify the calculated Weibull distributions and to define the possible fracture origin types, the fracture surfaces of the different grades were analyzed. To compare the TRS with the well-defined mechanical properties, namely the hardness and fracture toughness the mean value and the standard deviation of TRS for all grades were calculated. At the end, mechanical properties were correlated with chemical composition and microstructure parameters.

4.2 Materials and experimental procedure

Three different commercial cemented carbides with 6.5, 9.0 and 12.0 wt.% of Co were selected (Table IV - 1).

Grade	WC (wt.%)	WC powder size (μm)	Co (wt.%)	D_{Co} (μm)	Cr_3C_2 (wt.%)
A	93.2	0.8	6.5	1.0	0.3
B	90.7	0.8	9.0	1.0	0.3
C	88.0	1.1	12.0	1.0	0.0

Table IV – 1. Composition details of the two studied commercial WC-Co.

Using the method explained in Chapter III, a complete microstructural characterization with the determination of D_{WC} , λ and C was carried out. Murakami's reagent (100 ml distilled water, 7g KOH, 7g $\text{K}_3[\text{Fe}(\text{CN})_6]$) [Petzow, 1999], was used for selective etching of WC particles.

Three-point bend tests defined by ISO 3327 and ASTM B406-96, were carried out on twenty-five samples for each WC-Co grades and the experimental configuration is summarized in Figure IV – 5.

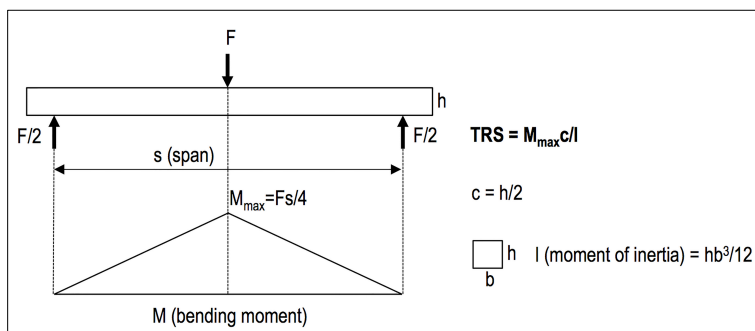


Figure IV – 5. Three-point bend test configuration and the bending moment distribution.

For TRS measurement of WC-Co, sample geometry of a prismatic (Type B) with ground dimensions reported in Table VI – 2 was selected.

Type	L (mm)	b (mm)	h (mm)	s (mm)
B	20 ± 1	6.50 ± 0.25	5.25 ± 0.25	14.5 ± 0.5

Table VI – 2. Test piece dimensions.

In case of Type B configuration, test piece must be placed on two cylindrical supports and the force is applied using a ball. In this condition, TRS was evaluated by the equation [4.7].

$$TRS = \frac{3 \cdot k \cdot F \cdot s}{2 \cdot b \cdot h^2} \quad [4.7]$$

where k is the chamfer correction factor, F the rupture force, s the span between supports, b the width and h the high of sample.

Both supports and ball must be in WC-Co in order to reduce the possible deformation obtained by applied force. In this work, support cylinders of a 6 mm diameter and a composition of grade K5UF and a force ball of 12 mm diameter and a composition of grade TCK20 were selected. The test pieces shall be grounded on the four faces which are parallel to the length and the four long edge shall be chamfered to around 0.15 mm at an angle of 45°. In these conditions, the chamfer correction factor k, used for the evaluation of TRS is equal to 1.00. For this reason, the equation [6.8] becomes equal to equation [4.7].

$$TRS = \frac{3 \cdot F \cdot s}{2 \cdot b \cdot h^2} \quad [4.8]$$

Ten SEM images at 5000X of the microstructure, with oportune correction of brightness and contrast, were used in order to investigate the residual microporosity by means of ImageJ software. This software is able to select and quantify the residual microporosity working on grey scale. In this condition the resulting percentage refers to an investigated area equals to 4.75 mm².

The fracture surfaces of the different grades were investigated by SEM analysis.

4.3 Results and discussion

4.3.1 Microstructure and residual microporosity analyses

The microstructural characterization of the three different WC-Co grades was summarized in Table IV – 3.

Grade	WC (wt.%)	Co (wt.%)	Cr ₃ C ₂ (wt.%)	D _{wc} (μm)	I _{av} (μm)	C (-)	λ (μm)
A	93.2	6.5	0.3	1.0	0.42 ± 0.25	0.58 ± 0.10	0.14 ± 0.03
B	90.7	9.0	0.3	1.0	0.40 ± 0.22	0.55 ± 0.10	0.18 ± 0.04
C	88.0	12.0	0.0	1.4	0.68 ± 0.39	0.54 ± 0.13	0.44 ± 0.12

Table IV – 3. Microstructural characterization of the studied WC-Co grades.

As shown in Chapter III, the carbide contiguity slightly decreases and the mean binder free path increases by increasing Co content and D_{wc}. The dependence of carbide contiguity on Co content and D_{wc} results weak because of the too large standard deviation of the contiguity values. Differently, the dependence of mean binder free path on Co content and D_{wc} is evident.

The image analysis of the residual microporosity of the studied WC-Co grades is shown in Figure IV – 6.

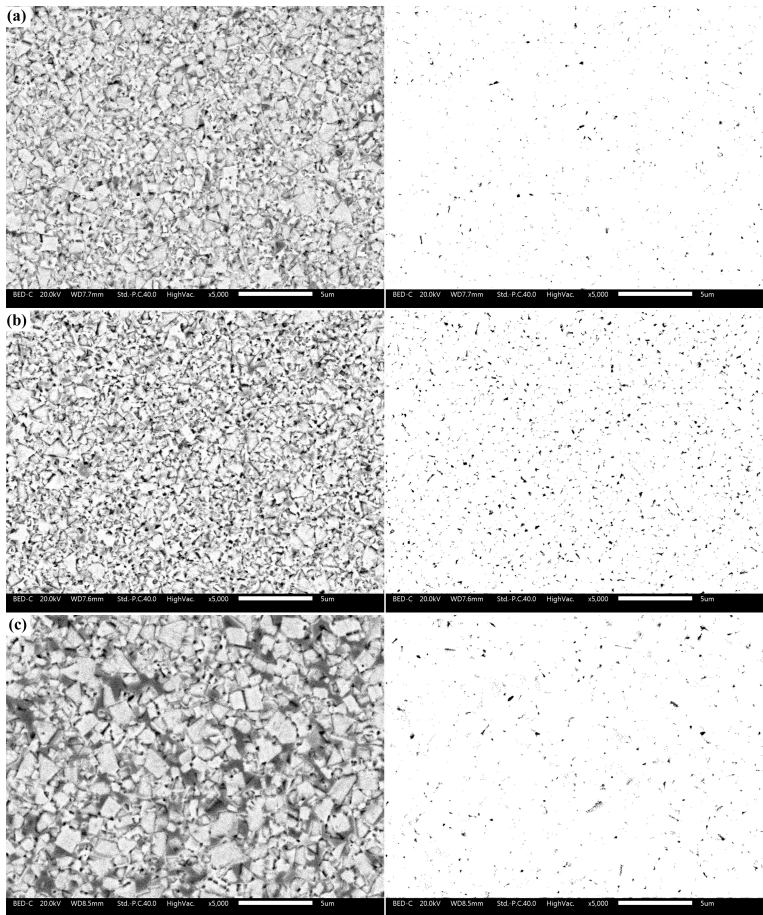


Figure IV – 6. Residual microporosity evaluation by image analysis of grade A (a), B (b) and C (c).

From Figure IV – 6 it is evident that grade B is characterized by a higher residual microporosity respect to grades A and C, as highlighted by the percentage values reported in Table IV – 4.

Grade	WC (wt.%)	Co (wt.%)	Cr ₃ C ₂ (wt.%)	D _{wc} (μm)	Microporosity (%)
A	93.2	6.5	0.3	1.0	0.5 ± 0.2
B	90.7	9.0	0.3	1.0	1.6 ± 0.6
C	88.0	12.0	0.0	1.4	0.8 ± 0.4

Table IV– 4. Microporosity of the studied WC-Co grades.

4.3.2 Mechanical strength distribution: Weibull theory

The rupture force in the three-point bend test of twenty-five samples for each grades were measured and the TRS values were determined by equation [4.8]. The Weibull parameters for the mechanical strength distributions were calculated according to standard EN 843-5 by equation [4.9].

$$\ln[-\ln(1 - P_f)] = m \cdot \ln \sigma_f - m \cdot \ln \sigma_0 \quad [4.9]$$

where P_f is the failure probability, σ_f refers to TRS, and the Weibull parameters σ_0 and m are the characteristic strength and the Weibull modulus, respectively.

Using equation [4.8], the mechanical strength distribution of the three investigated WC-Co grades is plotted in a Weibull diagram defined by the logarithmic of the TRS versus the double logarithmic reciprocal of the probability of failure (P_f), as shown in Figures IV – 7, VI – 8 and IV – 9. The dotted lines in the three figures refer to the best fit of the data according to equation [4.8].

Weibull Probability Plot of TRS - grade A

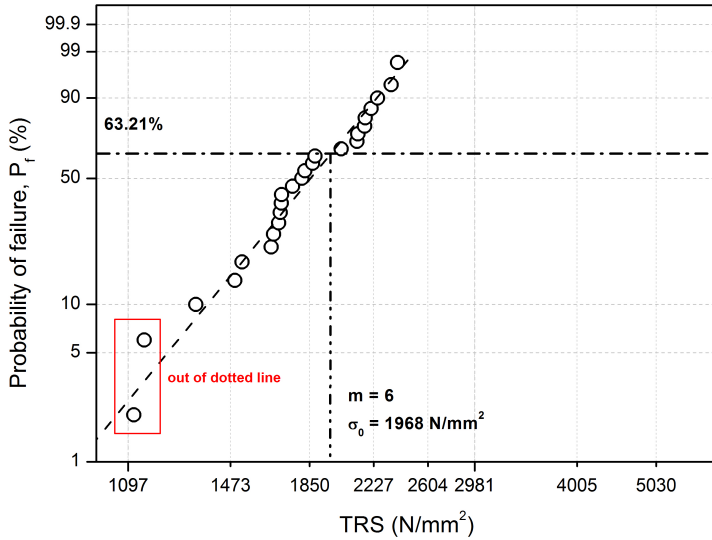


Figure IV – 7. TRS versus the probability of failure for grade A.

Weibull Probability Plot of TRS - grade B

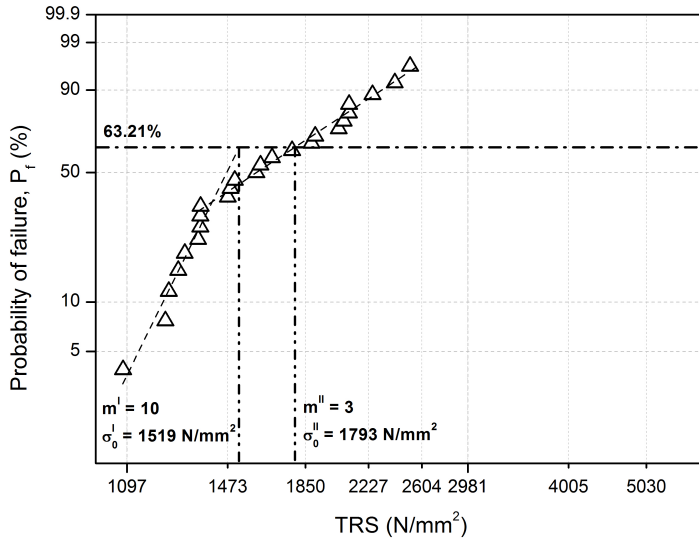


Figure IV – 8. TRS versus the probability of failure for grade B.

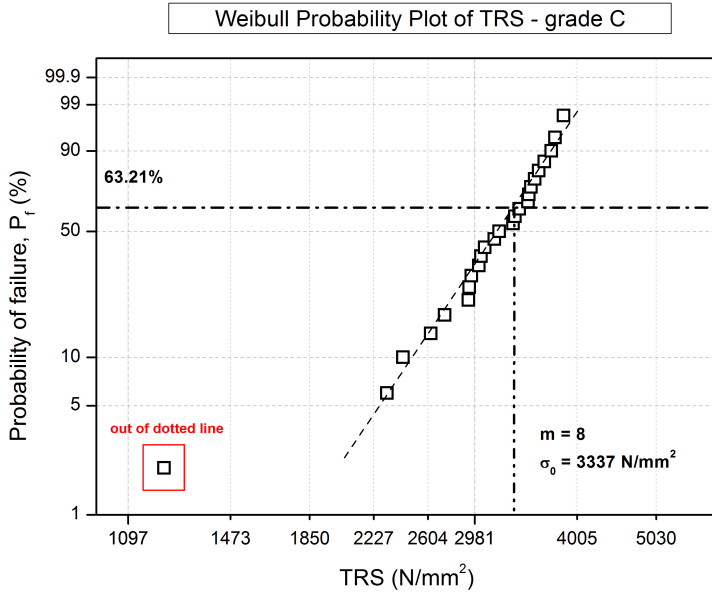


Figure IV – 9. TRS versus the probability of failure for grade C.

Figures IV – 7 and IV - 9 show the fitted data of grade A and C. In these grades, data display a uni-modal Weibull distribution of TRS, excepted for the lower values that are out of fitted lines in both grades. This means that grade A and C are characterized mostly by only a type of critical defect that leads to failure. Differently, considering Figure IV – 8, grade B is characterized by a bi-modal Weibull distribution of the mechanical strength, which is attributed to two different types and/or sizes of critical defect that bring about the failure [Weibull, 1951; Tarragó, 2017].

Figure IV – 10 shows the comparison between the grade A, B and C.

Weibull Probability Plot of TRS - Comparison between grades A,B and C

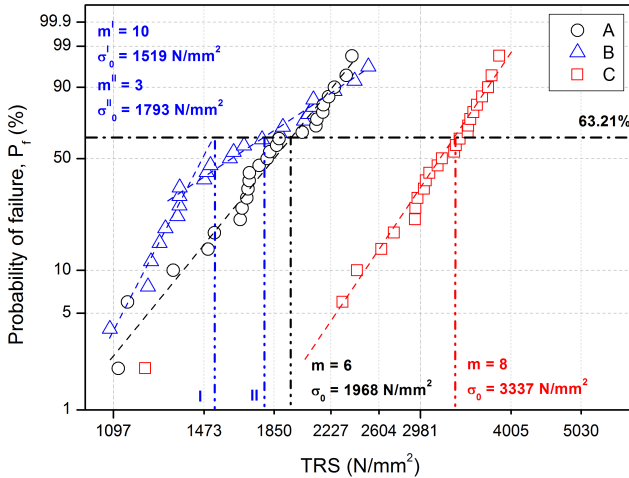


Figure IV – 10. TRS versus the probability of failure for grade A, B and C.

Grade B is characterized not only by a bi-modal Weibull distribution but also presents TRS values lower or equal to grade A even if with a higher Co content. Higher Co amount should be correlated to a higher mechanical strength, as shown in the comparison between grade A and C. This is not true, considering the A and B grades. This could be justified considering that grade B is characterized by a higher residual microporosity that could affect the global strength of the WC-Co, as summarized in Table IV – 5 [Li, 2013; Prokopiv, 2008].

Grade	m (-)	σ_0 (N/mm ²)	Microporosity (%)
A	6	1968	0.5 ± 0.2
B	10 3	1519 1793	1.6 ± 0.6
C	8	3337	0.8 ± 0.4

Table IV - 5. TRS Weibull parameters and residual microporosity of grade A, B and C.

In order to better understand the different mechanical behaviour of grade B, fracture surfaces of the different samples were investigated below.

4.3.3 Fracture surface analysis

Even if grades A and C present a uni-modal Weibull distribution of the mechanical strength, the lower values are not fitted correctly by the equation [4.9] and the respectively defined Weibull parameters. Fracture surface analysis of the different grades was conducted in order to understand better the bi-modal Weibull distribution of grade B and the presence of values that are not fitted by the uni-modal distribution in grade A and C.

In case of three-point bend test, a compressive and a tensile area characterize the fracture surface of the tested sample. Obviously, the investigated surface must be the tensile side in order to define the origin of the fracture.

The fracture surface of grade A sample with a TRS value out of the dotted line was reported in Figure IV – 11.

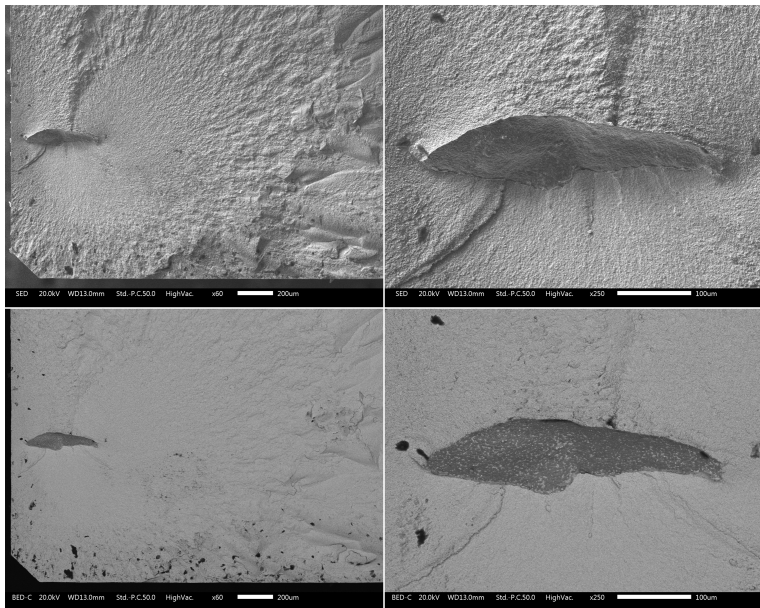


Figure IV – 11. Fracture surface of grade A sample with a TRS value out of the dotted line using SED and BED modes.

It is evident that the fracture origin in this sample is an agglomerate rich of Co inside the tensile area, to one side. The presence of the mirror-mist region and the surrounded hackle region mention in the introduction [Morrell, 1999] is visible.

The fracture surface of grade A sample with an intermediate TRS value well fitted by the dotted line was reported in Figure IV – 12.

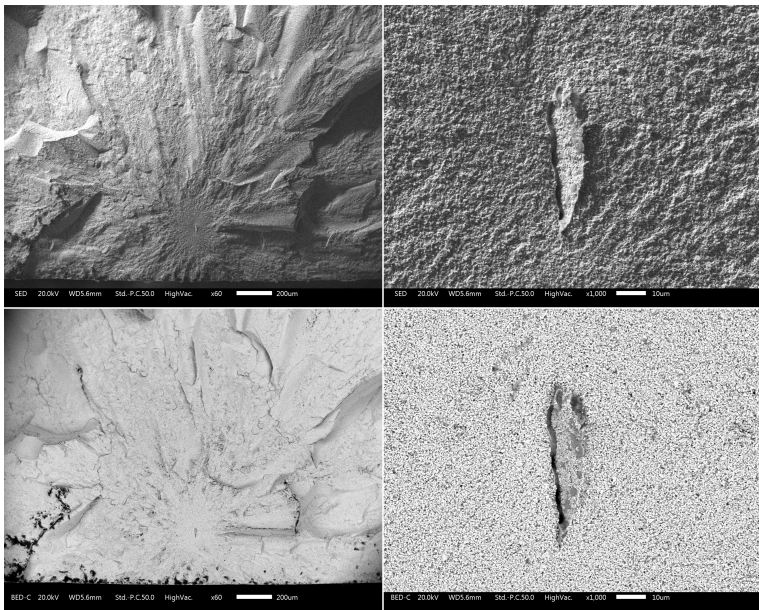


Figure IV – 12. Fracture surface of grade A sample with a TRS value well fitted by dotted line using SED and BED modes.

In this case, the defect is a compositional inhomogeneity rich of Co inside the tensile area. Also in this case the mirror-mist region and the surrounded hackle region are present.

In conclusion, the rupture of grade A pieces in the three-point bend test is mainly due to the presence of compositional inhomogeneity. Differently, when a different defect, such as agglomerate, is present the resulting rupture force is different and the associated TRS is not defined by the dotted line in the Weibull diagram.

The fracture surface of grade C sample with a TRS value out of the dotted line is reported in Figure IV – 13.

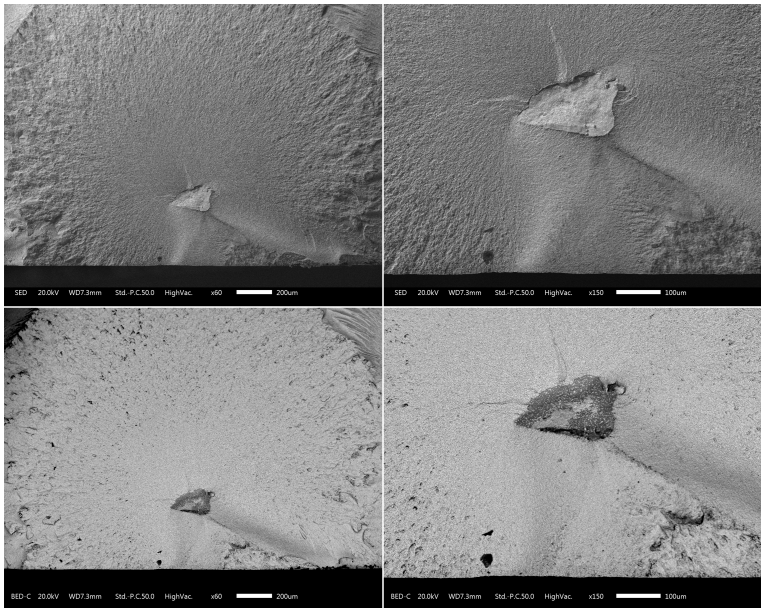


Figure IV – 13. Fracture surface of grade C sample with a TRS value out of the dotted line using SED and BED modes.

As for the TRS out of the dotted line in grade A, the fracture origin is an agglomerate rich of Co inside the tensile area with the presence of the mirror-mist region and the surrounded hackle region.

The fracture surface of grade C sample with a TRS value well fitted by the dotted line was reported in Figure IV – 14.

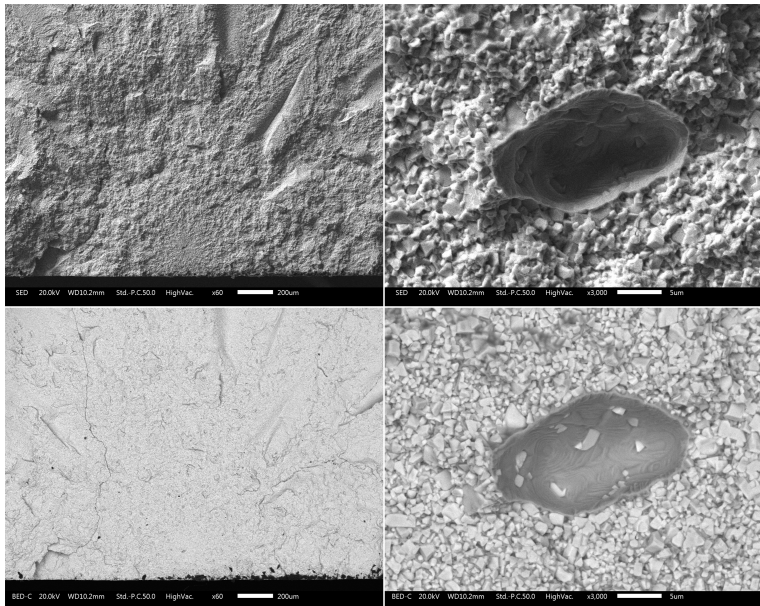


Figure IV – 14. Fracture surface of grade C sample with a TRS value well fitted by dotted line using SED and BED modes.

In this case, the defect is a pore inside the tensile area. Also in this case the mirror-mist region and the surrounded hackle region are present.

In conclusion, the rupture of grade C specimens in the three-point bend test is mainly due to the presence of pores. Differently, when a different defect, such as agglomerate, is present the resulting rupture force is different and the associated TRS is not defined by the dotted line finds for grade C.

Comparing the Weibull parameters of grade A and C reported in Table VI - 5, it is clear that the higher characteristic strength of grade C is due to the higher C_o content and D_{wc} . Differently, the slightly lower Weibull modulus of grade A is justified considering a smaller scatter of the TRS values due to the presence of compositional inhomogeneity rather than pores.

Considering the grade B with a bi-modal Weibull distribution, the fracture surfaces of samples fitted by Weibull distribution I and II, are shown in Figure IV – 15 and IV – 16, respectively.

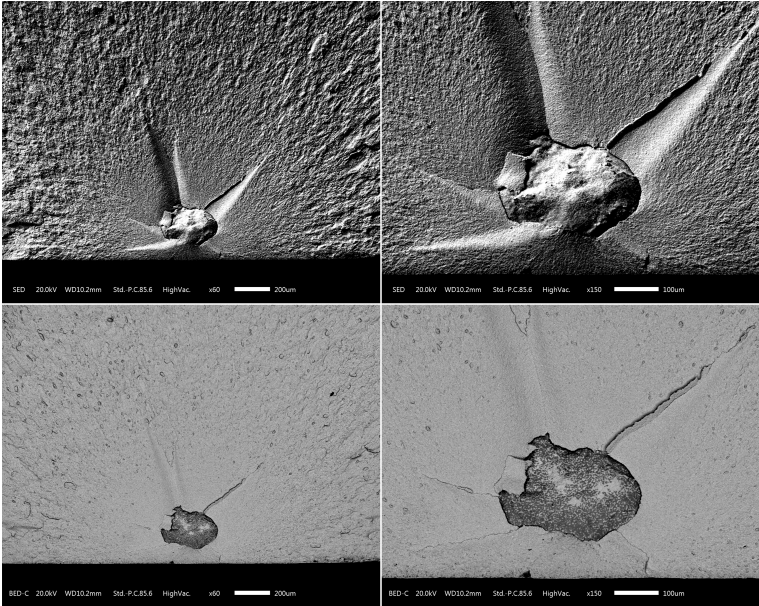


Figure IV - 15. Fracture surface of grade B sample - I using SED and BED modes.

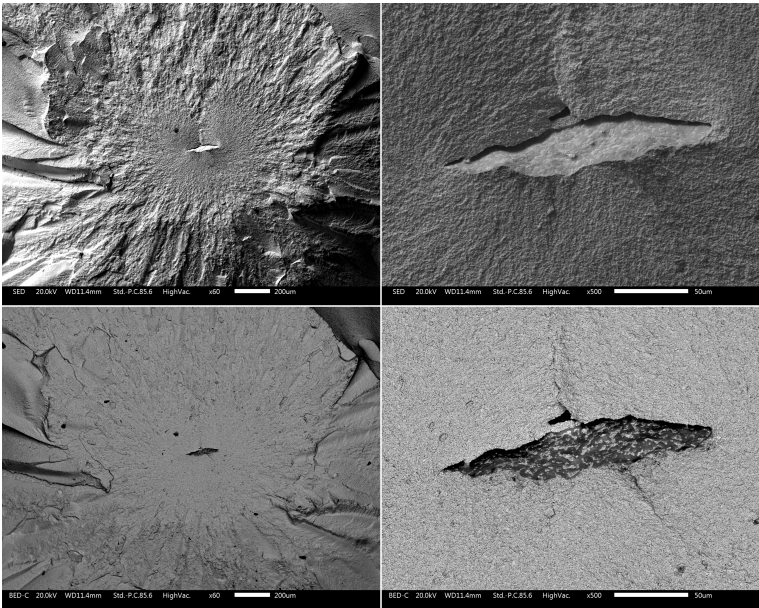


Figure IV - 16. Fracture surface of grade B sample - II using SED and BED modes.

Figure IV – 15 shows the presence of agglomerate in the tensile area close to the surface. Differently, in Figure IV – 16 is evident that the defect type is a compositional inhomogeneity into the tensile area. Indeed, it is possible to conclude that the bi-modal Weibull distribution in grade B is due to two different defect types: agglomerates in case of Weibull distribution I and compositional inhomogeneity in case of Weibull distribution II. Also, considering the Weibull parameters reported in Table IV – 5, it is evident that the Weibull modulus and the characteristic strength are lower in case of agglomerates than in case of compositional inhomogeneities. This means that the rupture of grade B samples occurs earlier and with a little variation of strength when agglomerations rather than compositional inhomogeneities are present.

In conclusion, grade A and C present a uni-modal Weibull distribution since most of the samples are characterized by only one type of defect that is compositional inhomogeneity in grade A and pore in grade C. Moreover, the presence of compositional inhomogeneities leads to a smaller variation of the rupture strength respect to pores, as highlighted by the different Weibull modulus of grade A and C. Nevertheless, in both grades, only a very few samples are characterized by a different defect type and, therefore, they are not well fitted by the calculated uni-modal distribution. Differently, in grade B one part of samples presents agglomerates and the other part is characterized by compositional inhomogeneities. This justifies the necessity to fit data of grade B with a bi-modal Weibull distribution. Furthermore, the rupture of the grade B samples occurs earlier and with a little variation of the mechanical strength when agglomerations are present rather than compositional inhomogeneities, as highlight by Weibull parameters.

4.3.4 Mechanical properties and correlation with microstructure

In order to correlate the mechanical strength with hardness and fracture toughness, the mean value and the standard deviation of TRS for all grades were evaluated. These mechanical properties and the residual microporosity of all grades are reported in Table IV – 6.

Grade	K_{IC} (MPa m ^{1/2})	HV30 (Kg/mm ²)	TRS (N/mm ²)	Microporosity (%)
A	9.66 ± 0.20	1763 ± 16	1828 ± 348	0.5 ± 0.2
B	10.72 ± 0.15	1606 ± 13	1679 ± 403	1.6 ± 0.6
C	13.85 ± 0.93	1330 ± 10	3130 ± 571	0.8 ± 0.4

Table IV - 6. Mean values and standard deviations of mechanical properties and residual microporosity of grade A, B and C.

From data reported in Table IV – 6 and graph in Figure IV – 17, it is evident that fracture toughness decreases by increasing hardness, as shown in Chapter III. This highlights that the residual microporosity does not affect these mechanical properties.

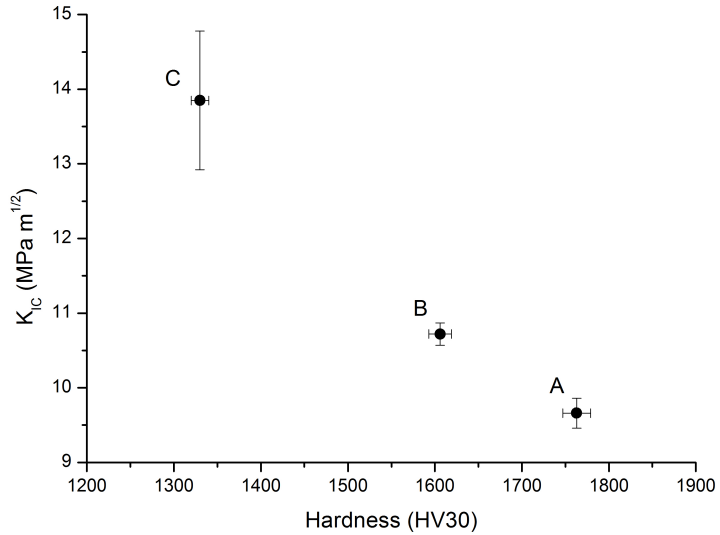


Figure IV – 17. Fracture toughness vs hardness for all studied grades.

Differently, considering data reported in Table IV – 6, the correlation between TRS and fracture toughness and hardness is not so clearly understood. Figure IV – 18 and IV - 19 show the correlation between TRS and hardness and TRS and fracture toughness, respectively.

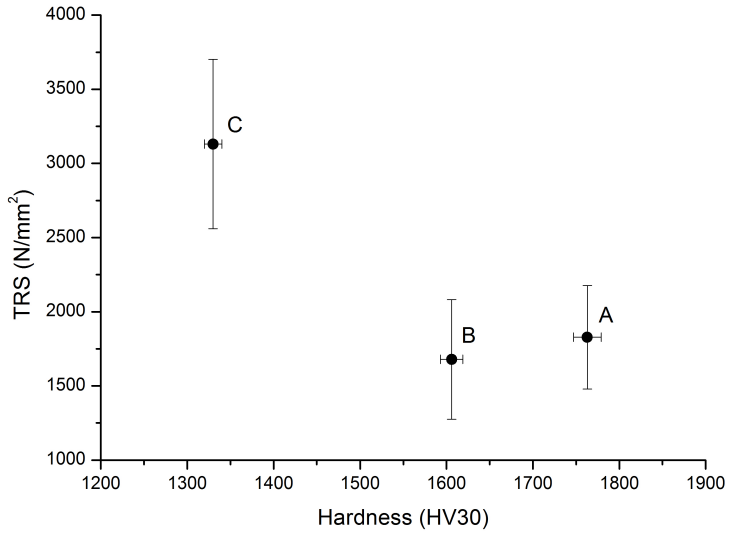


Figure IV – 18. TRS vs hardness for all studied grades.

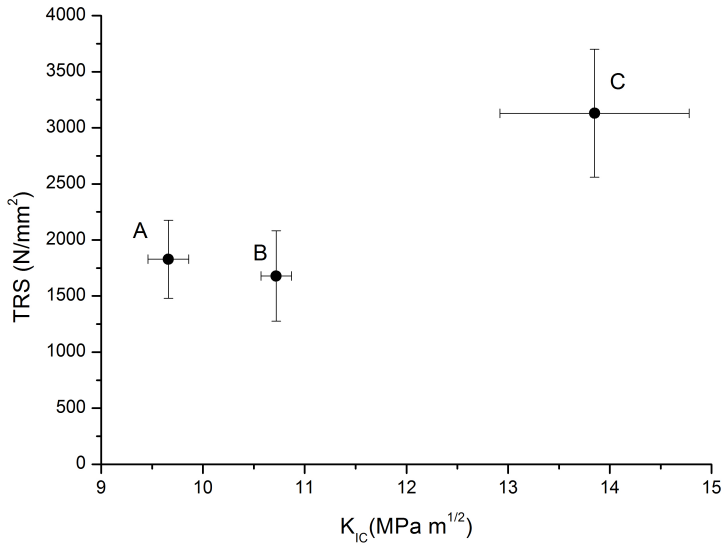


Figure IV – 19. TRS vs fracture toughness for all studied grades.

From these graphs, it is only possible to define a rough trend of TRS with the other mechanical properties: TRS increases when hardness decreases and fracture toughness increases. This is justified considering the residual microporosity that affect the TRS and not the hardness and the Palmqvist fracture toughness [Li, 2013; Prokopiv, 2008].

In Table IV – 7 are summarized the chemical composition, the microstructural parameters and the mechanical properties of the studied grades.

Grade	Co (wt.%)	D _{wc} (μm)	C (-)	λ (μm)	K _{IC} (MPa m ^{1/2})	HV30 (Kg/mm ²)	TRS (N/mm ²)
A	6.5	1.0	0.58 ± 0.10	0.14 ± 0.03	9.66 ± 0.20	1763 ± 16	1828 ± 348
B	9.0	1.0	0.55 ± 0.10	0.18 ± 0.04	10.72 ± 0.15	1606 ± 13	1679 ± 403
C	12.0	1.4	0.54 ± 0.13	0.44 ± 0.12	13.85 ± 0.93	1330 ± 10	3130 ± 571

Table IV - 7. Chemical composition, microstructural parameters and the mechanical properties of the studied grades.

In Figure IV – 20 is reported the correlation between mechanical properties and Co content.

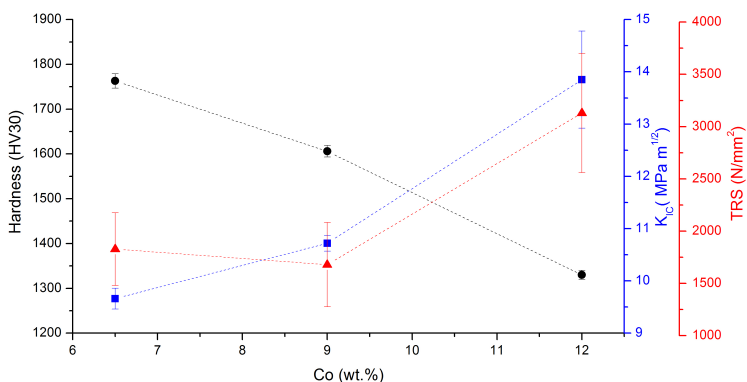


Figure IV – 20. Mechanical properties vs Co content for all studied grades.

From these results, it is evident that the fracture toughness and the hardness vary correctly with the Co content: higher Co amount increases the fracture toughness and decreases the hardness of the material. Differently, TRS slightly decreases by increasing Co content from 6.5 to 9.0 wt.% and increases by increasing Co amount from 9.0 and 12.0 wt.%. This is justified again considering the higher microporosity of grade B

that affects the mechanical strength of the material, decreasing the mean TRS value at 9.0 wt.% of Co.

Figure IV – 21 shows the correlation between mechanical properties and D_{WC} .

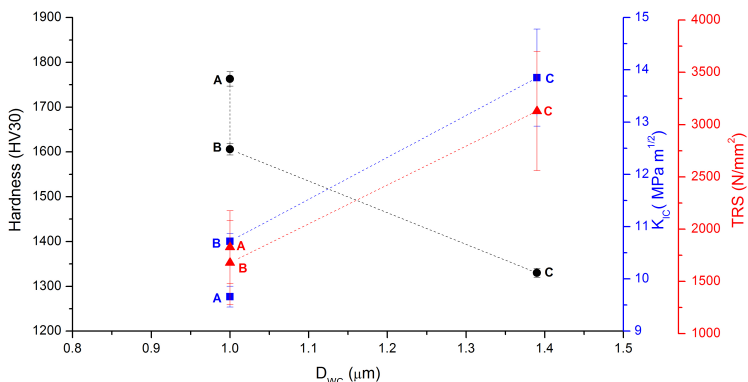


Figure IV – 21. Mechanical properties vs Co content for all studied grades.

In this case, due to the fact that grade A and B are characterized by the same D_{WC} , it is evident that the different values of mechanical properties are due to the different Co content. An increase of the D_{WC} from 1.0 to 1.4, associated with an increase of the Co amount, leads to an increased fracture toughness and TRS and to a decreased hardness.

In conclusion, the hardness and the fracture toughness depend on the Co content and the D_{WC} : increasing the Co amount and the D_{WC} , the hardness decreases and the fracture toughness increases as widely demonstrated in Chapter III. Considering the TRS, the effects of Co content and D_{WC} are affected by the presence of a high residual microporosity in grade B respect to grade A and C that affect the mechanical strength of the material.

As shown in Chapter III, the dependencies of fracture toughness and hardness with Co content and D_{WC} are justified considering that the Co content and the D_{WC} act on the contiguity and the mean binder free path, which affect the hardness and the fracture toughness of the material. Therefore, it is more accurate to correlate the mechanical proprieties of WC-Co with the contiguity and the mean binder free path as reported in Figure IV – 22 and IV – 23.

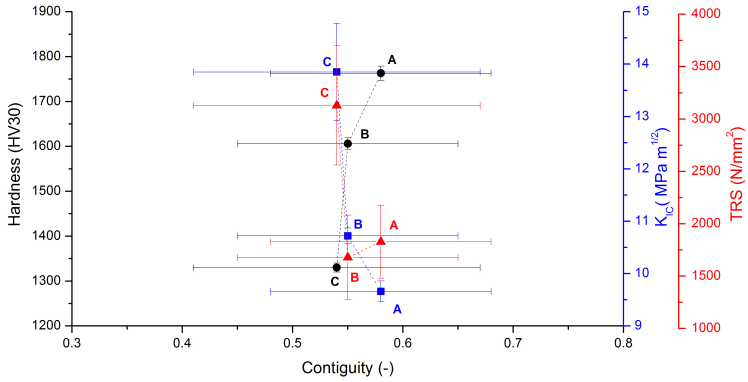


Figure IV – 22. Mechanical properties vs contiguity for all studied grades.

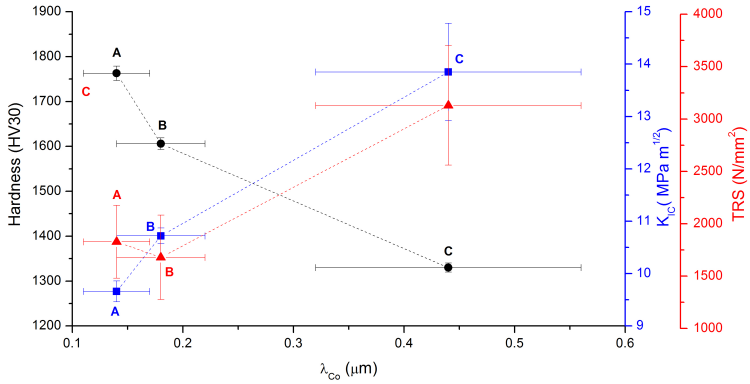


Figure IV – 22. Mechanical properties vs mean binder free path for all studied grades.

As shown in Figure IV – 21, the high standard deviations of the contiguity values in the analyzed materials make data interpretation difficult. As reported in Chapter III, the difficulty in the measurement of contiguity leads to a high scatter. Therefore, it is not possible to define a particular trend comparing the mechanical properties and the contiguity of studied WC-Co.

Considering the mean binder free path (Figure IV – 22), which increases by increasing both the Co amount and the D_{WC} , the hardness decreases and the fracture toughness increases by increasing the mean binder free path. Differently, the correlation between TRS and mean binder free path is affected by the residual microporosity.

4.4 Conclusion

The mechanical strength of three commercial WC-Co grades with different amount of binder and WC grain size were investigated by means of three-point bend test defined by ISO 3327 and ASTM B406-96. Due to the large scatter, the obtained results were analyzed through the Weibull theory. In order to justify the calculated Weibull distributions and to define the possible fracture origin types, the fracture surfaces of the different grades were analyzed. After that, the mean mechanical strength was compared with the mean hardness and the mean fracture toughness of the three WC-Co grades measured as reported in Chapter III. At the end, all these mechanical properties were correlated with the microstructure parameters and the residual microporosity. The overall conclusions of this study may be summarized as follows.

- Uni-modal Weibull distribution of the TRS for grades A and C were defined and only a very few data of both grades are not fitted by the defined Weibull distribution. Differently, grade B presents a bi-modal Weibull distribution of the TRS;
- The fracture analysis highlights that grade A and C present a uni-modal Weibull distribution since most of the samples are characterized by only one type of defect that is compositional inhomogeneity in grade A and pore in grade C. The data of both grades that are not fitted by the calculated uni-modal distribution are correlated with a different defect type, namely the presence of agglomerates. Differently, in grade B there is one part of samples that presents agglomerates and the other part that is characterized by compositional inhomogeneities. This justifies the presence of a bi-modal Weibull distribution. Furthermore, the rupture of the grade B samples occurs earlier and with a little variation of the mechanical strength when agglomerations are present rather than compositional inhomogeneities, as demonstrated comparing the Weibull parameters of the two distributions.
- Grade B is characterized also by TRS values lower or equal to grade A even if with a higher Co content. Higher Co amount should be correlated to a higher mechanical strength, as shown in the comparison between grade A and C. This is not true, considering the grade A and B. This could be justified considering that grade B is characterized by a higher residual microporosity that affects the global strength of the WC-Co. It is clear that the residual microporosity acts on the mechanical strength of WC-Co; Differently, hardness and fracture toughness are not affected by the residual microporosity. Indeed, all the correlations with the microstructure parameters defined in Chapter III are confirmed. As for hardness and fracture toughness,

no correlation between TRS and contiguity is present since the high standard deviation. Differently, there is a rough trend between the TRS and the mean binder free path but is affected by the residual microporosity.

Chapter V

Liquid Co migration in cemented carbide

Part of this chapter has been presented and published in:

L. Emanuelli, A. Molinari, G. Arrighetti, G. Garoli

“La migrazione del cobalto nella sinterizzazione del metallo duro”,

in Proceedings 36AIM, Parma, Italy: AIM, 2016. Atti di: 36AIM, Parma – IT, 21-23 September 2017.

L. Emanuelli, A. Molinari, G. Arrighetti, G. Garoli

“Effect of process parameters on the cobalt capping in WC-Co”,

in Proceedings EuroPM2017, Milan, Italy: EPMA, 2017. Atti di: EuroPM2017, Milan – IT, 1-5 October 2017.

L. Emanuelli, A. Molinari, G. Arrighetti, G. Garoli

“La migrazione del cobalto nella sinterizzazione del metallo duro”,

LA METALLURGIA ITALIANA, n. 11/12 (2017), p. 5-13.

L. Emanuelli, A. Molinari, G. Arrighetti, G. Garoli

“Effect of the sintering parameters on the liquid Co migration in WC-Co”,

Int. Journal of Refractory Metals and Hard Materials 70 (2018), p. 202-209.

In applications where the wear resistance is the most important requirement, usually cold applications as drawing dies, the surface of a cemented carbide part plays a fundamental role. In this condition, a modification of the surface during the production of the part affects the final performance of the component. An important phenomenon that occurs during sintering, under specific condition, is the liquid Co migration, which leads to the formation of a Co gradient from the surface to the bulk of sintered cemented carbide. It is clear that this phenomenon changes the surface and bulk condition of the part, affecting the local mechanical properties of WC-Co [Tsuada, 1996].

For this reason, the aim of this Chapter is to well understand this phenomenon in order to optimize the final local mechanical properties, acting on the sintering process. In this Chapter, which starts with the analysis of the state of art of the Co migration phenomenon, the influence of chemical composition and process parameters on the Co migration was studied. Therefore, at the end, the effect of these parameters and the geometry of the part on the Co migration phenomenon were investigated considering a common industrial sintering process.

5.1 Introduction of liquid Co migration

The liquid Co migration, which leads to the formation of a Co gradient from the surface to the bulk of sintered cemented carbide, occurs during sintering, under specific condition. This phenomenon is important in order to optimize the mechanical properties of WC-Co for specific application [Tsuada, 1996].

The WC-Co that is produced with this gradient between surface and bulk takes the name of “functionally graded WC-Co” (FG-WC-Co). The formation of this material is widely investigated in literature [Brookes, 2010; Eso, 2008; Eso, 2005; Fan, 2008; Fan, 2009A; Fan, 2009B; Fan, 2009C; Fan, 2013; García, 2016; Guo, 2010; Guo, 2011; Janisch, 2010; Konyashin, 2012; Konyashin, 2013; Konyashin, 2014; Liu, 2004; Liu, 2006; Sachet, 2013; Sachet, 2012; Taniguchi, 1989]. A Co gradient produced by a lower Co amount on the surface and higher Co content in the bulk permits a trade-off between the wear resistance and the fracture toughness [Eso, 2008; Eso, 2005; Fan, 2008; Fan, 2009A; Fan, 2009B; Fan, 2009C; Fan, 2013; Guo, 2011; Konyashin, 2012; Konyashin, 2013; Liu, 2004; Liu, 2006]. This combination of properties becomes important in case of cold applications as drawing dies or tool applications. Differently, a higher surface Co content respect to the bulk, which could lead to the formation of a Co layer on the surface, is preferred in the WC-Co joining process. The formation of the Co layer on the surface of WC-Co is called “Co capping” [Brookes, 2010; Fan, 2008; Fan, 2009A; Fan, 2009B; Fan, 2009C; García, 2016; Guo, 2010; Janisch, 2010; Taniguchi, 1989; Sachet, 2013; Sachet, 2012].

From literature it is certain that the Co gradient formation depends on the composition of WC-Co and on the production process conditions. It also occurs during cooling, specifically in the solidification temperature range. What it is still not fully defined is the mechanism for its formation. Below, all the theories reported in literature regarding the liquid Co migration are summarized.

5.2 Liquid Co migration theories

In *the pressure migration theory* the driving force for the Co migration is the pressure migration that is connected with the liquid phase fraction, the carbon content in the liquid Co and the WC grain size [Fan, 2008; Fan, 2009A; Fan, 2009B; Fan, 2009C; Fan, 2013].

The carbon gradient theory [Guo, 2010; Taniguchi, 1989], which studies the effect of different chemical potential of carbon between the atmosphere and the WC-Co surface, finds that a decarburizing condition of the surface reduces the carbon content into the surface liquid Co increasing its solidification temperature [Upadhyaya, 1998]. For this reason, during cooling, the liquid Co on the surface solidifies prior than that on the bulk forming a gradient of liquid Co between the bulk and the surface and the

consequent Co migration towards the surface. On the contrary, a prior solidification of the liquid in the bulk and its migration from the surface to the core occurs due to a carburizing condition of the surface that increases the C content into the surface liquid Co.

The theory that is in contradiction with the others is *the thermal contraction theory* [Brookes, 2010; Janisch, 2010]. It affirms that the liquid Co migration towards the core occurs due to a decarburizing condition. Indeed, the prior solidification of the surface liquid and the linked volume shrinkage spreads the residual Co liquid towards the core.

The surface tension theory [Sachet, 2013; Sachet, 2012] focused its attention on the capping phenomenon. It considers that the so fast formation of the surface Co layer is not only related to the material transport but also to the surface energy minimization. Indeed, the process starts with an initial mass transport due to a decarburizing condition and proceeds due to the higher surface tension of the liquid Co that leads to the formation of domes on the surface to minimize surface energy.

Nevertheless, in all these theories, the influence of the wettability of WC by liquid Co on its migration was not taken into account. Konyashin et al. [Konyashin, 2017A; Konyashin, 2016] considers the capillarity phenomena in the carbides near surface layer as the driving force for Co capping.

It is well known that a liquid in a capillary of a composite body is subject to two opposite pressures: the capillary pressure and the migration or suction pressure [Lisovsky, 1993]. The capillary pressure is related with the wettability of the capillary material by liquid and with the capillary dimension. Indeed, the capillary pressure increases with increased wettability and decreased channel diameter. In this condition, the liquid tends to enter the channel. Differently, the pressure migration, which depends on the liquid content, decreases by increasing the liquid amount. For this reason, in an ultrafine grade, the capillary pressure is high due to the thin channel and the migration pressure depends on the Co amount. In details, an increased migration pressure is obtained by a decreased Co content. At a certain Co amount, the pressure migration is so high to overcome the capillary pressure and the liquid does not fill the channel.

Considering the wettability of WC by liquid Co, it is known that it results modified by impurities [García, 2016; Konyashin, 2016] and by the carbon content in solution [Konyashin, 2017A]. Indeed, the C content reduces the wettability of WC by liquid Co leading to a lower capillary pressure.

For this reason, it is possible to conclude that the Co migration from high carbon regions to low carbon regions is caused not only by the liquid Co gradient that is formed during cooling but also by wettability of WC by liquid with different C content.

5.3 Effect of the process parameters on the Co migration

As reported previously, it is sure that the Co migration is promoted by a carbon gradient in liquid Co. An inhomogeneous distribution of carbon may result not only from a decarburizing or carburizing atmosphere but also from the efficiency of the dewaxing step. Indeed, a not complete or homogeneous elimination of the wax, usually paraffin, may result in an inhomogeneous distribution of C activity in the material. Considering the paraffin wax, it is well known that it decomposes into olefin and free carbon at 400°C [Chen, 2008; Upadhyaya, 1998] and contaminates the material by carbon if not completely removed at a lower temperature.

In this subchapter, the influence of dewaxing stage, Co content, cooling rate and isothermal holding at the sintering temperature in the production of drawing dies on the Co migration were studied.

5.3.1 Materials and experimental procedure

Two different commercial cemented carbides with 6.5 and 9.0 wt.% of Co were selected (Table V – 1).

Grade	WC (wt.%)	D _{wc} (μm)	Co (wt.%)	D _{Co} (μm)	Cr ₃ C ₂ (wt.%)
A	93.2	0.8	6.5	1.0	0.3
B	90.7	0.8	9.0	1.0	0.3

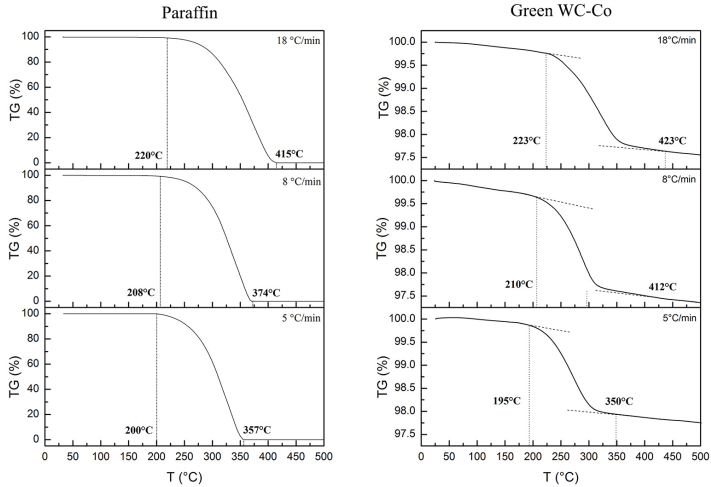
Table V – 1. Composition details of the two studied commercial WC-Co.

Green specimens were produced by cold compaction of the two powders by adding the 2.0 wt.% of paraffin.

In order to determine the melting and solidification intervals of the two grades, Differential Scanning Calorimetry (DSC) analyses were carried out with a heating rate of 5°C/min in a N₂ flux up to 1450°C and a cooling rate of 40°C/min.

The paraffin evaporation was studied by ThermoGravimetric Analyses (TGA) firstly on pure paraffin and secondly on the green WC-Co in order to evaluate the resistance offered by the cross section to the outwards flux of evaporated paraffin. Tests were carried out in a N₂ flux of 200 ml/min with three different heating rates (5, 8 and 18°C/min) up to 600°C. The effect of an isothermal stage at 300°C for 1h was studied on the green material. These analyses, that are reported in Figure V – 1, underline that almost all the paraffin evaporates within 400°C and it is completely eliminated in 6 minutes with the isothermal stage at 300°C.

EFFECT OF HEATING RATE



EFFECT OF ISOTHERMAL STAGE AT 300°C

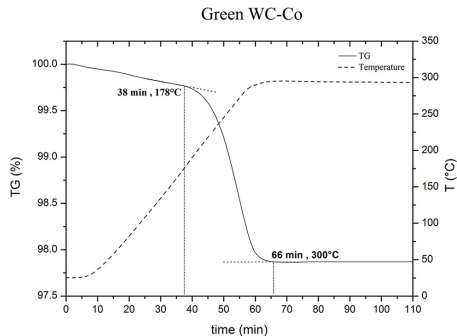


Figure V – 1. TGA on both pure paraffin and the green WC-Co.

Four different sintering cycles were defined (S1, S2, S3 and S4) on the base of the TGA results. They are carried out in a graphite furnace that leads to a slight carbon enrichment of the surface due to the high temperature reached. Because of limitation on our sintering furnace, the sintering temperature in all cycles was 1350°C. The different cycles are summarized as follows.

- S1. This cycle consists of a fast heating rate and a static N₂ atmosphere, which lead to the paraffin evaporation on the surface only, in order to reproduce the decarburizing condition of the surface respect to the bulk. The carbon activity

in the core is higher than that on the surface since the residual paraffin in the core is higher than the C surface enrichment provided by the graphite of the furnace.

- S2. In this cycle the complete dewaxing through an isothermal step at 300°C and a vacuum atmosphere was achieved, and the carbon enrichment of the surface due to the graphite furnace leads to the carburizing condition of the surface respect to the bulk.
- S3. This cycle differs from cycle S1 because of a lower heating rate. This is done in order to reproduce a slight decarburizing condition of the surface.
- S4. In this cycles, the slight decarburizing condition of the surface was obtained by fluxing N₂ respect to cycle S1.

Once the conditions to obtain the Co layer formation were individuated, the effect of the cooling rate on the Co capping was investigated by cycle S5.

At the end, the effect of the isothermal holding at the sintering temperature on the Co migration was studied by cycles S6, S7 and S8. Table V – 2 summarizes the different sintering cycles used in this study.

Cycles	Heating	Dewaxing	Heating	Sintering	Atmosphere	Cooling	Expected condition
	(RT-300°C) (°C/min)	(°C, h)	(300-1350°C) (°C/min)	(°C, h)	(200 mbar)		
S1	18	-	18	1350, 2	N ₂ static	Furnace cooling	Strong Decarburizing
S2	5	300,1	8	1350, 2	Vacuum	Furnace cooling	Carburizing
S3	8	-	8	1350, 2	N ₂ static	Furnace cooling	Slight Decarburizing
S4	18	-	18	1350, 2	N ₂ flux	Furnace cooling	Slight Decarburizing
S5	18	-	18	1350, 2	N ₂ static	Forced cooling	Strong Decarburizing
S6	18	-	18	1350, 0	N ₂ static	Furnace cooling	Strong Decarburizing
S7	18	-	18	1350, 0	N ₂ static	Forced cooling	Strong Decarburizing
S8	5	300, 1	8	1350, 0	Vacuum	Furnace cooling	Carburizing

Table V – 2. Sintering cycles details.

The furnace cooling consists in the turning off of the furnace. Differently, the forced cooling regards the turning off of the furnace and the introduction of a cooling gas (below 1250°C in order to avoid the furnace damage).

Standard metallographic procedure was used in order to investigate the sintered drawing dies.

Murakami's reagent (100 ml distilled water, 7g KOH, 7g $K_3[Fe(CN)_6]$) [Petzow, 1999], was used for selective etching of WC particles.

EDXS analysis on areas of 450 μm^2 was used to determine the Co concentration profile along the cross section from internal to external surface. Due the impossibility to quantify the carbon content with the EDXS analysis, the Co content measured results slightly higher than the real one. Therefore, data were corrected considering the C amount due to WC and Cr_3C_2 .

The outer and inner surfaces of the drawing dies were investigated in order to highlight different behaviors of the Co migration because of possible geometry effects owed to the small diameter of the hole. The schematization of the outer and inner surface of a drawing die is reported in Figure V – 2.

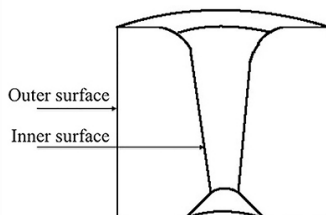


Figure V – 2. Schematization of the inner and outer surfaces of the drawing die.

Due to the formation, in specific condition, of a Co concentration profile between the surface and the core of the material that affect the local mechanical properties, microhardness profile from the outer to the inner surface was performed.

5.3.2 Results and discussion

5.3.2.1 Differential scanning calorimetry

Table V – 3 shows the melting and solidification intervals of the two investigated grades.

Grade	Melting interval (°C)			Solidification interval (°C)		
	Start	Finish	ΔT	Start	Finish	ΔT
A	1328	1380	52	1360	1307	53
B	1345	1385	40	1365	1317	48

Table V – 3. Melting and solidification intervals for grade A and B.

The grade A melts and solidifies at lower temperatures than the grade B and the melting and solidification intervals are wider in grade A.

5.3.2.2 Grade A

Micrographs of specimens with and without the surface Co layer are reported in Figure V - 3, along with the EDXS analysis of some selected regions.

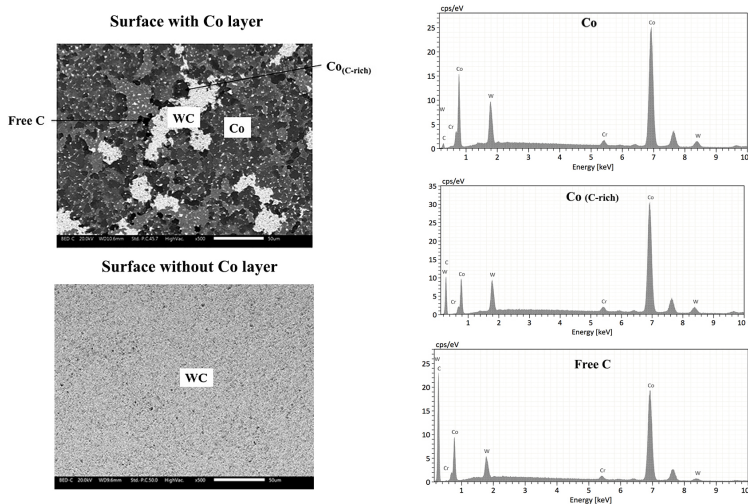


Figure V – 3. Surface details with and without the Co layer.

The different gray scale on the Co enriched surface refers to Co with more or less carbon in solid solution and the black areas are free carbon.

SEM micrographs of the outer and inner surfaces of the grade A drawing die after the cycles S1, S2, S3, and S4 are shown in Figure V - 4.

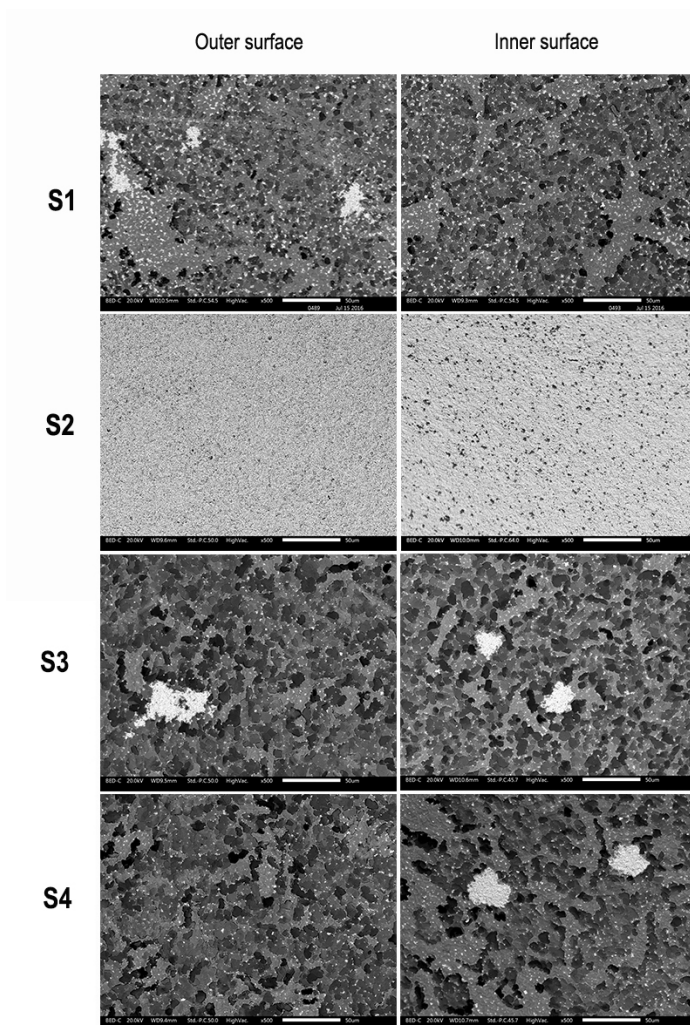


Figure V – 4. Grade A outer and inner surfaces of drawing dies after cycles S1, S2, S3 and S4.

The formation of a Co layer on the surface is observed in the decarburizing condition of the surface obtained by either avoiding or limiting dewaxing (S1, S3 and S4). The surfaces of the drawing sintered with cycles S3 and S4 present the same condition as that obtained with the cycle S1. Differently, the surface depletion of Co is obtained by a carburizing condition of the surface (S2). In cycles S1, S3 and S4 where the Co migration towards the surface occurs, no evident differences were found between the outer and the inner surfaces. On the contrary, in cycle S2, the inner surface is characterized by a slightly higher amount of Co. This is due to the small diameter of the hole that leads to a less efficient effect of the atmosphere circulation. The cobalt concentration profiles underline these differences between cycle S1 and S2, as shown in Figure V – 5.

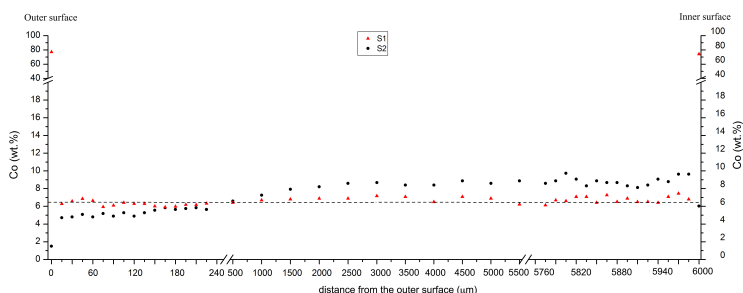


Figure V – 5. Co concentration profiles after cycles S1 and S2 of grade A.

The Co content is constant between 1.50 mm and 5.94 mm from the outer surface. For this reason, in order to better investigate what happens in and near the surfaces, the Co profiles after cycles S1 and S6 without the area where the Co amount is constant, are shown in Figure V – 6.

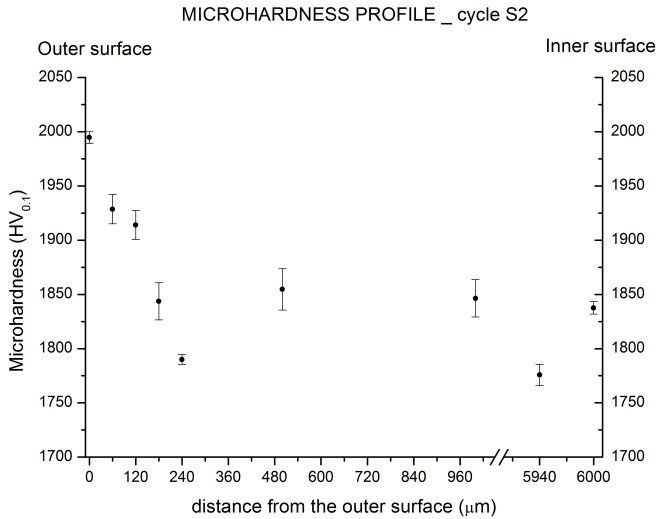


Figure V – 7. Microhardness profile after cycle S2.

The influence of the cooling rate on the Co capping was investigated comparing cycles S1 and S5 (Figure V – 8).

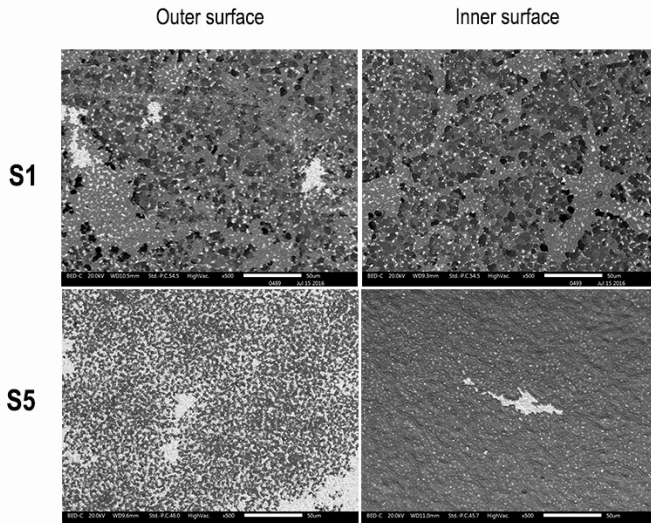


Figure V – 8. Grade A outer and inner surfaces of drawing dies after cycles S1 and S5.

Considering the solidification intervals measured by DSC (Table V - 3), the forced cooling starts after the complete solidification in both grades. Nevertheless, the S1 and S5 micrographs reported in Figure V - 5 underline that the surface Co amount decreases by using a forced cooling between 1250°C and RT. This is attributed to the fact that in this cycles, due to the residual paraffin and the graphite of the furnace, the carbon content of the core and the surface is higher than the stoichiometric one. In the DSC analysis this does not happen. Indeed, due to the low heating rate and the small dimension of samples, all the paraffin evaporates and no graphite is present into the DSC furnace. Therefore, the sintered drawings with cycles S1 and S5 are characterized by a start and finish solidification temperatures lower than that of grades with C stoichiometric value, due to higher carbon content. In cycles S5 the forced cooling starts when both grades are not completely solidified, affecting Co capping.

Considering the outer and the inner surfaces, in cycles S5, due to the small diameter of the hole that leads to a less efficient effect of the cooling rate, the inner surface is characterized by a slightly higher amount of Co.

These differences between cycles S1 and S5 are highlighted comparing the Co concentration profiles, as shown in Figure V - 9.

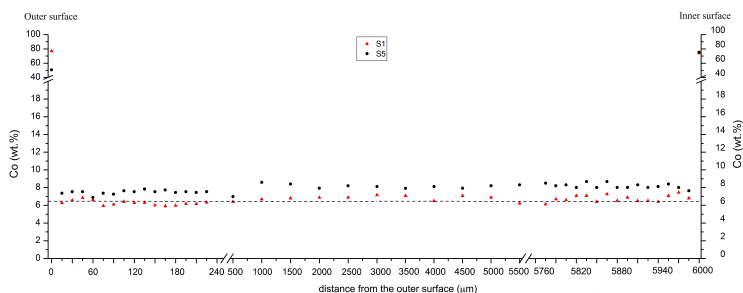


Figure V - 9. Co concentration profiles after cycles S1 and S5 of grade A.

As shown before, the Co content is constant between 1.50 mm and 5.94 mm from the outer surface. For this reason, it is better to study the Co concentration profile reported in Figure V - 10.

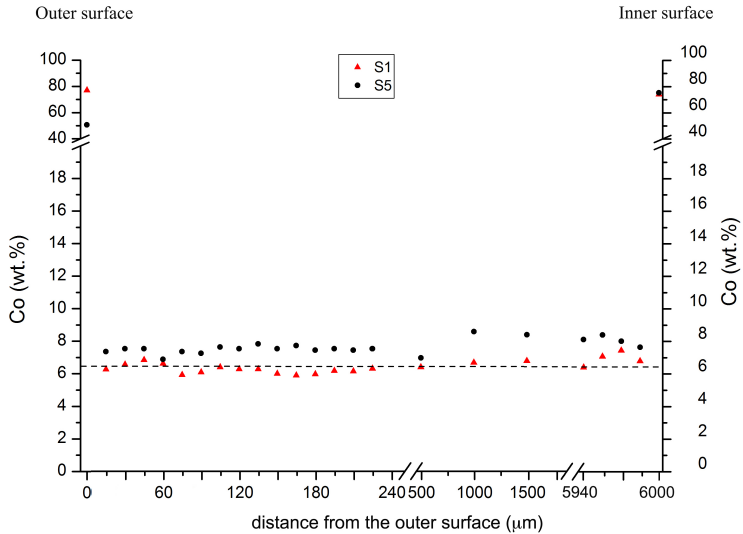


Figure V – 10. Co concentration profiles after cycles S1 and S5 of grade A without the area between 1.50 mm and 5.94 mm.

From these profiles it is evident that in both cases the Co layer formation occurs but cycle S1 presents a higher Co content on both surfaces and a lower amount in the bulk respect to cycles S5. This confirms what is shown before: an increased cooling rate in the interval between 1250°C and RT (cycles S5) brings about a decreased Co content on the surface and an increased one in the bulk.

In order to evaluate the effect of the isothermal holding on the Co migration, Figure V – 11 shows the micrographs of the inner and outer surface of sintered drawings after cycles S6, S7 and S8.

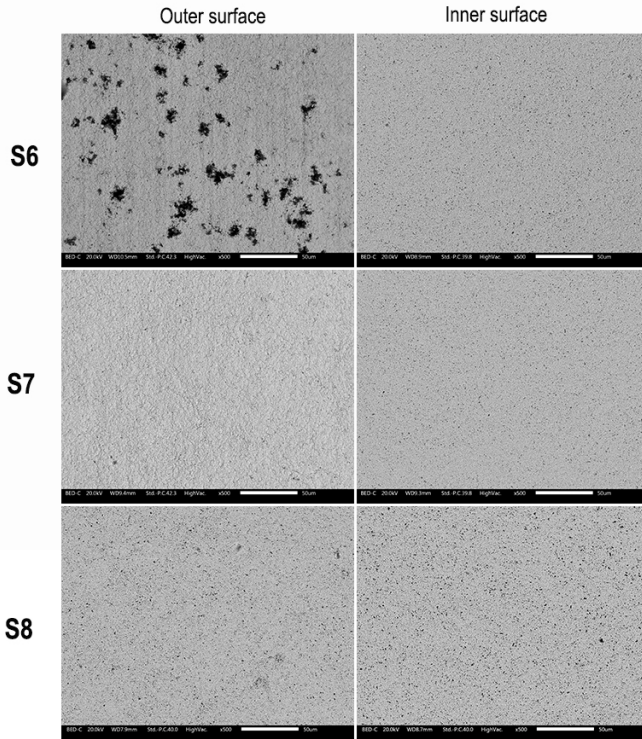


Figure V – 11. Grade A outer and inner surfaces of drawings after cycles S6, S7 and S8.

The effect of the isothermal holding on the decarburizing condition of cycles S1 and S5 was investigated in cycles S6 and S7, respectively. From the micrographs is evident that, even if in the decarburizing condition, the formation of the Co layer is prevented without the sintering dwell before cooling. It may be correlated with the temperature gradient in the drawing die at the end of the heating stage. Indeed, the bulk is at a lower temperature respect to the surfaces. The effect of the carbon gradient is outclassed by the effect of the temperature gradient. Therefore, during cooling, because of the prior solidification of the liquid at the core, the residual liquid Co migrates towards the interior of the material.

The effect of the isothermal dwell at high temperature on the carburizing conditions is appreciated by comparing cycles S2 and S8. In this condition, both the temperature and the carbon gradients work together in favour of the Co migration towards the interior of the material.

Considering the outer and the inner surfaces, differences are evident only in cycle S6 and S8. In cycles S6 the outer surface presents a lot of black spots respects to the inner surface. These areas are present also on the surfaces after cycles S1, S3 and S4 and refer to free C, as shown in Figure V – 3. The presence of free carbon, as reported previously, is mainly attributed to the high carbon amount due to the residual paraffin that precipitates as free carbon. Differently, a slightly higher Co content characterizes the inner surface after cycles S8. This is attributed to the small diameter of the hole as reported previously for cycles S2 and S5.

In order to confirm these results, the influence of the isothermal holding at the sintering temperature in the different surface condition where investigated by comparing the cobalt profiles of cycles S1 and S6 and cycles S2 and S8.

In the case of the decarburizing condition of the surface, the cobalt profiles of cycles S1 and S6 are compared in Figure V – 12.

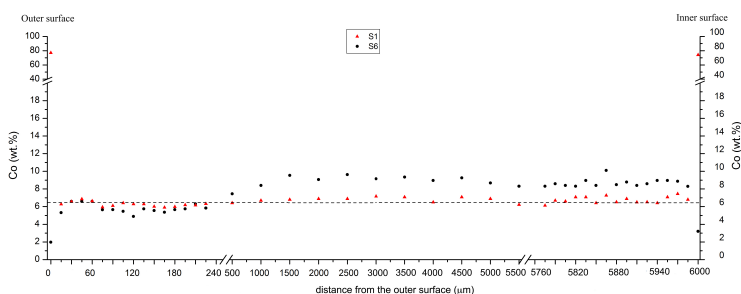


Figure V – 12. Co concentration profile after cycles S1 and S6 of grade A.

Also in this case, the Co content is constant between 1.50 mm and 5.94 mm from the outer surface. For this reason, the Co profiles after cycles S1 and S6 without the area where the Co amount is constant, are shown in Figure V – 13.

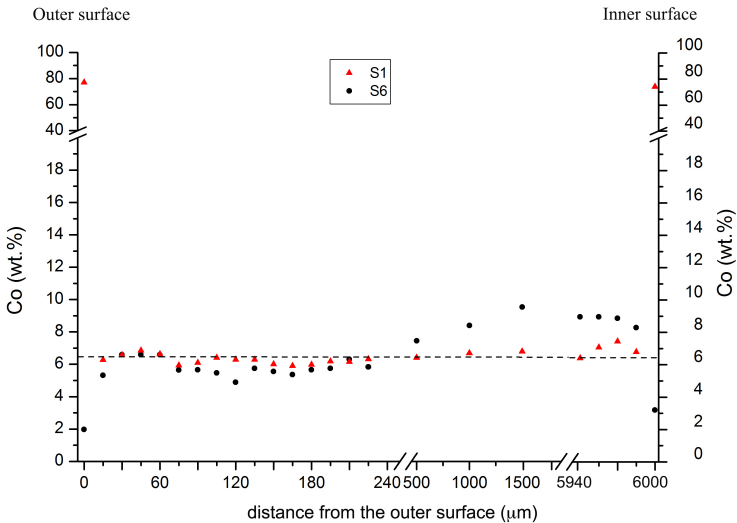


Figure V – 13. Co concentration profiles after cycles S1 and S6 of grade A without the area between 1.50 mm and 5.94 mm.

In cycle S1 is evident a large Co enrichment on the two surfaces, with an almost flat Co profile around the nominal value in the whole of the thickness. Differently, S6 shows the Co depletion of both surfaces. Furthermore, a small Co depletion is present from the subsurface layers of the outer surface until 225 μm . Differently, Co enrichment is evident between 500 μm and the subsurface layers of the inner surface. This is attributed to the fact that in cycles S6 the temperature gradient due to the absence of the sintering dwell prevails on the carbon gradient leading to the Co migration towards the interior of the material. A Co gradient is present in the first 1.5 mm from the outer surface, after that it remains higher than the nominal value and decreases only on the inner surface. This is associated to temperature gradient between the outer surface and the core that is higher than that between the inner surface and the core. Differently, the temperature gradient is eliminated in cycles S1 due to the sintering dwell and, during cooling, the carbon gradient promotes the Co migration towards the surface. This leads to a homogeneous distribution of the Co into the part and a surface Co enrichment.

Same behavior is evident comparing the cycles S5 and S7, as displayed in Figure V – 14.

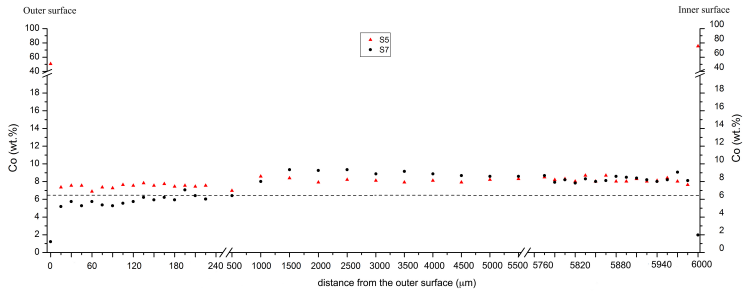


Figure V – 14. Co concentration profile after cycles S5 and S7 of grade A.

In Figure V – 15 are reported the cycles S5 and S7 without the area between 1.50 mm and 5.94 mm from the outer surface, where the Co content results constant.

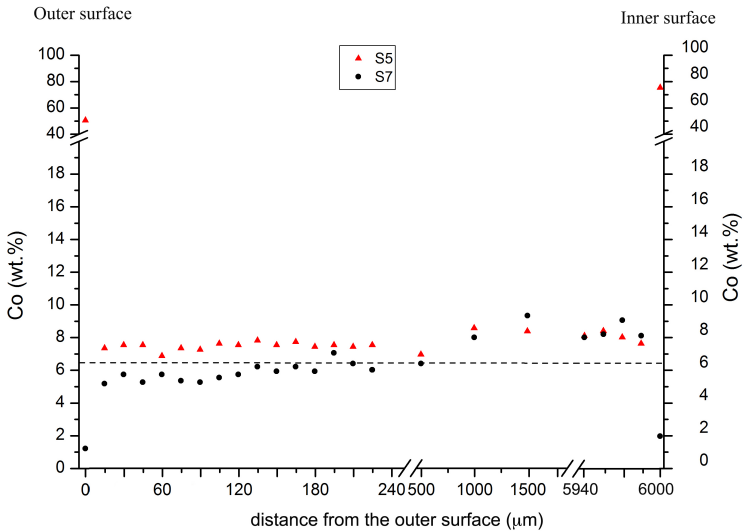


Figure V – 15. Co concentration profiles after cycles S5 and S7 of grade A without the area between 1.50 mm and 5.94 mm.

Differently, the Co concentration profiles regarding the effect of the sintering dwell on the carburizing condition of cycles S2 are reported in Figure V - 16.

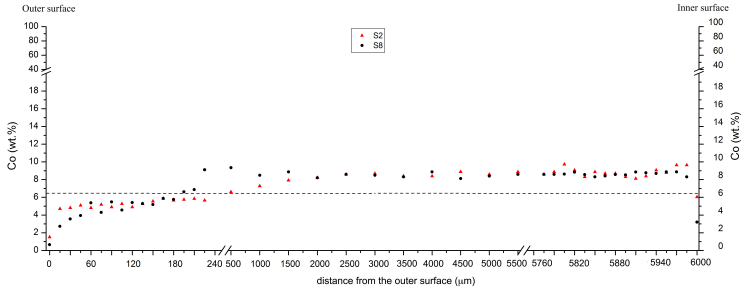


Figure V - 16. Co concentration profiles after cycles S2 and S8 of grade A.

Figure V - 17 shows the Co profiles after cycles S2 and S8 without the area between 1.50 mm and 5.94 mm where there is a constant Co distribution.

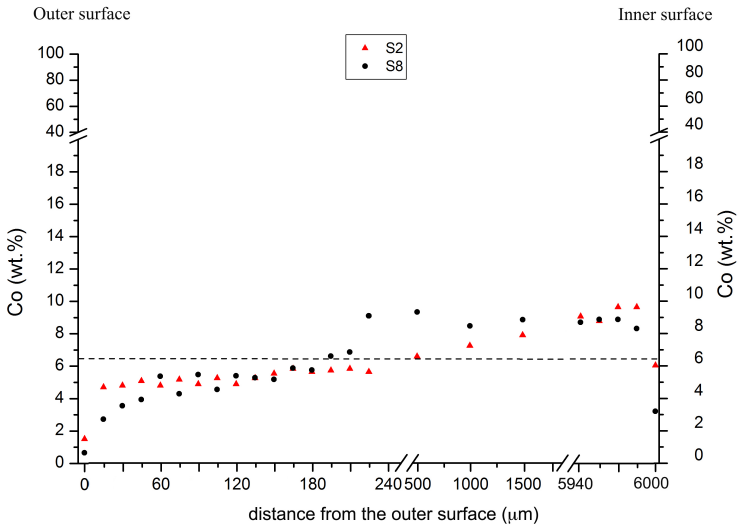


Figure V - 17. Co concentration profiles after cycles S2 and S8 of grade A without the area between 1.50 mm and 5.94 mm.

The cycle S2 exhibits a large Co depletion on the outer surface with an almost flat Co profile, lower than the nominal concentration, from the subsurface layers of the outer surface until 225 μm . After that the Co content increases up to reach 9.5 wt.% in the subsurface layers of the inner surface and decreases down to the nominal concentration on the inner surface. In S8, the Co content increases from a very low value on the outer surface to the nominal value at 210 μm . It increases up to around 9.0 wt.%, remains

constant throughout the subsurface layers of the inner surface and drastically decreases on the inner surface. These behaviours are justified considering that, without the sintering dwell, the temperature gradient between the core and the outer surface is added to the carbon gradient leading to a greater Co gradient. Differently, due to the very small temperature gradient, no differences are present between the core and the inner surface.

The influence of the cooling rate in the condition without the sintering holding on the Co migration is investigated comparing the cycles S6 and S7 (Figure V – 18).

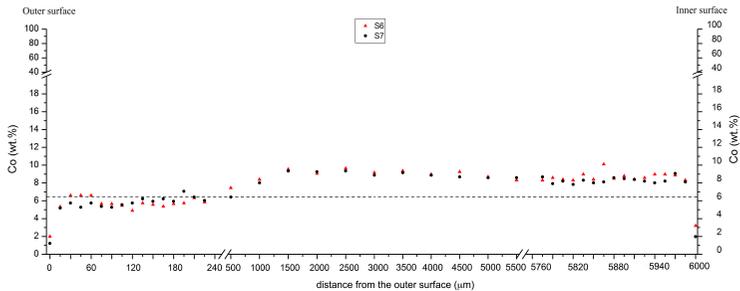


Figure V - 18. Co concentration profiles after cycles S6 and S7 of grade A.

Figure V – 19 exhibits the cobalt profiles after cycles S6 and S7 without the Co constant distribution between 1.50 mm and 5.94 mm in order to better highlights the different behaviour in and near the surfaces.

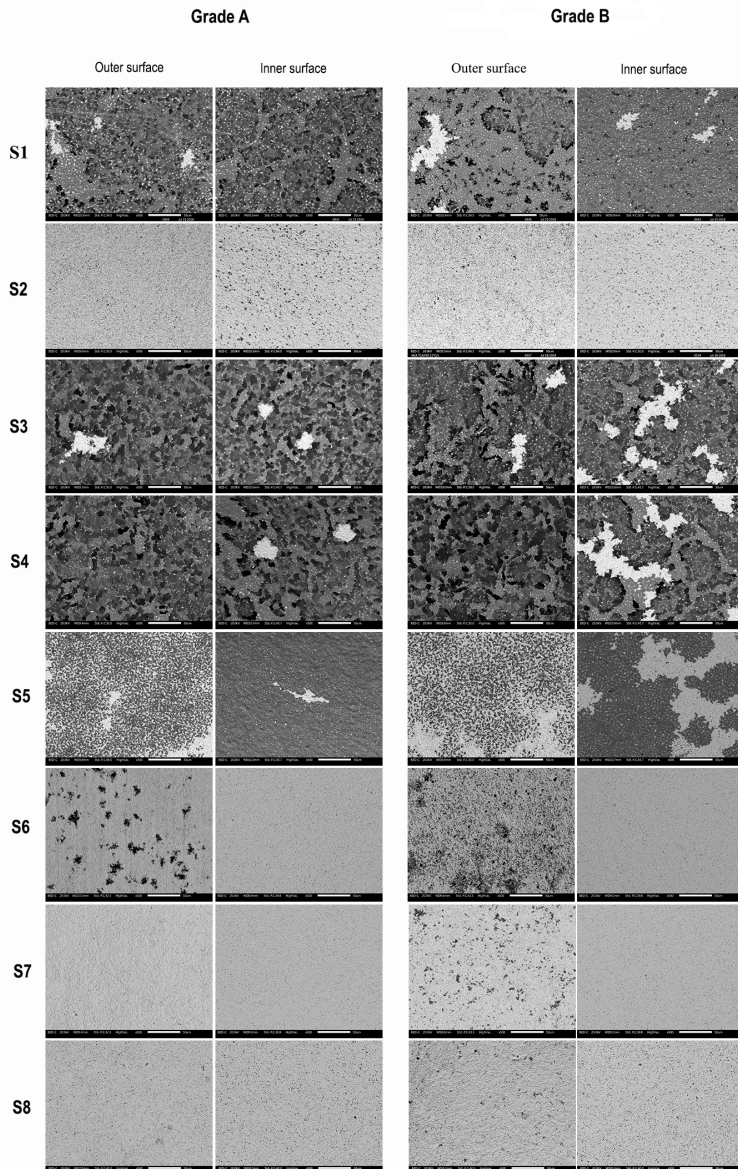


Figure V - 20. Grade A and B inner and outer surfaces after all the different sintering cycles.

Grade A and B present the same behaviour in all cycles except for the cycles S6 and S7.

In these cycles, a slightly higher Co content on the outer surface respect to the inner one characterizes the grade B as shown in detail in Figure V – 21.

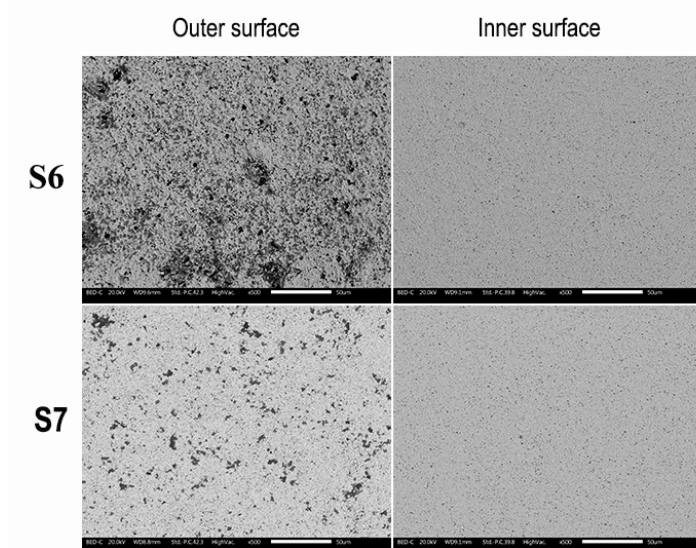


Figure V - 21. Grade B outer and inner surfaces of drawings after cycles S6 and S7 that differ from the cycles S6 and S7 of the grade A.

The reason is closely linked to the solidification interval and to the different cooling rate of the inner and the outer surfaces: in grade B only the inner surface is characterized by a low cobalt content since, it is subject to a slower cooling.

This behaviour is confirmed by the Co distribution profiles of Grade B after cycles S6 and S7 (Figure V – 22).

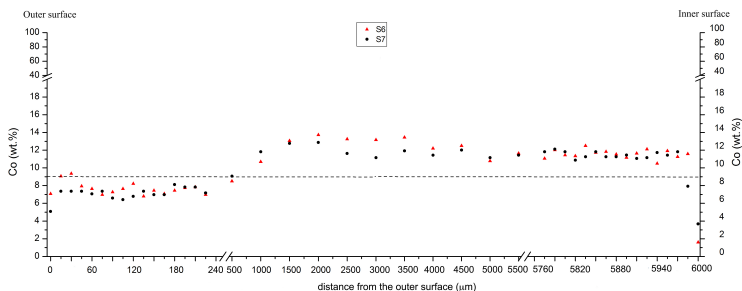


Figure V - 22. Co concentration profiles after cycles S6 and S7 of grade B.

As for grade A, the Co content is constant between 1.50 mm and 5.94 mm from the outer surface. For this reason, in order to better investigate what happens in and near the surfaces, the Co profiles after cycles S6 and S7 without the area where the Co amount is constant, are shown in Figure V – 23.

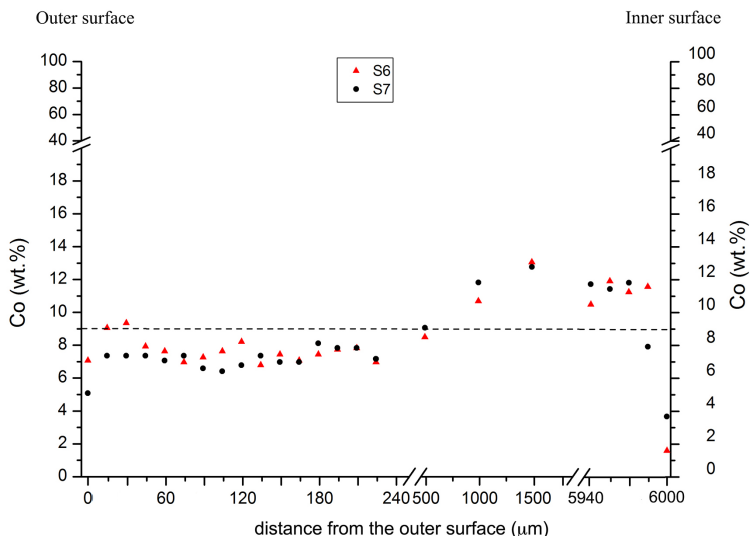


Figure V - 23. Co concentration profiles after cycles S6 and S7 of grade B without the area between 1.50 mm and 5.94 mm.

5.3.2.4 Co migration mechanism

As reported previously, the Co migration is strongly influenced by the carbon gradient in the material. By means of experimental analyses, it was observed that Co migrates from a region with high C amount to a region with lower C content. This confirms what is reported in literature [Fan, 2008; Fan, 2009A; Fan, 2009B; Fan, 2009C; Fan, 2013; Guo, 2010; Konyashin, 2017B; Konyashin, 2016; Sachet, 2013; Sachet, 2012; Taniguchi, 1989] and is in contradiction with the thermal contraction theory [Brooks, 2010; Janisch, 2010].

The solidification temperature [Upadhyaya, 1998] and the wettability of the WC by the liquid binder [Konyashin, 2017A; Konyashin, 2016] are affected by the C content in the liquid Co. The liquid Co with a lower C content solidifies prior than the liquid Co with higher C amount. The thermodynamic driving force for the liquid phase migration is the minimization of the total interfacial energy of the system that is related with the difference between the WC-WC and the WC-liquid Co interfacial energies, as demonstrated in the “liquid migration pressure” [Fan, 2008; Fan, 2009A; Fan, 2009B;

Fan, 2009C; Fan, 2013]. Considering a small liquid Co amount in the material, it leads to the formation of large WC-WC and small WC-liquid Co interfacial areas and, consequently, to a high total interfacial energy. Differently, there are a lot of WC-liquid Co and less WC-WC interfaces in case of high liquid Co content and this brings about a low interfacial energy. Therefore, the liquid migration occurs from areas with high liquid amount to areas with low liquid content to reduce the total interfacial energy. However, an increased C content in solution in liquid Co is responsible for a decreased wettability of WC by liquid Co, namely a decreased capillary pressure [Konyashin, 2017A; Konyashin, 2016]. In this way, the liquid Co migrates from high C regions to low C regions not only because of the different liquid content but also due to the difference in the WC wettability by liquid Co with heterogeneous carbon amount.

From the experimental analyses reported previously, it was observed that the conditions for the Co migration towards the interior of the material act mainly between the outer surface and the core respect to the inner surface and the core. The result is the formation of a Co gradient in the first 1.5 mm between the outer surface and the core and only a surface Co depletion in case of inner surface.

The morphology of the Co layer, which is formed in decarburizing condition and a sintering isothermal holding, is reported in Figure V – 24.

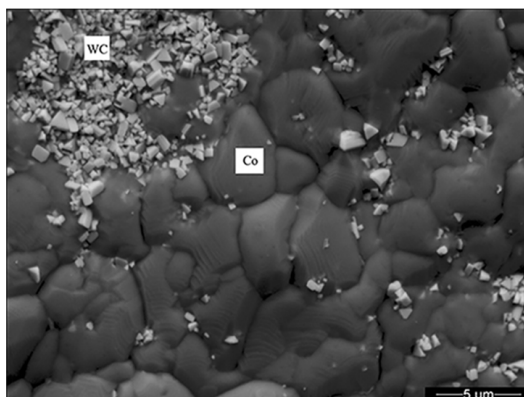


Figure V - 24. Detail of the Co layer morphology.

It is clear that the Co capping occurs with the formation of Co cupules. This is attributed to the minimization of surface energy: the surface/volume ratio of the liquid Co on the surface is reduced by the formation of domes [Sachet, 2013; Sachet, 2012].

It possible to conclude that, the migration of Co towards the surface leads to the formation of a surface Co layer and a Co depletion into all the material without any Co gradient in the near surface region.

5.3.3 Conclusion

The effect of Co amount, dewaxing stage, cooling rate and sintering holding at the sintering temperature in the production of drawing dies on the Co migration were investigated. Two different commercial cemented carbides were studied. The carburizing and decarburizing conditions of the surfaces were obtained by varying the dewaxing step in order to create different carbon gradients between the surface and the core of the material.

Using a cooling media and working on the sintering dwell, the effect of the cooling rate and sintering holding was investigated, respectively.

The conclusions obtained by these experimental analyses may be summarized as follows.

- The melting and solidification intervals of WC-Co are narrower and shifted to lower temperature on decreasing Co amount.
- The decarburizing condition of the surface, which is obtained by a partial dewaxing, brings about the Co layer formation on the WC-Co surface.
- The cooling rate affects the Co layer formation: a lower cooling rate increases the time for the cobalt migration towards the surface, thus increasing Co capping.
- The carburizing condition of the surface, which is obtained by a complete dewaxing stage and a partial surface enrichment due to the graphite of the furnace leads to a surface Co depletion.
- A carburizing condition or a decarburizing condition without the sintering holding brings about to the Co migration towards the interior of the material.
- The liquid Co migration affects not only the surface properties but also the hardness and consequently the fracture toughness of the material.
- In Co capping, since the high surface tension, the liquid Co forms domes on the surface which can extend and leading to the Co layer formation.

Based on these results, it is possible to conclude that the Co migration occurs from a region with higher C amount to a region with lower C content. This is attributed to the fact that the C in solution in the liquid Co affects the solidification temperature and the wettability of WC. Furthermore, if the Co migration occurs towards the surface, the necessity to minimize the surface energy, leads to the surface Co layer formation since the coalescence of the domes.

5.4 Co migration from an industrial point of view

In this subchapter, based on the experimental results reported previously, a typical industrial sintering cycle used for the production of commercial cemented carbides with 6.0, 6.5 and 9.0 wt.% and different hole diameters was modified working on different process parameters. The effects of the modified parameters such as the dewaxing holding, the N₂ flux rate, the cooling media and the pressure of the furnace in the sintering stage, on the Co migration phenomenon, were investigated.

5.4.1 Materials and experimental procedure

Three different WC-Co grades with 6.0, 6.5 and 9.0 wt.% of Co were used in order to produce drawing dies having different hole diameters. The composition details and the different diameters of the holes are summarized in Table V – 4.

Sample	Grade	Φ foro (mm)	Co (wt.%)	WC (wt.%)	Cr C _{3 2} (wt.%)
Grade A _{0.60}	A	0.60	6.5	93.2	0.3
Grade A _{1.60}	A	1.60	6.5	93.2	0.3
Grade A _{2.15}	A	2.15	6.5	93.2	0.3
Grade B _{1.60}	B	1.60	9.0	90.7	0.3
Grade C _{0.60}	C	0.60	6.0	94.0	0.3

Table V – 4. Composition and hole size details of the studied drawing dies.

Green specimens were produced by cold compaction of the three powders by adding 2.0 wt.% of paraffin.

The hole diameter (d_{hole}) refers to the size of the hole in the bearing area of the drawings as shown in Figure V – 22.

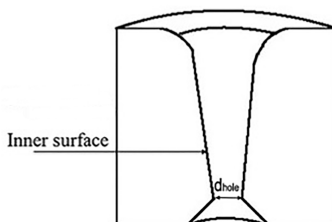


Figure V – 22. Details of the hole diameter, outer and inner surface in the drawings.

Considering the same sintering condition, these samples were selected in order to investigate the possible effect of the drawing die geometry and of the composition on the Co migration phenomenon. The effect of the different hole diameters was investigated comparing the three different drawings of grade A. Differently, the effect of the composition was investigated comparing grade A and B with the same hole diameter of 1.60 mm and grade A and C with the hole diameter of 0.60 mm.

Four different sintering cycles were defined by varying the typical industrial sintering cycle (cycle N) used for the production of grade A, B and C reported in Figure V – 23.

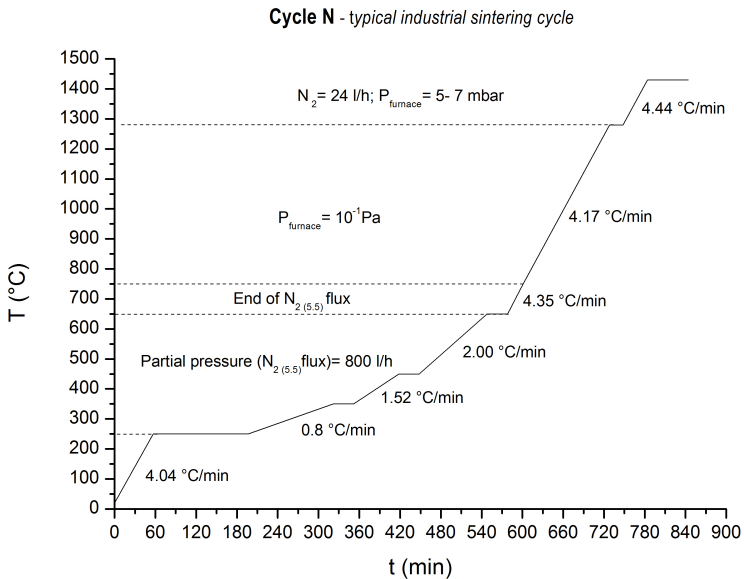


Figure V – 23. Typical industrial sintering cycle used for the production of WC-Co with a low Co content.

The different variation of the cycle N, used for the production of cycles 1, 2, 3 and 4 are summarized as follow.

- Cycle 1. Addition of 1h dwell at 250°C respect to cycle N.
- Cycle 2. During dewaxing stage the N₂ flux rate was increased to 1200 l/h respect to the 800 l/h of the cycle N.
- Cycle 3. Higher cooling rate using Argon respect to the cycle N.

Cycle 4. The furnace pressure during the sintering stage was increased to 10 - 14 mbar respect to the 5 – 7 mbar of the cycles N.

After the different sintering cycles, the Co content on the inner surface of the different drawings, which is the working surface during drawing, was investigated by SEM analysis.

5.4.2 Results and discussion

The different specimens obtained by the sintering cycles N, 1, 2, 3 and 4 were investigated in terms of surface analysis, as shown below.

The surface analysis consists on the comparing, through SEM micrographs, the Co amount on the inner surface of the drawings after the different sintering cycles.

First of all it is important to specify that, from the micrographs taken at the same magnification, the drawings with the same composition and dimension obtained with the different cycles seem to have a different hole diameter even if, actually, it is the same. This is attributed to the different position of the cutting section during the samples preparation.

The comparison between the different inner surfaces for the grade A_{0.60} after cycles N, 1, 2, 3 and 4 is shown in Figure V – 24.

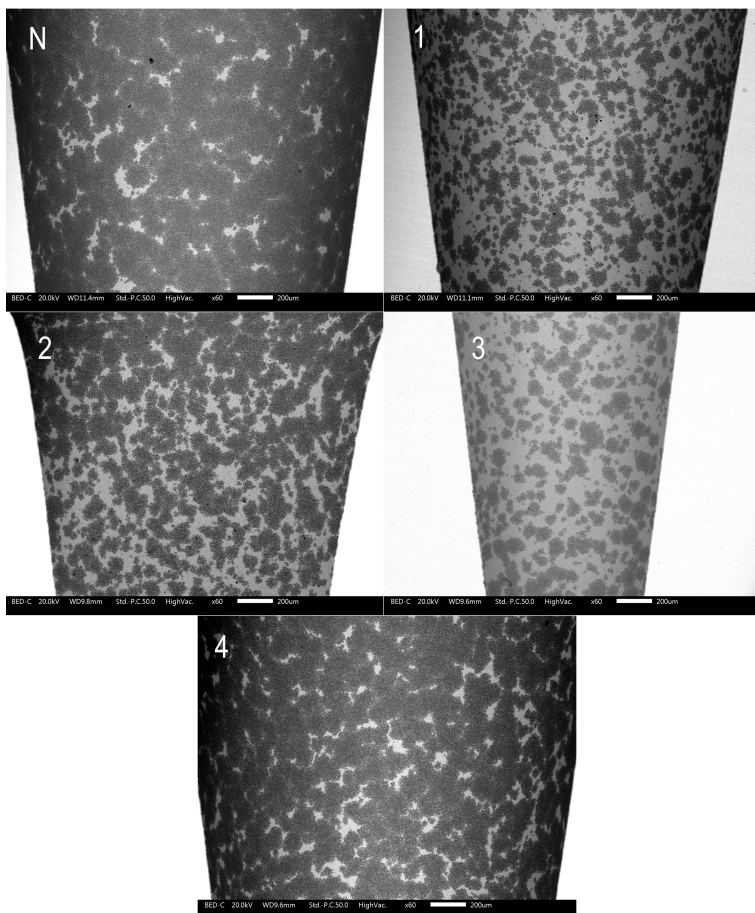


Figure V – 24. Grade A 0.60 inner surface analysis after cycles N, 1, 2, 3 and 4.

Comparing the different inner surfaces, it is evident that the cobalt amount is lower after cycles 1 and 3, slightly increases after cycles 2 and covers almost all the inner surface after cycles 4 and N. The lower Co content after cycles 1 and 3 is related with the long dwell at 250°C that increases the paraffin evaporation and with the higher cooling rate that reduces the time to Co migration towards the surface, respectively. These results are in agreement with the results in the subchapter 5.3.

Furthermore, also the cycle 2 is characterized by a better dewaxing stage since a higher N_2 flux rate. Nevertheless, the effect of the higher flux rate is not so effective as the higher cooling rate or the longer dewaxing holding on the reduction of the Co layer formation, probably since the very small hole diameter. Differently the cycle 4,

even if with a higher partial pressure, presents the same Co content observed after the typical industrial sintering cycle (N). This is justified taken into account that the higher pressure is introduced in the sintering stage when the paraffin evaporation is already finished. For this reason this modification does not act on the Co migration towards the surface.

Considering the grade A_{1.60}, the inner surface analysis regarding the Co content is reported in Figure V – 25.

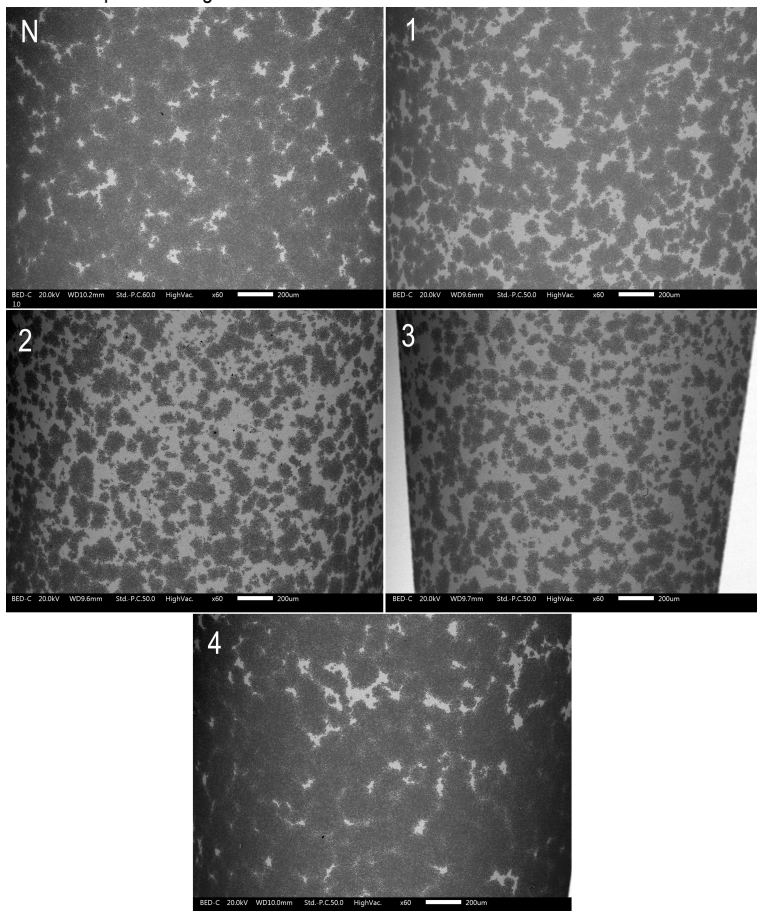


Figure V – 25. Grade A_{1.60} inner surface analysis after cycles N, 1, 2, 3 and 4.

In the grade A_{1.60} the cobalt amount is lower after cycles 2 and 3, slightly increases after cycles 1 and covers almost all the inner surface after cycles 4 and N. This grade after cycles 3, 4 and N shows the same results observed for grade A_{0.60}.

However, differently from the grade A_{0.60}, after the cycle 2, it presents a lower Co content on the surface than the cycle 1, maybe since the wider hole permits a greater effectiveness of the N₂ flux.

Figure V-26 shows the different inner surfaces after cycles N, 1, 2, 3 and 4 for the grade A_{2.15} that is characterized by a wider hole respect to the grade A_{0.60} and grade A_{1.60}.

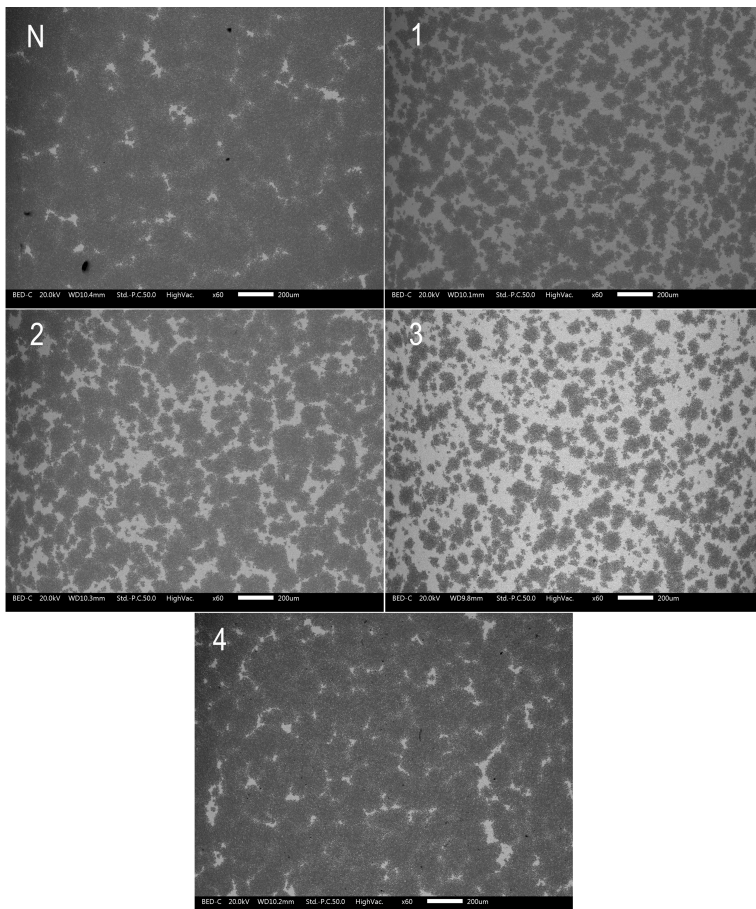


Figure V – 25. Grade A_{2.15} inner surface analysis after cycles N, 1, 2, 3 and 4.

In this grade the cobalt content results lower after cycle 3, slightly higher after cycles 1 and 2 and covers almost all the inner surface after cycles 4 and N. This grade after cycles 4 and N shows the same results observed for grade A_{0.60} and grade A_{1.60}.

Differently, the dewaxing stage of cycle 3 result slightly more effective respect to the cycles 1 and 2, which seem to present the same Co migration. This is probably attributed to the fact that a higher hole permits a more effective cooling stage with Argon that reduce the time for the Co migration. Cycles 1 and 2 present the same Co content maybe since the so wide hole permits a good dewaxing by working both on the dewaxing holding and on the N₂ flux rate.

In conclusion, comparing the different hole diameters with the same composition, same results were observed considering the effect of the cooling rate, the pressure of the furnace during sintering and the traditional cycle. Differently, considering the better dewaxing stage obtained working with a long dewaxing holding or with a higher flux rate, different results were observed. Increasing the hole diameter, the most effective dewaxing stage on the reduction of the Co amount of the surface changes from the one obtained working on the dewaxing holding, the one that is done with a higher N₂ flux rate and both conditions considering the higher hole diameter.

Considering a different composition, the inner surface analysis after cycles N, 1, 2, 3 and 4 for grade B_{1.60} is shown in Figure V – 26.

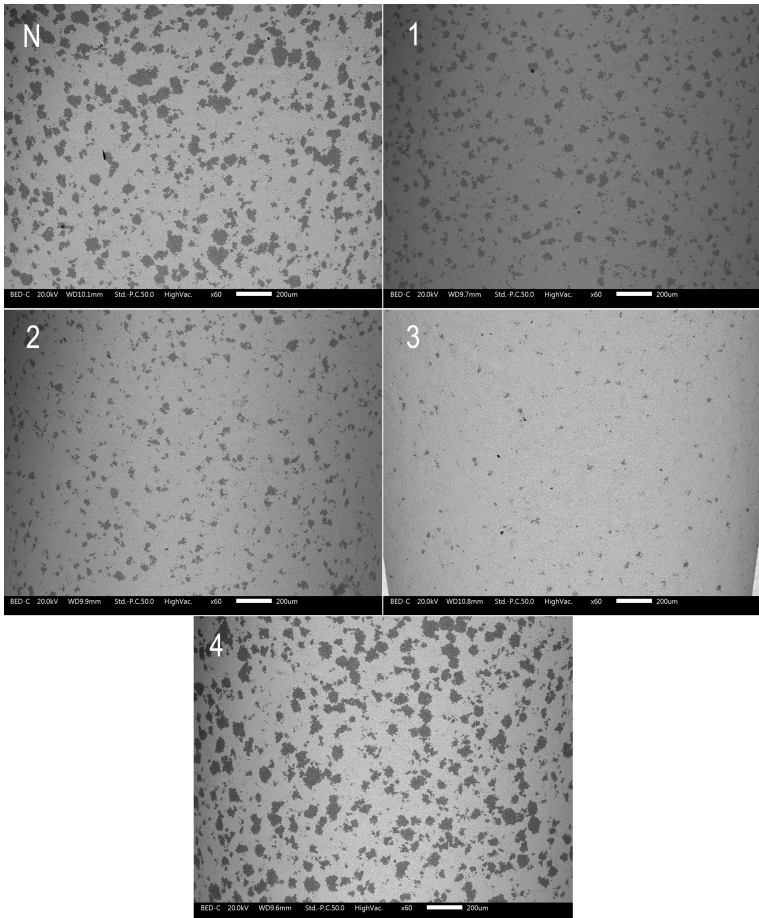


Figure V – 26. Grade B _{1.60} inner surface analysis after cycles N, 1, 2, 3 and 4.

Comparing the grade B _{1.60} with the grade A _{1.60}, there is a little Co content on the inner surface of the grade B _{1.60} drawings after all the different sintering cycles. This is associated with the higher cobalt content of the grade B respect to grade A. Indeed, due to the different composition, the melting and solidification interval are different comparing the two grades, as shown in the Table V – 1 in the subchapter 5.3.2.1. For this reason, the cycles N, 1, 2, 3, and 4 provide little support the Co migration toward the surface.

Nevertheless, comparing the inner surfaces after the different cycles, it is evident that the cobalt content slightly increases by passing from cycle 3 to cycles 1 and 2 and finally to cycles 4 and N as for the grade A _{2.15}. It differs from the grade A _{1.60}, even if with the same hole diameter, probably since the higher cooling rate in cycle 3 acts

mainly on the grade B that is characterized by a smaller solidification interval as shown in Table V – 1 in the subchapter 5.3.2.1.

The Co migration phenomenon after the different cycles in grade C_{0.60} is shown in Figure V – 27.

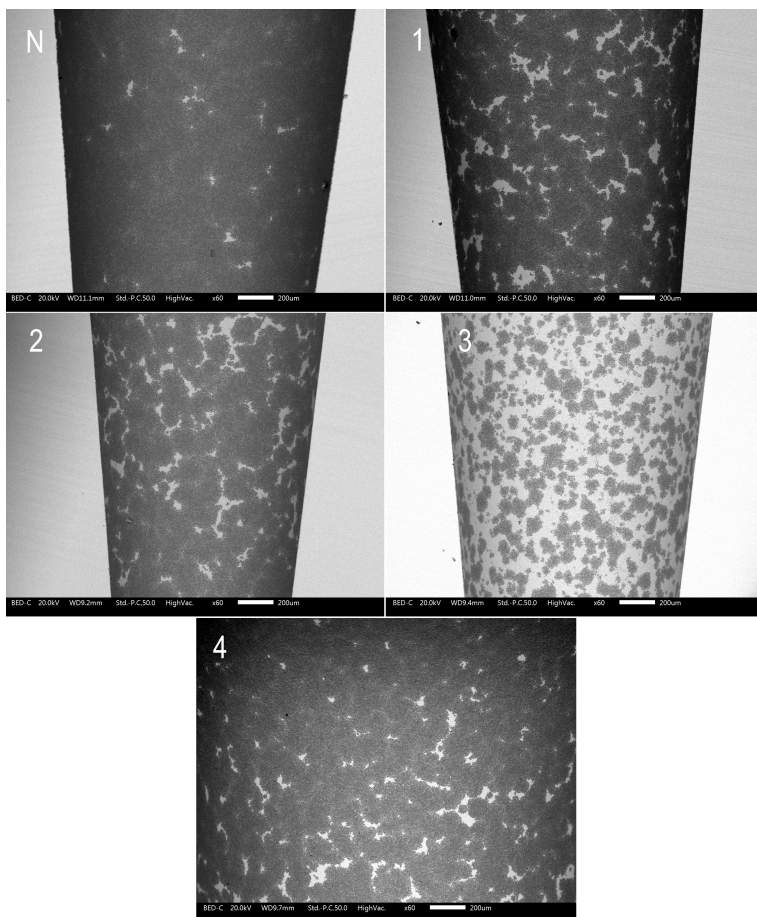


Figure V – 27. Grade C_{0.60} inner surface analysis after cycles N, 1, 2, 3 and 4.

Comparing the grade C_{0.60} with the grade A_{0.60}, there is a slightly higher Co content on the inner surface of the grade C_{0.60} drawings after all the different sintering cycles. This is associated with the slightly lower cobalt content of the grade C respect to grade A that affects the melting and solidification interval of the part.

In this grade, the cobalt content results lower after cycle 3, slightly higher after cycles 1 and 2 and covers almost all the inner surface after cycles 4 and N. This grade after cycles 4 and N shows the same results observed for grade A_{0.60}. Differently, the dewaxing stage of cycle 3 result slightly more effective respect to the cycles 1 and 2, which seem to present the same Co migration as for grade A_{2.15}. In case of grade A_{2.15} this maybe has been associated with the higher hole that permits a more effective cooling stage with Argon. Differently, in case of grade C_{0.60} it could be associated with a slightly lower Co content that slightly increases the width of the solidification interval and consequently gives more time to Co migration towards the surface.

In conclusion, comparing the three different compositions, the material with 9.0 wt.% of Co presents a very small amount of Co on the inner surface. Differently, a great Co content, which is slightly higher in grade with 6.0 wt.%, is present on the surface of grade with 6.0 and 6.5 wt. % of Co. This is associated with the influence of the Co content on the melting and solidification interval of the cemented carbide as shown in the subchapter 5.3.2.1.

Considering the effect of the different sintering parameters, it is possible to conclude that in all materials, the cycles 3, which has a higher cooling rate respect to cycle N, is responsible for a lower Co migration towards the surface. Differently, the typical sintering cycle N and the cycle 4, which is characterized by a higher partial pressure during sintering, resulting in the more effective in terms of Co capping. Considering the cycles 1 and 2, they act in a different way considering different compositions and hole dimensions.

5.4.3 Conclusion

The effects of the Co content, hole diameter of the drawing die, dewaxing stage, cooling rate and the pressure of the furnace during a typical industrial sintering cycle in the production of commercial WC-Co drawing dies, were investigated. The effect of a better dewaxing stage was studied by increasing the dewaxing holding or the N₂ flux rate during the dewaxing stage. Differently, a different cooling media was used in order to investigate the effect of the cooling rate. At the end, the effect of a different pressure of the furnace during the sintering holding on the Co migration was investigated.

The conclusion obtained by these analyses may be summarized as follows.

- Considering the effect of the cooling rate, the cycle with a higher cooling rate reduced the Co layer formation on the inner surface confirming what has been already demonstrated in the subchapter 5.2.
- Considering the traditional cycle and the higher pressure of the furnace during sintering, no differences were observed. This is justified taken into account that the higher pressure during sintering stage does not affect the paraffin

evaporation that is already finished and therefore no effect on the Co migration towards the surface was observed.

- Considering the different dewaxing conditions, obtained working on the dewaxing dwell or on the flux rate, they act in a different way on the Co migration depending on the composition and hole diameter.
- Considering the same composition with different hole diameters, same results were observed considering the effect of the cooling rate, the pressure of the furnace during sintering and the traditional cycle. Differently, considering the better dewaxing stage obtained either with a long dewaxing holding or with a higher flux rate, different results were observed. Increasing the hole diameter, the most effective dewaxing stage on the reduction of the Co content on the surface changes from the one obtained working on the dewaxing holding, the one that is done with a higher N₂ flux rate and both conditions considering the higher hole diameter.
- Considering the effect of the compositions, increasing Co content, the solidification interval is reduced giving less time to liquid Co to migrate towards the surface leading to a lower Co content on the surface.

From these results, it is possible to conclude that all results obtained in the subchapter 5.3 are confirmed but, considering an industrial process, the effect of the different composition is more pronounced and the geometry of the drawing die acts an important role in the Co capping.

Chapter VI

Thermal fatigue and oxidation behaviour of cemented carbide

Part of this chapter has been published in:

L. Emanuelli, M. Pellizzari, A. Molinari, F. Castellani, E. Zinutti,
“**Thermal fatigue behaviour of WC-20Co and WC-30(CoNiCrFe) cemented carbide**”,
Int. Journal of Refractory Metals and Hard Materials 60 (2016), p. 118–124.

L. Emanuelli, M. Pellizzari, A. Molinari, F. Castellani, E. Zinutti,
Reprint of “**Thermal fatigue behaviour of WC-20Co and WC-30(CoNiCrFe) cemented carbide**”,
Int. Journal of Refractory Metals and Hard Materials 62 (2017), p. 176-182.

In applications, where cyclic temperature variations are present, important damage phenomena that must be taken into account are Thermal Fatigue (TF) and oxidation. Indeed, in cemented carbide, the high difference in thermal expansion coefficients between the binder and the hard phase leads to the formation of high stresses that promote the nucleation and propagation of TF cracks. The WC-Co is typically used for its excellent wear resistance since the high hardness. Nevertheless, in high temperature applications the material needs also to guaranty a certain level of fracture toughness in order to increase the resistance to the nucleation and propagation of cracks. For this reason, the common WC-Co used for the hot applications is characterized by a high Co amount and D_{wc} . Moreover, in hot applications, due to the high temperature and the presence of a cooling media, also the oxidation phenomena must be taken into account.

In this chapter, TF and oxidation behaviour of two typical commercial cemented carbides used in case of hot applications were studied. The TF damage was evaluated by means of a custom test configuration inducing a biaxial state of stress. The oxidation behaviour was measured by ThermoGravimetric Analysis (TGA) and the results were compared with the oxides formed on the surface of samples after TF test. Possible correlations between the TF and oxidation damages were investigated.

6.1 Introduction

In hot applications, since the rapid temperature variations, cemented carbide parts undergo TF damage. Milling is an example of thermo-mechanical cyclic loads, which lead to the formation of comb cracks perpendicular to the cutting edge in the hardmetal component [Klocke, 2011]. J. García et al. widely investigated this kind of damage

[García, 2015]. TF, that is a typical oligo-cyclic fatigue phenomenon [Weronki, 1991], promotes the initiation of a fine crack network also called heat cracking, on the surface with small penetration depth. In most cases, heat-cracking affects the tool surface finishing and consequently the worked material surface. TF damage alone leads rarely to the catastrophic failure, while together with a secondary damage phenomenon, such as wear or contact fatigue, enhances crack propagation and promotes a untimely loss of structural integrity. The TF damage could be prevented or delayed by the selection of a most appropriate material or/and by the development of best operational practices.

Based on the theory of thermo-elasticity and fracture mechanics, the maximum allowable temperature difference (ΔT) in a body under quick cooling condition [Li, 2009] and the thermal shock (TS) resistance (R_{TS}) of cemented carbides [Santhanam, 1990; Upadhyaya, 1998] is defined by the equation [6.1] and [6.2] respectively.

$$\Delta T = \sigma_m \cdot (1 - \nu) / E \cdot \alpha \quad [6.1]$$

$$R_{TS} = \sigma_m \cdot (1 - \nu) \cdot \lambda / E \cdot \alpha \quad [6.2]$$

Where σ_m is the transverse rupture strength (TRS), ν is the Poisson's ratio, λ is the thermal conductivity, E is Young's modulus and α is the coefficient of thermal expansion. Even if these equations are often used to predict the TF resistance, it is necessary not to confuse the TS with TF. Indeed, a repeated temperature variation, as repeated quenching, leads to a different final damage respect to the simple quenching of material and this is not taken into account in these equations. For this reason, the values of ΔT and R_{TS} obtained by these equations are not in agreement with the experimental results obtained by a repeated quenching [Ezquerria, 2017].

Tumanov et al. [Tumanov, 1966] investigated cemented carbides under repeated TS created by immersion of a preheated specimen in a cooling media and found that the different thermal expansion coefficients of Co and WC cause the accumulation of micro-stresses in the material. A Co content reduction decreases the TS resistance since the increase in tensile stresses in the metal matrix. Lagerquist [Lagerquist, 1975] studied The TF damage of cemented carbide in hot roll and concluded that higher cobalt content and WC grain size increase the nucleation of new cracks but decrease their propagation rate. They found that the effect of grain size becomes relevant only in case of low cobalt amount.

The common fracture modes that take place in WC-Co are cleavage of WC particles, fracture at the WC/Co interface and WC/WC grain boundary, and shear fracture of binder phase. Increasing the WC grain size, the ratio of transgranular/intergranular fracture of WC increases [Upadhyaya, 1998]. In cemented carbides, cracks nucleate at the surface and propagate preferentially at the WC/WC grain boundary and the WC/Co interface.

In literature is observed that thermal cracking proceeds by nucleation, growth and aggregation of micro-voids at the interface between WC/Co [Ning, 1997]. The overall damage resulted proportional to the maximum temperature during thermal cycling and more evident cracks are present with a higher cooling rate. This behaviour is confirmed by studying cemented carbide with a composition of 72WC-8TiC-8TaC-2NbC-10Co. In this material, the cracks mostly propagate through the metal binder or at the interface with the WC phase, following a zigzag path [Ishihara, 1999].

The other important damage that must be considered in applications where high temperatures are reached is the oxidation. Most of authors investigated the oxidation resistance of WC-Co alloys in the temperature range between 500-1000°C in different atmospheres (air, Ar/O₂ mixture or O₂) [Basu, 1996; Bhaumik, 1992; Casas, 2001; Del Campo, 2009; Gu, 2012; Voitovich, 1996]. In all the works, WO₃, CoWO₄ and Co oxides were observed. The oxidation resistance of cemented carbide increases by increasing the binder content since the formation of a higher amount of CoWO₄, which is denser and more protective than the WO₃. It was also demonstrated that the oxidation of Co occurs before that of WC since its faster oxidation kinetics [Chen, 2015]. The effect of partial and complete substitution of Co by Ni on the oxidation resistance of cemented carbide was investigated [Voitovich, 1996]. In the temperature range between 500 and 800°C the oxidation of Co is faster than that of Ni. In this condition, the addition of Ni reduces the oxidation resistance of cemented carbide since WO₃ becomes the main oxidation product. The oxidation resistance increases with the binder content but decreases on increasing the Ni/Co ratio as confirmed also by Aristizabal et al. [Aristizabal, 2009; Aristizabal, 2010; Aristizabal, 2011]. Nevertheless, this negative effect of the substitution of Ni is negligible in case of 15 wt.% binder and becomes important at 25 wt.% binder.

As mentioned before, a few data are available in literature on the TF resistance of cemented carbides with high Co content. Moreover, no author has investigated the combination of TF and oxidation damage in cemented carbides. For this reason, in this Chapter, TF and oxidation resistances of two typical commercial cemented carbides used in hot applications were investigated.

6.2 Materials and experimental procedure

Two different commercial cemented carbides containing 20wt.%Co (WC-20Co) and 19wt.%Co-9.5wt.%Ni-1wt.%Cr-0.5wt.%Fe (WC-30CoNiCrFe) were selected for present investigation. Using the method explained in Chapter III, a complete microstructural characterization with the determination of D_{wc} , λ and C was carried out. Murakami's reagent (100 ml distilled water, 7g KOH, 7g K₃[Fe(CN)₆]) [Petzow, 1999], was used for selective etching of WC particles. The composition of the two materials was investigated by EDXS.

TF tests were carried out by means of a test configuration that induce a biaxial state of stress and the experimental configuration is shown in details in Figure VI- 1 [Pellizzari, 2013].

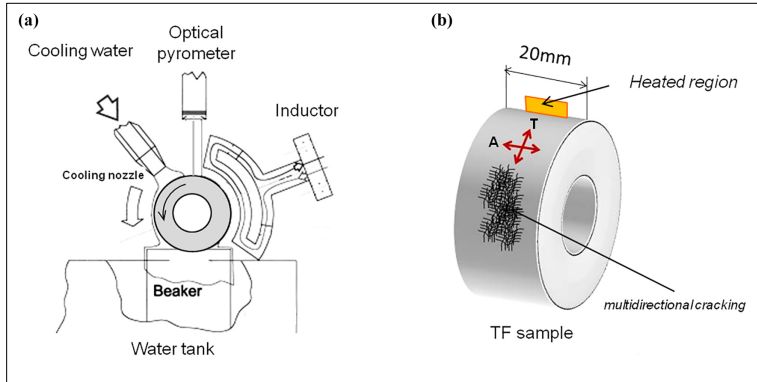


Figure VI- 1. Customary rig used for TF cracking (a). TF sample showing multiaxial stress state (T=tangential, A=axial) and multidirectional thermal cracking (b).

This test configuration consists in the induction heating (100 kHz) up to 600°C and, subsequently, in the cooling down to 80°C by a water jet (18°C, 2 l/min) of a surface of a disc specimen, which rotates at 4rpm. The maximum temperature of 600°C at the exit of the inductor, monitored by an infrared pyrometer, was defined considering the typical temperature reached in many commercial applications involving rapid temperature variations. Geometry of the disc specimen is reported in Figure VI - 2.

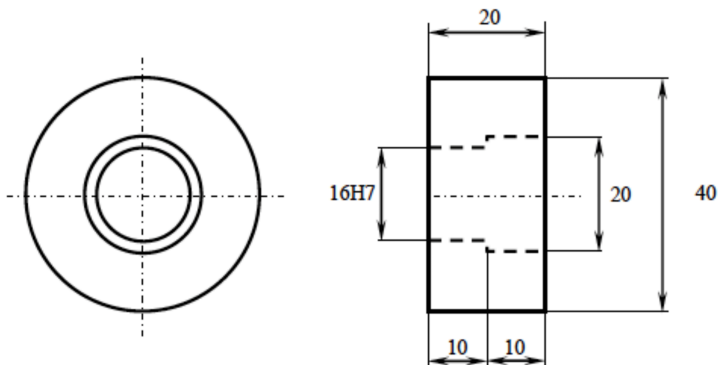


Figure VI- 2. Geometry of the TF disc specimen with dimension values in mm.

In hot applications, even if working temperature is much higher than 600°C, since the very short contact time, thermal equilibrium conditions cannot be reached. Furthermore, according to literature, 600°C is the maximum operating temperature of cemented carbides, because of the significant decrease of mechanical strength and hardness above this temperature [Lee, 1983]. During the TF tests, the temperature gradients are induced in tangential and axial direction since the heating was limited to a portion of the outermost surface, individuated by an angle of 105° and 10mm width. The resulting biaxial state of stress leads to the formation of a crack network, as observed in many components undergoing TF during service.

The first test underlines that the formation of TF cracks started to be visible at 1300 cycles on the WC-30(CoNiCrFe) surface. Indeed, to monitor the damage evolution, TF tests were carried out up to 3000 cycles, with interruptions after 1300 and 2000 cycles. A quantitative image analysis on more than ten SEM images of the surface is used in order to evaluate the thermal cracking.

An automated image-processing route was set up using a Leica Qwin software in order to measure the total crack length and the number of the cracks for each SEM micrograph as shown in Figure VI - 3.

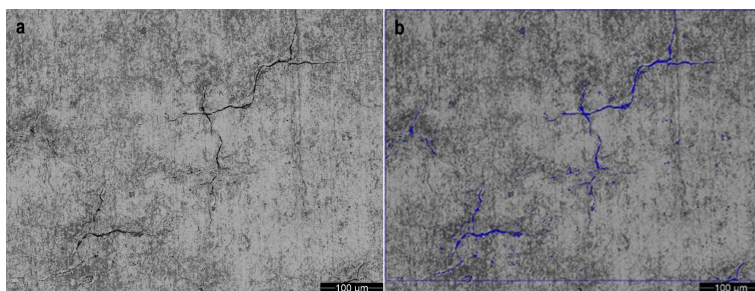


Figure VI- 3. TF cracks (a) and elaboration of the damage by Leica Qwin software (b).

With this software, the mean surface crack length (total surface crack length divided by the number of cracks) and the crack density (number of cracks divided by the reference area) were evaluated.

The metallographic cross section of the sample by SEM was used in order to investigate also the damage mechanisms and the oxidation phenomena. The surface region and the oxide scales were preserved from damage during cutting and metallographic preparation by nickel-plating.

Oxidation kinetic was evaluated by means of TGA: the two cemented carbides were oxidized isothermally in an air flux at 500°C, in order to investigate the oxidation

process in case of a lower kinetic, and at 600°C, which is the maximum TF test temperature, for 2h.

According to UNI EN ISO 6507, hardness tests (HV10) were carried out on the cross section of the specimens after TF test in order to evaluate any possible thermal softening of the cemented carbides.

6.3 Results and discussion

6.3.1 Microstructural analysis

As explained in Chapter III, with the linear intercept method applied on the micrographs of the two commercial cemented carbides show in Figure VI- 4, the microstructural parameters D_{wc} , C and λ are measured and reported in Table VI - 1.

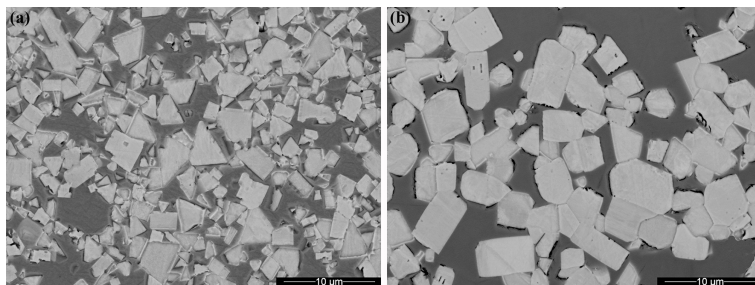


Figure VI- 4. WC-20Co (a) and WC-30(CoNiCrFe) (b) SEM micrographs.

Grade	D_{wc} (μm)	C (-)	λ (μm)
WC-20Co	2.65	0.53 ± 0.10	1.41 ± 0.19
WC-30(CoNiCrFe)	4.71	0.43 ± 0.11	3.54 ± 0.41

Table VII – 1. Microstructural parameters of WC-20Co and WC-30(CoNiCrFe).

Analysing the microstructural parameters it is evident that increasing the binder content and the D_{wc} , the mean binder free path increases and contiguity decreases, since the carbide spatial coincidence decreases as demonstrated in Chapter III.

6.3.2 TF damage

Figure VI- 5 shows the surface TF cracking for WC-20Co and WC-30(CoNiCrFe) after 1300, 2000 and 3000 cycles.

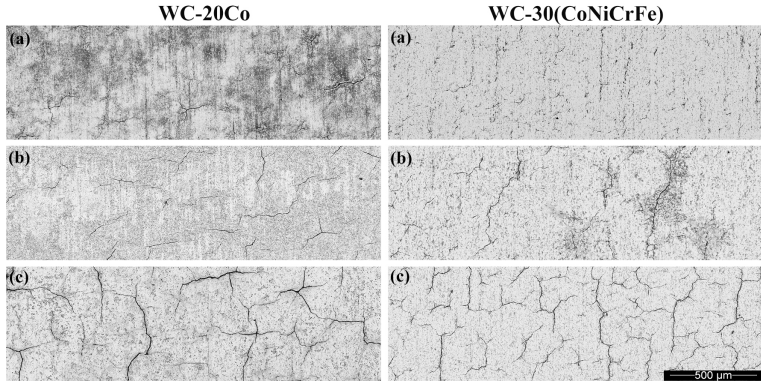


Figure VI- 5. Surface TF cracking for WC-20Co and WC-30(CoNiCrFe) after 1300 (a), 2000 (b) and 3000 (c) cycles.

The surface analysis underlines that, after the nucleation of TF cracks, the crack network propagates on increasing the number of cycles. Indeed, TF leads to the nucleation and propagation of cracks. After a certain number of cycles, an increase in the crack density and in the mean crack length leads to the formation of a mesh. Comparing the two different compositions, WC-30(CoNiCrFe) is characterized by a higher nucleation rate and lower crack propagation respect to the WC-20Co. For this reason, the TF damage of WC-30(CoNiCrFe) starts with the formation of many small cracks slightly branched and only at 3000 cycles, the formation of a mesh occurs due to an increased crack density and a reduced propagation rate. Differently, on the surface of WC-20Co, which presents a high propagation rate to the detriment of a low nucleation rate, a reduced number of long branched cracks is formed after 1300 cycles. Moreover, increasing the number of cycles, the crack density does not change while the mean crack length and ramification increase. Already after 2000 cycles, cracks start to be interconnected and, at 3000 cycles, form a mesh. It is clear that, the high propagation rate in case of WC-20Co leads to a large crack extension on the surface and in depth.

Figure VI - 6 shows the variation of mean crack length with the number of cycles.

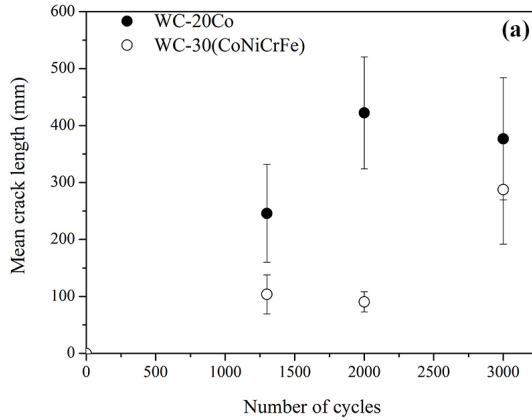


Figure VII – 6. Mean crack length vs number of cycles.

It is evident that the mean crack length increases with of the number of cycles, but the increase until 2000 cycles is higher in the case of WC-20Co. Indeed, after 2000 cycles, WC-30(CoNiCrFe) shows a quick increase while WC-20Co shows a plateau. Differently, after 3000 cycles the two materials present similar mean crack length.

Another important parameter that must be considered in the TF damage is the mean crack density as shown in Figure VI– 7.

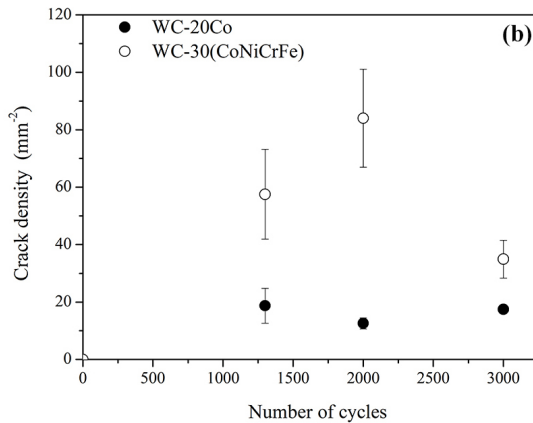


Figure VII – 7. Mean crack density vs number of cycles.

After an initial transient period, the crack density in WC-20Co reaches a steady value, whilst; in WC-30(CoNiCrFe), it increases up to a maximum and then decreases. This is

justified taking into account the increase in toughness provided by the increase in the binder content, which results in a lower propagation rate. Indeed, this condition promotes the possible nucleation of new cracks, since shorter cracks preserve the local constraint inducing higher thermo-mechanical stresses [Ning, 1997].

In other words, the propagation of long thermal cracks allows the free deformation in their neighbourhood and avoids the nucleation of new cracks, as confirmed by the inverse correlation between mean crack length and crack density shows in Figure VI– 8.

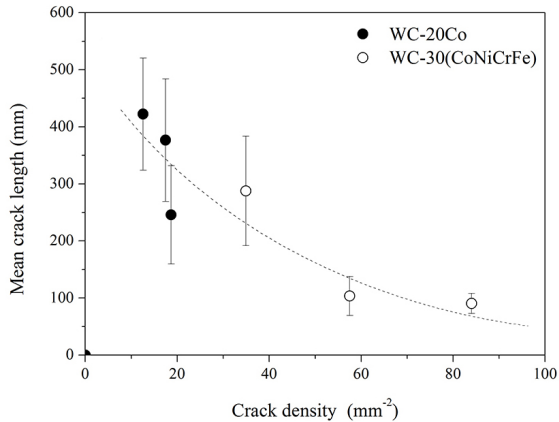


Figure VI– 8. Correlation between mean crack length and crack density.

This behaviour is justified considering the influence of microstructure on the crack density and the mean crack length. A decrease of the contiguity and an increase in the mean binder free path brings about a reduction of the crack length and an increase of the crack density (Table VI - 2).

Grade	D_{WC} (μm)	C (-)	λ (μm)	TF crack nucleation	TF crack propagation
WC-20Co	2.65	0.53 ± 0.10	1.41 ± 0.19	low	high
WC-30(CoNiCrFe)	4.71	0.43 ± 0.11	3.54 ± 0.41	high	low

Table VII – 2. Microstructural parameters and TF behaviour of WC-20Co and WC-30(CoNiCrFe).

Figure VI - 9 shows the two specimen cross-sections after 3000 cycles, to underline the cracks propagating in depth and the crack width.

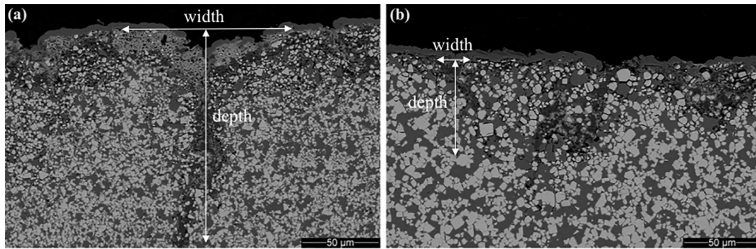


Figure VI- 9. WC-20Co (a) and WC-30(CoNiCrFe) (b) penetration depth of TF cracks after 3000 cycles.

From these micrographs, it is clear that the WC-20Co is characterized mainly by straight sharp cracks whilst the WC-30(CoNiCrFe), since the slow propagation, exhibits more tortuous crack paths. This is widely confirmed by the higher penetration depth and the larger crack width measured in WC-20Co than in WC-30(CoNiCrFe) as shown in Table VI - 3. These data extend the result obtained for the surface crack propagation to the in depth propagation. As a matter of fact, a higher penetration depth means a low crack density because of a reduction of the local constraint.

Grade	Depth (μm)	Width (μm)
WC-20Co	142 ± 25	22 ± 12
WC-30(CoNiCrFe)	70 ± 14	16 ± 5

Table VII – 3. The penetration depth and the width of the cracks after 3000 cycles for WC-20Co and WC-30(CoNiCrFe) cemented carbides.

Another important point that it is evidenced by micrographs reported in Figure VII – 9 is that, decreasing the binder content, cracks propagate approximately parallel to the temperature gradient, i.e. perpendicular to the external surface. Differently, an increase of the binder amount brings about deviations and branching of cracks [Lagerquist, 1975]. In this condition, the slower propagation gives time to a stronger interaction with oxidizing phenomena, as evidenced in the next subchapter.

The main propagation mechanisms in WC-20Co and WC-30(CoNiCrFe) are shown in the micrographs reported in Figure VI– 10.

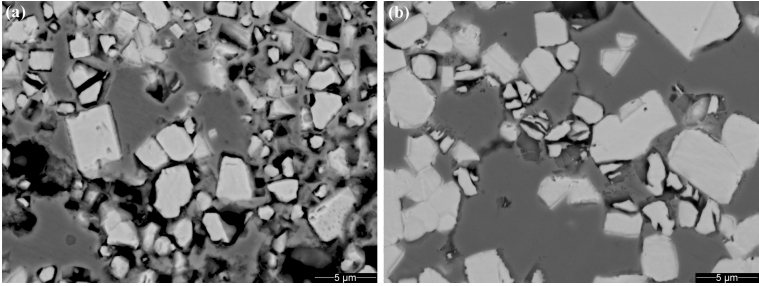


Figure VI- 10. WC-20Co (a) and WC-30(CoNiCrFe) (b) propagation mechanisms after 3000 cycles.

From Figure VI- 10 a, it is clear that the main fracture mechanisms in WC-20Co are the crack propagation at the WC/WC grain boundary and at WC/Co interface. On the other hand, in WC-30 (CoNiCrFe) prevails the cleavage fracture of WC particles and shear fracture of binder phase, as shown in Figure VI- 10 b. This different behaviour is explained considering that the ratio of transgranular/intergranular fracture of WC increases with a rise of the WC grain size [Upadhyaya, 1998]. Differently, increasing the binder content, cracks are more often forced to propagate in the binder phase due to a reduction of the contiguity and of a higher mean binder free path [Lagerquist, 1975] as mentioned in the Chapter III. In view of this evidences, it is more understandable the influence of the microstructure on the correlation between the mean crack length and the mean crack density shown in Figure VI - 8.

The possible softening effect due to the high temperature reached is measured by HV10 hardness profile as shown in Figure VI- 11.

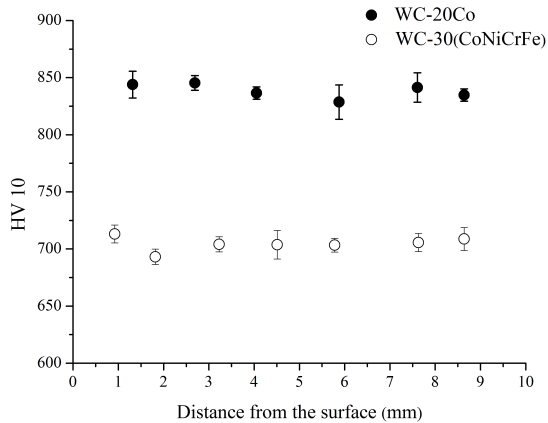


Figure VI- 11. Hardness profiles from the surface to the core for WC-20Co and WC-30(CoNiCrFe).

From the hardness profiles of WC-20Co and WC-30(CoNiCrFe) it is evident that there is no softening effect due to the high temperature reached. This means that the TF damage is not correlated with a decrease of mechanical properties due to high temperature.

6.3.3 Oxidation behaviour

TGA at 500°C and 600°C for 2h was carried out in order to investigate the possible effect of the oxidation on the TF damage. The oxidation kinetics at the different temperatures of WC-20Co and WC-30(CoNiCrFe) are reported in Figure VI– 12.

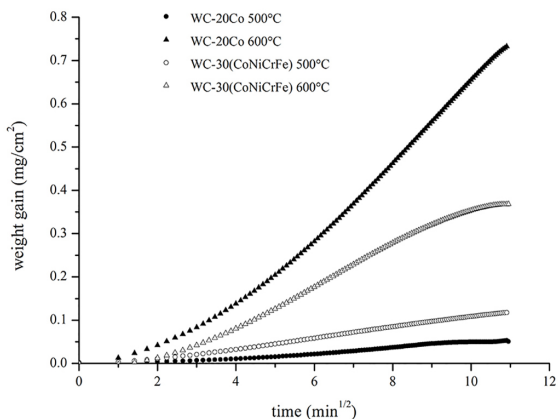


Figure VI– 12. Oxidation kinetics of WC-20Co and WC-30(CoNiCrFe) at 500 and 600°C.

It is evident that the oxidation follows a parabolic kinetic. At 500°C the curves of the two materials are very similar and the oxidation rate is very low. Differently, at 600°C, WC-20Co is characterized by a higher oxidation rate.

In Table VI– 4 are reported the parabolic constants calculated as the higher slope of all curves.

$T_{oxidation}$ (°C)	WC-20Co [mg ² /(cm ⁴ min)]	WC-30(CoNiCrFe) [mg ² /(cm ⁴ min)]
500	0.11E-03	0.15E-03
600	8.30E-03	2.44E-03

Table VI– 4. Parabolic rate constant of WC-20Co and WC-30(CoNiCrFe) at 500°C and 600°C.

The oxidation resistance of cemented carbide depends on the binder amount and composition [Aristizabal, 2009; Aristizabal, 2010; Aristizabal, 2011]. As reported in literature, a decrease in the binder amount and a partial or complete substitution of Co with Ni lead to a reduced oxidation resistance. These results highlight that, even if a partial substitution of Co with Ni in WC-30(CoNiCrFe), the higher binder content leads to higher oxidation resistance.

The cross-sections and EDXS analysis of the two materials after 3000 cycles are investigated in order to define the oxide scales form and find a possible interaction between TF and oxidation.

Figure VI– 13 shows the cross-section of WC-20Co and the EDXS analysis of the formed oxides.

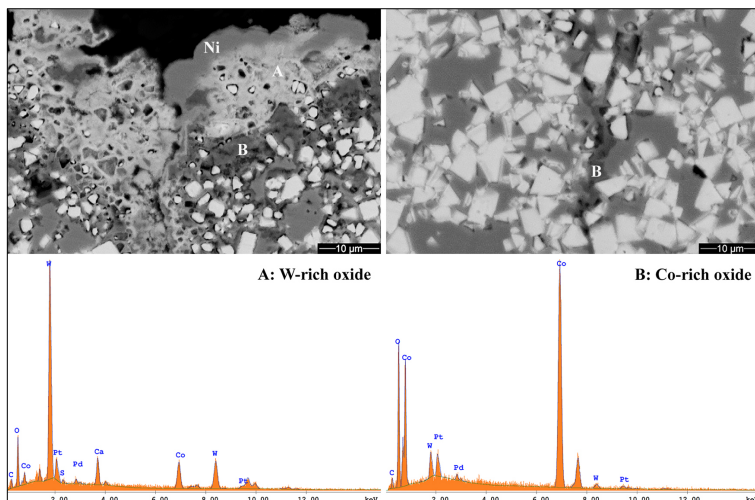


Figure VI– 13. Cross-sections of WC-20Co after 3000 cycles of TF test and the oxide composition patterns.

Two types of oxide are recognized in WC-20Co, namely a W-rich light grey oxide (WO_3), and a Co-rich dark grey oxide ($CoWO_4$). It is evident that the W-rich oxide mostly fills the deeper region of the crack while the Co-rich oxide covers the outermost crack surface. This behaviour is attributed to the fact that the Co oxidation occurs before that of WC [18].

Differently, Figure VI– 14 shows the cross-section of WC-30(CoNiCrFe) and the EDXS analysis of the formed oxides.

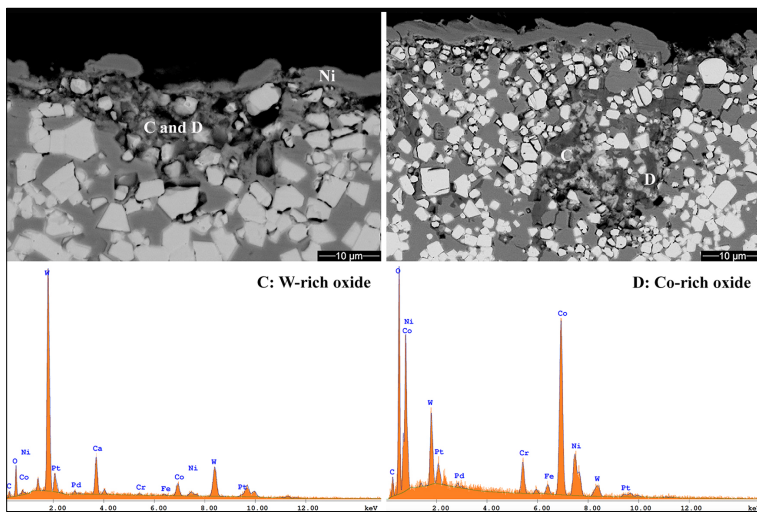


Figure VI- 14. Cross-sections of WC-30(CoNiCrFe) after 3000 cycles of TF test and the oxide composition patterns.

In WC-30(CoNiCrFe), the presence of Ni is not able to moderate the rate of oxygen interaction with WC [16] and a mixture of the two oxides is present into the crack of WC-30(CoNiCrFe). For this reason, even if increasing the binder amount the WO_3 amount decreases, the amount of this oxide is higher than in the case of WC-30Co.

6.3.4 Correlation between TF and oxidation

Considering the correlation between TF and oxidation, WC-30Co seems to be characterized by a greater amount of oxide inclusions rather than cracks. This is attribute to the slower crack propagation that induces a stronger interaction with oxidizing phenomena. Differently, on the surface of WC-20Co are present oxide rich cracks rather than oxide inclusions since faster crack propagation. For this reason, the WC-20Co oxidation at 600°C, that is characterized by a higher oxidation kinetics, can be responsible for such a high propagation rate.

This statement is confirmed by the Pilling Bedworth ratio (PBR) [Pilling, 1923] of WC-Co oxides that are > 1 [Basu, 1996; Bhaumik, 1992; Casas, 2001; Del Campo, 2009]. This means that the volume expansion due to the formation of both oxides, namely the WO_3 and the $CoWO_4$, inside the crack induces an additional tensile state at crack tip.

The PBR of the two main WC-Co oxides, calculated using the equation [6.3], is equal to 3.33 and 2.25 for WO_3 and $CoWO_4$, respectively.

$$PBR_{M1_nM2_mO_x} = \frac{V_{oxide}}{V_{metal}} = \frac{MW_{M1_nM2_mO_x}}{\delta_{M1_nM2_mO_x}} \cdot \left(\frac{\delta_{M1}}{n \cdot MW_{M1}} + \frac{\delta_{M2}}{m \cdot MW_{M2}} \right) \quad [6.3]$$

where $M1_nM2_mO_x$ is the generic oxide composed by two different metal M1 and M2, V refers to volume, MW is the molecular weight and δ is the density.

When the oxides are formed, the higher PBR of WO_3 causes a higher additional tensile state at crack tip respect to the $CoWO_4$. For this reason, it is clear that a higher propagation rate in the WC-20Co is firstly due to lower binder content but also due to higher oxidation rate and to greater amount of WO_3 .

In conclusion, an oxide induced crack propagation mechanism is confirmed.

Schematization of TF and oxidation behaviour of WC-20Co and WC-30(CoNiCrFe) is shown in Figure IV -15.

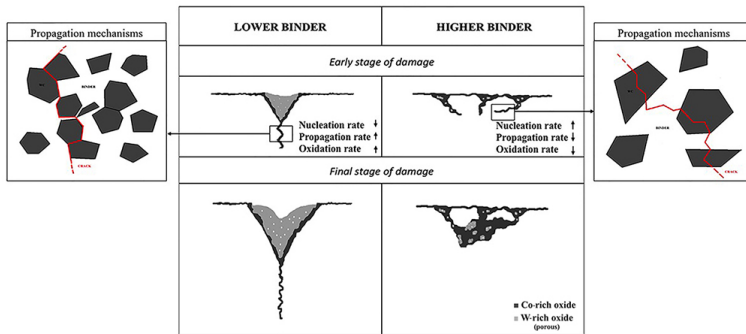


Figure VI- 15. Binder amount influence on TF and oxidation behaviours in WC-Co.

6.4 Conclusion

The TF and oxidation behaviours of two commercial WC-Co grades with different amount of binder, composition and WC grain size were investigated. The overall conclusions of this study may be summarized as follows.

- An increase in the WC grain size leads to a variation of the main crack propagation mechanism changes from an intergranular to a transgranular fracture of the WC.
- The crack propagation rate increases by decreasing the binder content. This condition avoids the nucleation of new cracks due to a reduction in the local constraint close to the crack.

- An oxidation induced crack propagation mechanism is confirmed, especially in WC-20Co, since a higher oxidation rate and the formation of a higher amount of WO_3 , which is characterized by a higher PBR.

From a practical point of view, is preferable to have a high crack density and low mean crack length. Indeed, the removal of cracks by wear phenomena or grinding is easier in case of short cracks and the risk to have catastrophic failure is lower. From this viewpoint, WC-30(CoNiCrFe) has a better TF behaviour that WC-20Co.

Chapter VII

Conclusions

From literature, it is well known that the mechanical properties of WC-Co are strongly related to the microstructural characteristics, namely the mean binder free path and the carbide contiguity. This PhD thesis stems with the purpose of understanding if the mechanical properties of WC-Co could be really defined by these microstructural parameters also in case of parts taken from industrial production. First of all, the influence of the contiguity and the mean binder free path on the mechanical properties of cemented carbides applied to the production of wire drawing dies was investigated. The conclusion of the first part of this PhD thesis may be summarized as follows.

- Among the two microstructural parameters investigated, only the mean binder free path displays the known correlation with hardness and fracture toughness. Differently, the carbide contiguity does not display the known correlation with mechanical properties since the high standard deviations, the microstructural fineness and also the high carbide grain size scatter. Therefore, only the mean binder free path results efficient in order to define the hardness and fracture toughness of industrial production.
- Differently from hardness and fracture toughness, the mechanical strength is influenced not only by the mean binder free path but also by the residual microporosity, that is a feature not easy to control in industrial production.

In conclusion, only the mean binder free path is a good characteristic to define the hardness and the fracture toughness of WC-Co parts taken from industrial production. Furthermore, considering the mechanical strength, not only the mean binder free path but also the residual microporosity must be taken into account. The residual microporosity occurs due to a not correct dewaxing stage. Therefore, in industrial production, not only the Co content and WC grain size but also the production process, such as the dewaxing stage, affects the microstructural parameters of the WC-Co parts and consequently, the mechanical properties. Considering the production process, another important modification of the final microstructure of WC-Co occurs due to the liquid cobalt migration phenomenon. For this reason, in the second part of this PhD thesis, the liquid cobalt migration that occurs during sintering was investigated. The conclusion obtained in the second part of this PhD thesis may be summarized as follows.

- Considering an industrial process, where the furnace and the atmosphere are fixed, it is possible to control the liquid cobalt migration working on the dewaxing stage. In details, a partial dewaxing brings about the Co migration towards the surface with a Co layer formation on the WC-Co surface; differently, a complete dewaxing and a partial surface enrichment due to the graphite of the furnace leads to a the Co migration towards the interior of the material with a surface Co depletion and the formation of a Co gradient into the material.

In conclusion, during the sintering of WC-Co parts in industrial production, the liquid cobalt migration occurs and affects not only the surface properties of the WC-Co part but also the mechanical properties of the material due to the modification of the cobalt amount into all the part.

After studying in details how to define the mechanical properties of WC-Co parts taken from industrial production, in the third part of this PhD thesis, Thermal Fatigue and its combination with oxidation damage in WC-Co were studied, since only a few data are available in literature. The conclusion of the third part of this PhD thesis may be summarized as follow.

- An increase in the WC grain size leads to a variation of the main crack propagation mechanism changes from an intergranular to a transgranular fracture of the WC.
- An increase in the Co content leads to a decreased crack propagation rate and to a increased crack nucleation rate and oxidation resistance.

In conclusion, in applications characterized by cyclic temperature variations, it is preferred to used a WC-Co with high Co content that leads to a higher crack density but lower mean crack length and higher oxidation resistance.

The overall conclusions of this PhD thesis is that the hardness and fracture toughness of WC-Co were defined by the mean binder free path, which is affected by the Co content and carbide grain size. Differently, in case of mechanical strength, also the residual microporosity that depends on the dewaxing stage must be defined. Furthermore, the dewaxing stage acts on the liquid cobalt migration that affects the surface properties and also the final microstructure of the WC-Co part in industrial production. At the end, considering a damage very poorly studied in case of WC-Co, the TF and oxidation resistance of WC-Co results affected by the Co content: high cobalt content leads to a better condition of TF damage and s higher oxidation resistance.

List of abbreviations and acronyms

BPR	ball to powder ratio
DSC	differential scanning calorimetry
EDXS	energy-dispersive X-ray spectroscopy
LPS	liquid-phase sintering
SEM	scanning electron microscopy
SSS	solid-state sintering
TF	thermal fatigue
TRS	transversal rupture strength

References

- Allibert**, C.H., *Sintering features of cemented carbides WC–Co processed from fine powders*. Int. Journal of Refractory Metals and Hard Materials, **2001**. 19 (1): p. 53-61.
- Almond**, E.A., *Deformation characteristics and mechanical properties of hardmetals*. Proceedings of science of hardmaterials, **1983**. 1: p. 517–561.
- Aristizabal**, M., N. Rodriguez, F. Ibarreta, R. Martinez, J.M. Sanchez, *Effect of the Binder Phase Content and Decarburization Phenomena on the Oxidation and Wear Resistance of WC-CoNiCr Materials*. Proceedings EuroPM2009 Congress and Exhibition, Copenhagen (Denmark), ed. EPMA, Shrewsbury (UK), **2009**. 1: p. 299-306.
- Aristizabal**, M., N. Rodriguez, F. Ibarreta, R. Martinez, J.M. Sanchez, *Phase sintering and oxidation resistance of WC-Ni-Co-Cr cemented carbides*. Int J of Refractory Met Hard Mater, **2010**. 28: p. 516-522.
- Aristizabal**, M., J.M. Sanchez, N. Rodriguez, F. Ibarreta, R. Martinez, *Comparison of the oxidation behaviour of WC-Co and WC-Ni-Co-Cr cemented carbides*. Corr Sci **2011**. 53: p. 2754-2760.
- Basu**, S.N., V.K. Sarin, *Oxidation behaviour of WC-Co*. Mater Sci and Eng, **1996**. A209: p. 206-212.
- Bennett**, E.G., B. Roebuck, *The Metallographic Measurement of Hardmetal Grain Size*. NPL Measurement Good Practice Guide, **2000**. 22: p. 1368-6550.
- Bermejo**, R., P. Supancic, R. Danzer, *Influence of measurement uncertainties on the determination of the Weibull distribution*. Journal of the European Ceramic Society, 2012. 32 (2): p. 251-255.
- Bhaumik**, S.K., R. Balasubramaniam, G.S. Upadhyaya, M.L. Vaidya, *Oxidation behaviour of hard and binder phase modified WC-10Co cemented carbides*. J Mater Sci Lett, **1992**. 11: p. 1457-1459.
- Bhushan**, A., S.K. Panda, D. Khan, A. Ojha, K. Chattopadhyay, H.S. Kushwaha, I.A. Khan, *Weibull Effective Volumes, Surfaces, and Strength Scaling for Cylindrical Flexure Specimens Having Bi-Modularity*. Journal of Testing and Evaluation, **2016**. 44(5): p. 1978-1997.
- Brookes**, K.J.A., *Hardmetals and other Hard Materials*. **1992**, United Kingdom: International carbide data.
- Casas**, B., X. Ramis, M. Anglada, J.M. Salla, L. Llanes, *Oxidation-induced strength degradation of WC-Co hardmetals*. Int J Refract Met Hard Mater, **2001**. 19: p. 303-309.
- Cha**, S.I., K.H. Lee, H.J. Ryu, S.H. Hong, *Effect of size and location of spherical pores on transverse rupture strength of WC-Co cemented carbides*. Materials Science and Engineering, **2008**. 486A (1-2), p. 404-408.
- Chen**, L., D. Yi, B. Wang, H. Liu, C. Wu, X. Huang, H. Li, Y. GaO, *The selective oxidation behaviour of WC-Co cemented carbides during the early oxidation stage*. Corr Sci, **2015**. 94: p.1-5.

- Chen, X.**, Y. Yan, *Study on the technology of thermal cracking of paraffin to alpha olefins*. J. Anal. Appl. Pyrolysis, **2008**. 81: p. 106–112.
- Chermant, J.L.**, F. Osterstock, *Fracture toughness and fracture of WC-Co composites*. Journal of Materials Science, **1976**. 11: p. 1939–1951.
- Chongbin, W.**, X. Song, J. Fu, Xi. Lv, H. Wang, Y. Gao, S. Zhao, X. Liu, *Effect of Carbon Addition on Microstructure and Properties of WC–Co Cemented Carbides*. Journal of Materials Science & Technology, **2012**. 28: p. 837-843.
- Da Silva, A.G.P.**, W.D. Schubert, B. Lux, *The Role of the Binder Phase in the WC-Co Sintering*. Materials Research, **2001**. 4 (2): p. 59-62.
- Danzer, R.**, *A general strength distribution function for brittle materials*. Journal of the European Ceramic Society, **1992**. 10: p. 461–72.
- Del Campo, L.**, S.R.B. Pérez, F.L. González, M.J. Tello, *Kinetics inversion in isothermal oxidation of uncoated WC-based carbides between 450 and 800°C*. Corr Scie, **2009**. 51: p. 707-712.
- Dobrzański, L.A.**, B. Dolżańska, *Hardness to toughness relationship on WC-Co tool gradient materials evaluated by Palmqvist method*. Archives of Materials Science and Engineering, **2010**. 43: p. 87-93.
- Engle, E.W.**, *Cemented carbides*. Powder Metallurgy (J. Wulff, ed.), ASM, **1942**. p.436.
- Engqvist, H.**, B. Uhrenius, *Determination of the average grain size of cemented carbides*. International Journal of Refractory Metals & Hard Materials, **2003**. 21: p. 31–35.
- Engle, E.W.**, *Cemented carbides*. Powder Metallurgy (J. Wulff, ed.), ASM, **1942**. p.436.
- Eso, O.**, P. Fan, Z. Fang, *A kinetic model for cobalt gradient formation during liquid phase sintering of functionally graded WC–Co*. Int. J. Refract. Met. Hard Mater., **2008**. 26: p. 91–97.
- Eso, O.**, Z. Fang, A. Griffo, *Liquid phase sintering of functionally graded WC–Co composites*. Int. J. Refract. Met. Hard Mater, **2005**. 23: p. 233–241.
- Exner, H.E.**, H.F. Fischermeister, *Structural dependence of the properties of tungsten carbide-cobalt alloys*. Archiv fur das Eisenhüttenwesen, **1966**. 37: p.417-499.
- Exner, H. E.**, J. Gurland, *A review of parameters influencing some mechanical properties of tungsten carbide-cobalt alloys*. Powder Metallurgy, **1970**. 13: p. 13–31.
- Exner, H.E.**, L. Sigl, M. Fripan, O. Pompe, *Fractography of critical and subcritical cracks in hard materials*. Int. Journal of Refractory Metals and Hard Materials, **2001**. 19: p. 329–334.
- Ezquerro, B. L.**, L. Lozada, J. M. Sánchez, H. Berg, M. Wolf, *Thermal Shock resistance of Cemented Carbides with high Binder Phase Content. Comparison Between Co and Co-Ni-Cr Based Binders*. Proceedings EuroPM2017, Milan, Italy, 1-5 October **2017**.
- Fan, P.**, J. Guo, Z. Z. Fang, P. Prichard, *Design of cobalt gradient via controlling carbon content and WC grain size in liquid-phase-sintered WC–Co composite*. Int. Journal of Refractory Metals & Hard Materials, **2009A**. 27: p. 256–260.

- Fan, P., J. Guo, Z. Fang, P. Prichard, Effects of Liquid-Phase Composition on Its Migration during Liquid-Phase Sintering of Cemented Carbide.** Metallurgical and materials Transactions, **2009B**. A 40: p. 1995-2006.
- Fan, P., O. Eso, Z. Fang, H.Y. Sohn. Effect of WC particle size on Co distribution in liquid-phase-sintered functionally graded WC–Co composite.** Int. Journal of Refractory Metals and Hard Materials, **2008**. 26: p. 98-105.
- Fan, P., Z. Fang, Numerical simulation of kinetics of the cobalt gradient change in WC–Co during liquid phase sintering.** Int. Journal of Refractory Metals and Hard Materials, **2009C**. 27: p. 37-42.
- Fan, P., Z. Z. Fang, J. Guo, A review of liquid phase migration and methods for fabrication of functionally graded cemented tungsten carbide.** Int. Journal of Refractory Metals and Hard Materials, **2013**. 36: p. 2–9.
- Fang, Z.Z., Correlation of transverse rupture strength of WC–Co with hardness.** Int. Journal of Refractory Metals and Hard Materials, **2005**. 23 (2): p. 119-127.
- Fernandes, C. M., A. M. R. Senos, Cemented carbide phase diagrams: a review.** Int. Journal of Refractory Metals and Hard Materials, **2011**. 29: p. 405-418.
- Fernandes, C. M., A. M. R. Senos,, M.T. Vieira, Control of eta carbide formation in tungsten carbide powders sputter-coated with (Fe/Ni/Cr).** Int. Journal of Refractory Metals and Hard Materials, **2007**. 25: p. 310-317.
- Formisano, A, F. Capece Minutolo, A. Caraviello, L. Carrino, M. Durante, and A. Langella, Influence of Eta-Phase on Wear Behavior of WC-Co Carbides.** Advances in Tribology, **2016**. p. 1-6.
- Garcia, J., S. Englund, F. Haglöf, Controlling cobalt capping in sintering process of cermets.** Int Journal of Refractory Metals and Hard Materials, **2016**. 62: p. 126-133.
- Garcia, J., T. Carvalho Miranda, H. C. Pinto, F. Soldera, F. Mücklich, 3D-FIB Characterization of Wear in WC-Co Coated Composites.** Mater Sci Forum, **2015**. 825-826: p. 995-1000.
- German, R. M., Sintering theory and practice.** **1996**, New York: John Wiley & sons, Inc.
- Gu, W.H., Y. S. Jeong, K. Kim, J. C. Kim, S. H. Son, S. Kim. Thermal oxidation behaviour of WC-Co hard metal machining tool tip scraps.** J Mater Process Technol, **2012**. 212: p. 1250-1256.
- Guo, J., P. Fan, X. Wang, Z. Z. Fang, Formation of Co-capping during sintering of straight WC–10wt% Co.** Int. Journal of Refractory Metals & Hard Materials, **2010**. 28: p. 317–323.
- Guo, J., Z. Z. Fang, P. Fan, X. Wang, Kinetics of the formation of metal binder gradient in WC–Co by carbon diffusion induced liquid migration.** Acta Mater., **2011**. 59: p. 4719-4731.
- Gurland, J., Practical Applications of Quantitative Metallography.** ASTM STP839, **1984**.
- Gurland, J., P. Bardzil, Relation of strength, composition, and grain size of sintered WC-Co Alloys.** Transactions of the metallurgical society of AIME, **1955**. 203. p.311-315.

- Huang**, S.G., R.L. Liu, L. Li, O. Van der Biest, J. Vleugels, *NbC as grain growth inhibitor and carbide in WC-Co hardmetals*. Int. Journal of Refractory Metals and Hard Materials, **2008**. 26 (5): p. 389-395.
- Hong**, J., J. Gurland, *A study of the fracture process of WC-Co alloys*. Proceedings of the science of hard materials, **1983**. 1: p. 649-669.
- Ishihara**, S., T. Goshima, K. Nomura, T. Yoshimoto, *Crack propagation behaviour of cermets and cemented carbides under repeated thermal shocks by the improved quench test*. J Mater Sci, **1999**. 34: 629- 636.
- Ivensen**, V.A., *The effect of conditions of preparation on the strength of WC-Co hard alloys and the relationship between the strength of these alloys and their structure and composition*. Poroshkovaya Metallurgiya, **1963**. 3 (15): p. 37-51.
- Janisch**, D.S., W. Lengauer, K. Rödiger, K. Dreyer, H. Van Den Berg, *Cobalt capping: Why is sintered hardmetal sometimes covered with binder*. Int. Journal of Refractory Metals & Hard Materials, **2010**. 28: p. 466-471.
- Jayatilaka**, A., K. Trustrum K. *Statistical approach to brittle fracture*. Journal of Materials Science, **1977**. 12: p.1426-30.
- Jefferies**, Z., A.K. Kline, E.B. Zimmer, *The determination of grain size in metals*. Trans AIME, **1916**. 57: p. 594-607.
- Jia**, K., T.E. Fisher, B. Gallois, *Microstructure, hardness and toughness of nanostructured and conventional WC-Co composites*. NanoStructured Materials, **1998**. 10: p. 875-891.
- Johannesson**, B., R. Warren, *Subcritical crack growth and plastic deformation in the fracture of hard metals*. Materials Science and Engineering, **1988**. A (105-106): p. 353-361.
- Joost** R., J. Pirso, M. Viljus, *The Effect of Carbon Content on the Mechanical and Tribological Properties of WC-Co Cemented Carbides*. **2008**, Nordtrib, Tampere, Finland.
- Klocke**, F., *Manufacturing Processes 1: Cutting*. **2011**, Berlin, Heidelberg, New York: Springer.
- Klünsner**, T., S. Wurster, P. Supancic, R. Ebner, M. Jenko, J. Glätzle, A. Püschel, R. Pippan, *Effect of specimen size on the tensile strength of WC-Co hard metal*. Acta Materialia, **2011**. 59 (10): p. 4244-4252.
- Konyashin**, I. A. A. Zaitsev, D. Sidorenko, E. A. Levashov, B. Ries, S.N. Konischev, Sorokin, M., A. A. Mazilkin, M. Herrmann, A. Kaiser, *Wettability of tungsten carbide by liquid binders in WC-Co cemented carbides: Is it complete for all carbon contents?*. Int. Journal of Refractory Metals and Hard Materials, **2017A**. 62: p. 134-148.
- Konyashin**, I., B. Ries, F. Lachmann, A. T. Fry, *A novel sintering technique for fabrication of functionally gradient WC-Co cemented carbides*. J. Mater. Sci., **2017B**. 47: p. 7072-7084.
- Konyashin**, I., B. Ries, F. Lachmann, A.T. Fry, *Gradient hardmetals: theory and practice*. Int. J. Refract. Met. Hard Mater., **2013**. 26: p. 10-21.

- Konyashin, I., B. Ries, S. Hlawatschek, A. Mazilkin, High temperature capillarity in hardmetal surface layers.** *Materials Letters*, **2016**. 16: p. 254-257.
- Konyashin, I., S. Hlawatschek, B. Ries, F. Lachmann, M. Vukovic, Co capping on WC–Co hardmetals. Part I: A mechanism explaining the presence or absence of cobalt layers on hardmetal articles during sintering.** *Int. Journal of Refractory Metals and Hard Materials*, **2014A**. 42: p. 142–150.
- Konyashin, I., S. Hlawatschek, B. Ries, F. Lachmann, M. Vukovic, Cobalt capping on WC–Co hard metals. Part II: A technology for fabrication of Co coated articles during sintering.** *Int. Journal of Refractory Metals and Hard Materials*, **2014B**. 42: p. 136–141.
- Lagerquist, M., A study of the thermal fatigue crack propagation in WC–Co cemented carbide.** *Powder Metall*, **1975**. 18: p. 71–88.
- Lee, M., High temperature hardness of tungsten carbide.** *Metallurgical Transactions A*, **1983**. 14:p. 1625-1629 .
- Leitner G., K. Jaenicke-Rössler, H. Wagner, Processes during dewaxing and sintering of hardmetal.** International conference on advances in hardmaterials production. **1992**. Germany.
- Li, A., J. Zhao, D. Wang, X. Gao, H. Tang, Three-point bending fatigue behavior of WC–Co cemented carbides.** *Materials & Design*, **2013**. 45: p. 271-278.
- Li, W., F. Yang, D. Fang, Thermal shock modeling of Ultra-High Temperature Ceramics under active cooling.** *Computers & Mathematics with Applications*, **2009**. 58 (11–12): p. 2373-2378.
- Lisovsky, A., Thermodynamics of isolated pores filling with liquid in sintered composite materials.** *Met. Mater. Trans.*, **1993**. 25A: p. 733–740.
- Liu, Y., H.Wang, J.Yang, B. Huang, Z. Long. Formation mechanism of cobalt-gradient structure in WC–Co hard alloy.** *J. Mater. Sci.*, **2004**. 39: p. 4397–4399.
- Liu, Y., H. Wang, Z. Long, P. K. Liaw, J. Yang, B. Huang, Microstructural evolution and mechanical behaviors of graded cemented carbides.** *Mater. Sci. Eng.*, **2006**. A 426: p. 346–354.
- Macedo, H.R., A.G.P da Silva, D.M.A de Melo, The spreading of cobalt, nickel and iron on tungsten carbide and the first stage of hard metal sintering.** *Materials Letters*, **2003**. 57 (24-25): p. 3924-3932.
- Mannesson, K., J. Jeppsson, A. Borgenstam, J. Ågren, Carbide grain growth in cemented carbides.** *Acta Materialia*, **2011**. 59 (5): p. 1912-1923.
- Mchugh, P.E., H. Riedel, A liquid phase sintering model: application to Si₃N₄ AND WC–Co.** *Acta Materialia*, **1997**. 45: p. 2995-3003.
- Morrell, R., A national measurement good practice guide No 15: Fractography of brittle materials.** **1999**, Teddington, UK: NPL.
- Ning, L., X. Genying, X. Yudong, Thermal shock fatigue behaviours of cemented carbide YG20.** *Trans Nonferrous Met Soc China*, **1997**. 7: p.149-154. **Ishihara, S., T. Goshima, K. Nomura, T. Yoshimoto, Crack propagation behaviour of cermets and cemented**

carbides under repeated thermal shocks by the improved quench test. *J Mater Sci*, **1999**. 34: 629– 636.

Okamoto, S., Y. Nakazono, K. Otsuka, Y. Shimoitani, J. Takada, *Mechanical properties of WC/Co cemented carbide with larger WC grain size*. *Materials Characterization*, **2005**. 55 (4–5): p. 281-287.

Osterstock, F., J.L. Chermant, *Some aspects of the fracture of WC-Co-composites*. *Proceedings of the science of hard materials*, **1983**. 1: p. 615–629.

Pellizzari, M., D. Ugues, G. Cipolloni, *Influence of heat treatment and surface engineering on thermal fatigue behaviour of tool steel*. *Int Heat Treat Surf Eng*, **2013**. 7: p.180-184.

Peters, C.T., R. Cooper, *Effect of the eta phase precipitation on the structure and mechanical properties of WC- 5% Hardmetals*. *Planseeber. Pulvermet*, 1987. 22: p. 181.

Petzow G., *Metallographic Etching*, Editor **1999** by ASM International.

Pilling, N.B., R.E. Bedworth, *The Oxidation of Metals at High Temperatures*. *J Inst Met*, **1923**. 29: p. 529–582.

Porat, R., S. Berger, A. Rosen, *Dilatometric study of the sintering mechanism of nanocrystalline cemented carbides*. *Nanostructured Materials*, **1996**. 7 (4): p. 429-436.

Poetschke, J., V. Richter, R. Holke, *Influence and effectivity of VC and Cr₃C₂ grain growth inhibitors on sintering of binderless tungsten carbide*. *Int. Journal of Refractory Metals and Hard Materials*, **2012**. 31: p. 218-223.

Prokopiv, M. M., *Study of the microporosity of WC-Co Alloys*. *Journal of Superhard Materials*, **2008**. 30: p. 67-74.

Quinn, G.D., *Weibull strength scaling for standardized rectangular flexure specimens*. *Communications of the American Ceramic Society*, **2003**. 86(3): p. 508–510.

Sachet, E., Mühlbauer G., Yukimua J., Kubo, Schubert W, *Understanding Cobalt Layer Formation: In Situ Observation and New Insights on the Mechanism*, 18th Plansee Seminar. *Int. Conference on Refractory Metals*, **2013**. HM3. Reutte (Austria).

Sachet, E., W.D. Schubert, G. Mühlbauer, J. Yukimura, Y. Kubo, *On the formation and in situ observation of thin surface layers of cobalt on sintered cemented carbides*. *Int. Journal of Refractory Metals and Hard Materials*, **2012**. 31: p. 96–108.

Šalák, A., *Ferrous powder metallurgy*. **1995**, Cambridge: Cambridge International Science Publishing.

Sandford, E.J., E.M Trent, *The physical metallurgy of sintered carbides*. *Symposium of Powder Metallurgy*, **1947**. 38: p.84.

Santhanam, A.T., P. Tierney, J.L. Hunt, *Properties and Selection: Non ferrous Alloys and Special Purpose Materials*, **1990**. ASM International. The Materials Information Company.

Sarin, V.K., *Comprehensive hard materials – Volume 1: Hardmetals*. **2014**, Boston (USA): Elsevier.

Schubert, W.D., H. Neumeister, G. Kinger, B.Lux, *Hardness to toughness relationship of fine-grained WC-Co hardmetals*. International Journal of Refractory Metals and Hard Materials, **1998**. 16: p. 133-142.

Shetty, D.K., I.G. Wright, P.N. Mincer, A.H. Clauer, *Indentation fracture of WC-Co cermets*. Journal of materials science, **1985**. 20: p. 1873-1882.

Sigl, L. S., H.E. Exner, *Experimental study of the mechanics of fracture in WC-Co alloys*. Metallurgical Transactions A, **1987**. 18: p. 1299–1308.

Sōmiya, S., *Advanced technical ceramics*. **1984**, San Diego: Academic Press, INC.

Spiegler, R., S. Schmauder, L.S. Sigl, *Fracture toughness evaluation of WC-Co alloys by indentation testing*. Journal of hard materials, **1990**. 1: p. 147-158.

Spriggs, G. E., *The importance of atmosphere control in hard-metal production*. Powder Metallurgy, **1970**. 13: p. 369-393.

Sun, J., f. Zhang, J. Shen, *Characterizations of ball-milled nanocrystalline WC–Co composite powders and subsequently rapid hot pressing sintered cermets*. Materials Letters, **2003**. 57: p. 3140-3148.

Taniguchi, *Surface-refined sintered alloy body and method for making the same*. **1989**, Patent US4830930.

Tarragó, J.M., D. Coureaux, Y. Torres, E. Jiménez-Piqué, L. Schneider, J. Fair, L. Llanes, *Strength and reliability of WC-Co cemented carbides: Understanding microstructural effects on the basis of R-curve behavior and fractography*. International Journal of Refractory Metals and Hard Materials, **2018**. 71: p. 221-226.

Thümmler, F., R. Oberacker, *An Introduction to Powder Metallurgy*. **1993**, London: the Institute of Materials.

Torres, Y., R. Bermejo, F.J. Gotor, E. Chicardi, L. Llanes, *Analysis on the mechanical strength of WC-Co cemented carbides under uniaxial and biaxial bending*, Materials & Design, **2014**. 55: p. 851-856.

Tsuada, K., A. Ikegaya, K. Isobe, N. Kitagawa, T. Nomura, *Development of functionally graded sintered hard materials*. Powder Metall, **1996**. 39: p. 296–300.

Tumanov, V.I., Z.A. Gol'dberg, V.V. Chernyshev, Z.I. Pavlova, *Thermal shock resistance of tungsten carbide-cobalt alloys*. Sov Powder Metall and Met Ceram, **1966**. 5: p. 818–822.

Uhrenius, B., *Carbon balances during presintering and sintering of cemented carbides*. Internal report Sandvik coromant. **1975**. Stockholm.

Uhrenius, B., J. Agren, S. Haglund, *On the sintering of cemented carbides*. In Sintering Technology, R. German, G. Messing, R. Cornwall, Editor **1996**, Marcel Dekker: New York (USA). p. 129–139.

Upadhyaya, G.S., *Cemented Tungsten Carbides: Production, Properties, and Testing*. **1998**, New Jersey: Noyes Publications.

Voitovich, V.B., V.V. Sverdel, R.F. Voitovich, E.I. Golovko, *Oxidation of WC-Co, WC-Ni and WC-Co-Ni Hard Metals in the Temperature Range 500-800°C*. Int J Refract Met Hard Mater, **1996**. 14: p. 289-295.

Weibull, W., *A statistical distribution function of wide applicability*. Journal of Applied Mechanics, Transactions of ASME, **1951**. 18: p. 293–297.

Weroncki, A., T. Hejwowski, *Thermal fatigue of metals*. **1991**, New York, N.Y.: Dekker.

Zackrisson, J., B. Jansson, G.S. Uphadyaya, H.-O. Andrén, *WC-Co based cemented carbides with large Cr₃C₂ additions*. International Journal of Refractory Metals and Hard Materials, **1998**, 16 (4-6): p. 417-422.

Scientific Production

International Journal

- [1] **L. Emanuelli**, M. Pellizzari, A. Molinari, F. Castellani, E. Zinutti, *Thermal fatigue behaviour of WC-20Co and WC-30(CoNiCrFe) cemented carbide*, Int. Journal of Refractory Metals and Hard Materials 60 (2016), p. 118–124.
- [2] **L. Emanuelli**, M. Pellizzari, A. Molinari, F. Castellani, E. Zinutti, Reprint of *Thermal fatigue behaviour of WC-20Co and WC-30(CoNiCrFe) cemented carbide*, Int. Journal of Refractory Metals and Hard Materials 62 (2017), p. 176-182.
- [3] **L. Emanuelli**, A. Molinari, G. Arrighetti, G. Garoli, *Effect of the sintering parameters on the liquid Co migration in WC-Co*, Int. Journal of Refractory Metals and Hard Materials 70 (2018), p. 202-209.
- [4] **L. Emanuelli**, A. Molinari, G. Arrighetti, G. Garoli, *Dependence of the mechanical properties on the microstructural parameters of WC-Co*, Submitted to Powder Metallurgy Progress.

National Journal

- [1] **L. Emanuelli**, *Caratterizzazione microstrutturale del WC-Co*, la metallurgia italiana, n. 11/12 (2017), p. 52-55.
- [2] **L. Emanuelli**, A. Molinari, G. Arrighetti, G. Garoli, *La migrazione del cobalto nella sinterizzazione del metallo duro*, la metallurgia italiana, n. 11/12 (2017), p. 5-13.

Proceedings

- [1] **L. Emanuelli**, A. Molinari, G. Arrighetti, G. Garoli, *La migrazione del cobalto nella sinterizzazione del metallo duro*, in Proceedings 36AIM, Parma, Italy: AIM, 2016. Atti di: 36AIM, Parma – IT, 21-23 September 2017.
- [2] **L. Emanuelli**, A. Molinari, G. Arrighetti, G. Garoli, *Effect of process parameters on the cobalt capping in WC-Co*, in Proceedings EuroPM2017, Milan, Italy: EPMA, 2017. Atti di: EuroPM2017, Milan – IT, 1-5 October 2017.
- [3] **L. Emanuelli**, A. Molinari, G. Arrighetti, G. Garoli, *Analysis of transversal rupture strength of different WC-Co Cemented carbides*, Accepted in Proceedings EuroPM2018, Bilbao, Spain, 14 - 18 October 2018.

Acknowledgments

I gratefully acknowledge Koner S.r.l for the supply of the WC-Co nibs. In details, I would like to thank G. Arrighetti and G. Garoli.

Last but not least, I would like to thank the Department of Industrial Engineering, especially Professor Molinari and Professor Pellizzari.

... e quelli meno formali ...

Desidero ringraziare sentitamente il Prof. Alberto Molinari per i suoi preziosi insegnamenti, la sua pazienza, fiducia e completa disponibilità.

Un grazie speciale a Cinzia, grande punto di riferimento in laboratorio ma, soprattutto, grande amica sempre pronta a farsi in quattro ad ogni necessità.

Un grazie a Lorena e Gloria per aver reso leggere e gioiose le innumerevoli ore al SEM.

Grazie di cuore anche allo staff della segreteria, in particolare Sara sempre disponibile e pronta ad aiutare.

Ci tengo a ringraziare di cuore anche tutti coloro che sono passati per il laboratorio di metallurgia e che hanno percorso con me questi anni di dottorato.

Un ringraziamento speciale e pieno di affetto va ai miei genitori ed a mio fratello che mi hanno sempre sostenuta, consigliata ed aiutata ad affrontare ogni momento!

Infine un immenso grazie a Dario, marito e migliore amico insostituibile, e Tommaso, new entry della famiglia che mi ha fatto capire cosa conta davvero nella vita.